STUDIES OF ION TRANSPORT PROPERTIES AND ION-MOLECULE INTERACTIONS IN A DRIFT TUBE MASS SPECTROMETER

A thesis

submitted in partial fulfilment

of the requirements for the Degree

of

Doctor of Philosophy in Chemistry

in the

University of Canterbury

by

Bruce J. McIntosh

University of Canterbury

1984

CONTENTS

LIST OF FIGURES

ABSTRACT

Mobilities of ions in helium buffer gas have been determined using a drift tube mass spectrometer. The ions are formed by dissociative charge transfer from electron impact generated He^+ to traces of compounds (<0.2%) added to the helium buffer. The electric field strength to gas number density ratio (E/N) was varied from $10\text{-}140 \times 10^{-21} Vm^2$. The design, construction and operation of the instrument is described in detail.

An important feature of the instrument constructed for this project is the ability to vary the drift distance from 1-10 cm by continuous movement of the ion source. This feature enables mobilities to be determined for ions formed by one or more reactions along the drift tube provided the reactions are largely completed during the early period of ion transit. Mobilities are derived from the slope of a plot of arrival time of maximum signal against drift distance. A mathematical analysis of this procedure is presented for various reaction schemes and used to determine optimum operating conditions and estimate systematic errors. Alternatively, the mobility may be determined iteratively by comparison of the experimental arrival time distributions with those calculated using an appropriate model. The total uncertainty in mobilities obtained by either technique is estimated not to exceed 5% and reproducibility between individual measurements is found to be better than 3%.

A series of ions containing the -CN group has been studied. Mobilities are presented for CN^+, HCN^+, H_2CN^+, C_2N^+, HC_2N^+, $C_2H_3N^+$ and $C_2N_2^+$ formed from hydrogen cyanide,

dicyanogen, methyl cyanide and methyl isocyanide. Momentum transfer collision integrals, $\Omega^{(1,1)}$, have been calculated as a function of effective temperature in accordance with the two-temperature theory of Viehland and Mason.

The mobilities of several selected organic ions formed from different precursor neutrals have been determined. The $C_3H_6^+$ ion produced from either cyclopropane or propene was found to exhibit the same mobility regardless of the precursor neutral molecule. This was also found for the $C_3H_3^+$ ions and in both cases is believed to signify structural equivalence. Ions of empirical formula $C_2H_4O^+$ formed from ethanol and ethylene oxide were found to exhibit different mobilities and $C_2H_5O^+$ ions from ethanol and dimethyl ether could be similarly distinguished. The different mobilities reflect structural differences and the use of mobility measurements as a technique for discrimination of isomeric ion structures is discussed.

CHAPTER 1

INTRODUCTION

The behaviour of ions in gases is an area of continually widening interest. Models of upper atmosphere chemistry, lasers, gaseous electronics and interstellar chemistry all require quantitative information concerning the properties of ion-neutral interactions. In many cases, a knowledge of the variation of these properties with energy or temperature is desirable. Below about 900K experimental methods such as mass spectrometry, ion cyclotron resonance and flowing afterglow can provide the necessary data. At very high temperatures, normally at least 10^4K, these data can be calculated from the results of ion-neutral beam experiments. The energy gap remaining, between 900 and 10^4K, can normally only be covered by means of drift tubes. Over the past fifteen years numerous theoretical and experimental advances have greatly increased the versatility and accuracy of drift tube measurements.

The work described in this thesis is primarily concerned with the measurement of drift velocities and hence mobilities of a range of ions in helium. Traditionally mobilities have been determined for the simplest possible systems, namely noble gas or alkali metal ions in noble gas buffers. An ion-neutral interaction potential can often be derived from the mobility data in these monoatomic systems and compared with the predictions of an appropriate theory.

The recently formulated two temperature theory of Viehland and Mason[1] quantitatively describes the equivalence

of the effects of temperature and electric field strength. Experimentally, this means that variation of the electric field strength (or more correctly E/N) which is easily performed over wide ranges can provide the same information as variation of temperature. Knowledge of the mobilities of the ions is essential for implementation of this theory. For example, in order to study an ion-neutral reaction at a given effective temperature the drift velocity of the ion is required so that the correct electric field can be established.

The ions studied in this work are formed as primary or secondary reaction products of charge transfer from He^+ ions. Previously, mobilities of ions formed by reaction in drift tubes have been determined by comparison of experimental and calculated ion arrival time distributions[2] with the mobility being treated as a variable parameter. Analytic expressions are only available for ions formed from direct reaction of primary ions[2,3] so this technique would be difficult to modify for ions formed by subsequent reaction. For accurate results the experimental arrival time spectra should closely resemble the expected model spectra; impurities and other experimental anomalies mean that this cannot always be guaranteed. Consequently, most of the data available for ions of chemical interest formed by reaction have been measured using the flow-drift technique.[4] The versatility of the method is offset only by the complexity and expense of the equipment required for its implementation and the constraints imposed by a limited range of single component buffer gases.

The present work makes use of a drift tube mass

spectrometer with a movable ion source. The advantages of a movable ion source in eliminating anomalous end effects have been well established by McDaniel.[5,6] This thesis describes the use of the instrument for the determination of mobilities from plots of the maximum signal intensity of ion arrival time distributions against drift distance. Variation of the drift distance permits effects due to finite reaction time to be effectively eliminated. This enables drift velocities to be measured for a wide range of ions formed by varying stages of reaction on a fairly routine basis. Knowledge of diffusion and rate coefficients is not necessary and data need only be collected over the range of highest signal intensity.

Compounds containing the -CN group were chosen for these studies because of their role in extraterrestrial systems. The CN radical and HCN have been detected in interstellar space and in comets and HCN has recently been identified in the atmosphere of Titan.[7] More complex molecules including HC_xN, where x=3,5,7 and 9, CH_3CN, NH_2CN and CH_2CHCN have also been observed[8] and the mechanism for their production is of considerable interest. The importance of ion-molecule reactions in the synthesis of these interstellar polyatomic molecules has been demonstrated and the observed abundances of several molecules successfully modelled.[9,10]

Much attention has been focussed in recent years on structure elucidation of isomeric ions. Mass filters are of course blind to structural differences and techniques such as collision induced dissociation,[11] appearance potential measurements[12] or analysis of the thermodynamics

of ion-molecule reactions are required to differentiate between isomeric structures. The application of mobility measurements to this problem could usefully supplement these techniques; particularly for analysis of ions formed in a flow tube experiment. Accordingly, the feasibility of this technique has been investigated using a variety of organic ions derived from isomeric precursors.

In keeping with modern practice, SI units are used as widely as possible throughout this thesis. However, units conventionally used by other workers in the field are retained here to ease comprehension and to facilitate the direct comparison of data. A table defining all non-SI units used is given in Appendix A.

CHAPTER 2

DEFINITIONS AND THEORY

(i) Mobility

An electric field (E) acting on a swarm of ions in a neutral buffer gas will cause them to acquire an average drift velocity (v_d) in the direction of the field. The constant of proportionality between these two quantities is the mobility K, i.e.

$$\underset{\sim}{v}_d = K\underset{\sim}{E} \qquad -(2.1)$$

The characteristic drift velocity v_d is attained when the momentum gained from the electric field equals that lost by collision with the neutral gas molecules. The mobility is therefore a joint property of the ions and the gas through which they drift. For tabulation[13,14] and comparison of data the mobility K is generally converted to a reduced mobility (K_o) defined by

$$K_o = K \cdot \frac{P}{760} \cdot \frac{273.16}{T} = \frac{NK}{N_o} \qquad -(2.2)$$

where P is the neutral gas pressure in Torr and T the temperature in Kelvin. N_o is the standard gas number density of 2.6872×10^{19} molec. cm^{-3}. The units most commonly and conveniently used for ion mobilities are $cm^2V^{-1}s^{-1}$ ($10^{-4}m^2V^{-1}s^{-1}$).

(ii) The parameter E/N

The variable which determines the amount of energy the ions can acquire from the field is the ratio of electric

field strength to gas number density, E/N. It can be rigorously shown[5] that the reduced mobility (K_o) is a function only of E/N and temperature for a given ion-neutral system. It is customary to denote the units of E/N by the Townsend[15] (Td) where $1Td = 10^{-21} Vm^2$.

When the energy acquired from the field is small compared to the thermal energy (E/N < 5Td) the field is descibed as "low". This criterion is reversed for a "high" field. When the thermal and field energies are of comparable magnitude the system is described in terms of an "intermediate" or "medium" field. Different theoretical treatments and assumptions may be appropriate to each of these ranges of field strength.[5]

In the limit of low E/N (and low temperature) the reduced mobility reaches a constant value. Extrapolation of mobility measurements at low E/N gives the zero field reduced mobility $K_o(0)$. Where a single figure is quoted for the mobility of a certain ion in a given buffer gas this will generally refer to $K_o(0)$.

(iii) Diffusion Coefficients

A localised collection of ions in a neutral buffer gas will become dispersed by diffusion. The diffusive flow will be proportional to, but in opposite direction to, the concentration gradient of the ions as described by Fick's Law of diffusion:

$$\underset{\sim}{J} = -D\underset{\sim}{\nabla}n \qquad -(2.3)$$

Here $\underset{\sim}{J}$ is the ionic flux density (the number of ions flowing in unit time through unit area normal to the direction of flow), n is the number density of the ions and D is the

diffusion coefficient with units cm^2s^{-1}.

In the presence of an electric field this diffusion will be superimposed on the drifting motion of the ions. Since the ions now diffuse as the result of both random thermal motion and motion induced by the field, the diffusion becomes anisotropic. The longitudinal diffusion coefficient, D_L, describes the rate of diffusion parallel to the electric field and the transverse diffusion coefficient characterizes diffusion in directions perpendicular to the field. In the limit of low E/N these diffusion coefficients become identical and are related to the mobility by the Einstein (or Nernst Townsend) equation[5a]:

$$\frac{qD}{K} = k_B T \qquad -(2\text{-}4)$$

where T is the gas temperature, q the ionic charge and k_B is the Boltzmann constant. Beyond the low field region the Einstein relationship is no longer valid and the diffusion coefficients increase rapidly.

Diffusion coefficients vary inversely with the gas number density; for this reason data are conveniently presented as the product DN.[13,14]

(iv) Elementary Theories

The most useful of the early theoretical treatments of gaseous ion transport is the free flight theory developed by Wannier.[16] This approach considers the acceleration of the ions by the field for a constant mean free flight time between collisions. The momentum loss on collision is determined by momentum and energy conservation principles and an approximate average over all collisions obtained.

This theory provides a number of reasonably accurate inter-relationships.

The "Wannier expression" gives the mean kinetic energy, E_k, of the ions in the laboratory frame of reference as they move through a single component neutral gas:

$$E_k = \frac{3}{2}k_B T + \frac{1}{2}mv_d^2 + \frac{1}{2}Mv_d^2 \qquad -(2.5)$$

Here T is the gas temperature, m and M are the ion and neutral masses, respectively, v_d is the drift velocity and k_B is Boltzmann's constant. Eq(2.5) gives the ion energy as the sum of the thermal energy, kinetic energy that the ions have due to motion in the direction of the field and energy that has also been acquired from the field but is exhibited as random motion due to ion-neutral collisions during transit.

Interparticle interaction will depend only on the relative energy of the collision partners. It is therefore advantageous to use a centre-of-mass reference frame i.e. one where the centre-of-mass of the colliding particles is at rest. The Wannier expression reduces to

$$E_{rel} = \frac{3}{2}k_B T + \frac{1}{2}Mv_d^2 \qquad -(2.6)$$

in the centre-of-mass frame. Eq(2.6) suggests that any combination of T and E/N that leads to the same E_{rel} should have the same coefficients. Thus in principle, temperature dependances may be evaluated by measuring these coefficients as a function of E/N.

Extension of the free flight treatment to diffusion provides useful generalizations to the Einstein relation.[16] Expressed in terms of drift velocities[5b] the diffusion coefficients at field strength E are given by

$$D_L(E) = D(0) + \frac{(M+3.72m)Mv_d^3}{3(M+1.908m)qE} \qquad -(2.7)$$

$$D_T(E) = D(0) + \frac{(M+m)Mv_d^3}{3(M+1.908m)qE} \qquad -(2.8)$$

where D(0) is the zero field value obeying the Einstein relation and all other variables are as defined previously. These expressions agree well with experimentally determined diffusion coefficients up to about 100 Td.[5]

Another elementary approach is that of momentum transfer,[17] many of the results being equivalent to those of free flight theory. This method, however, may be readily extended to multicomponent gas mixtures[18] giving in the limit of low E/N an expression for the mobility known as Blanc's Law:[5]

$$\frac{1}{K_{mix}} = \sum_j \frac{X_j}{K_j} \qquad -(2.9)$$

where $X_j = N_j/N$ is the mole fraction of neutral species j in the mixture. At high fields this expression is no longer valid. The determination of ion energy partitioning between drift and random field components is complex for a mixture and requires treatment with more sophisticated models.

The main limitation of these elementary theories is the difficulty of extending them significantly or of systematically improving their accuracy.[19]

A more general procedure to obtain T and E/N relationships for ion transport in gases is to solve the relevant Boltzmann equation by converting it into a set of moment equations of interest. The one-temperature theories derived by Kihara[20] and Mason and Schamp[21] with this method suffer from the limitation that they yield expressions for transport coefficients as power series in E/N which diverge at high field strengths.

(v) Two-Temperature Theory

The two-temperature theory of Viehland and Mason[1] overcomes problems of divergence at high field by the use of an effective ion temperature, T_{eff}, which may be greater than the neutral gas temperature:

$$\frac{3}{2}k_B T_{eff} = \frac{3}{2}k_B T + \frac{1}{2}Mv_d^2(1+\beta) \qquad -(2.10)$$

Note that the right hand side of Eq(2.10) is the same as the Wannier expression for E_{rel} (Eq 2.6) except for the correction factor β. The mobility of a swarm of atomic ions moving through a single component atomic gas can be respresented at all temperatures and field strengths by

$$K = \frac{3q}{8N}\left(\frac{\pi}{2\mu k_B T_{eff}}\right)^{\frac{1}{2}} \frac{1+\alpha}{\bar{\Omega}^{(1,1)}(T_{eff})} \qquad -(2.11)$$

where μ is the ion-neutral reduced mass and $\bar{\Omega}^{(1,1)}(T_{eff})$ is the temperature dependant momentum transfer collision integral. The correction terms α and β are complicated functions of T, E/N, m, M and the ion-neutral interaction potential. Numerical calculations[1] have shown α and β to normally be substantially less than 0.1 and as a first approximation these may be set to zero.

Neglecting α and β then, equation (2.11) shows that all of the influence of the ion-neutral interaction potential upon gaseous ion mobility arises through the momentum-transfer collision integral, $\bar{\Omega}^{(1,1)}$. This is the first of a series of integrals that arise in kinetic-theory calculations:

$$\bar{\Omega}^{(\ell,s)}(T) = \left[(s+\ell+1)!\,(kT)^{s+2}\right]^{-1} \int_0^\infty Q^{(\ell)}(E)\, e^{-E/kT}\, E^{s+\ell+1}\, dE \qquad -(2.12)$$

i.e. a normalised integration of the momentum transfer cross

section $Q^{(\ell)}(E)$ over relative ion-neutral collision energy E. The cross section $Q^{(\ell)}(E)$ is given classically by

$$Q^{(\ell)}(E) = 2\pi\left[1-\frac{1+(-1)^{\ell}}{2(1+\ell)}\right]^{-1}\int_0^{\infty}(1-\cos\theta)bdb \qquad -(2.13)$$

where θ is the deflection angle in an ion-neutral collision of energy E and impact parameter b. The normalization factors of eq(2.12) and (2.13) are chosen so that all of the $\bar{\Omega}^{(\ell,s)}$ and $Q^{(\ell)}$ are equal to πd^2 for the collision of rigid spheres of diameter d. The deflection angle θ is calculated as a function of b and E and the ion-neutral interaction potential $V_{(r)}$:

$$\theta(b,E) = \pi-2b\int_{r_o}^{\infty}\left[1-\frac{b^2}{r^2}-\frac{V(r)}{E}\right]^{-\frac{1}{2}}\frac{dr}{r^2} \qquad -(2.14)$$

where the distance of closest approach r_o is the outermost root of

$$1-\frac{b^2}{r_o^2}-\frac{V(r_o)}{E} = 0 \qquad -(2.15)$$

The application of these relationships as a direct link between the ion-neutral interaction potential and the mobility is discussed later.

The analysis of molecular ion-neutral systems is complicated by the presence of inelastic collisions and anisotropic interaction potentials. The two-temperature theory requires consideration also of an internal ion temperature, T_i, that characterizes the energy held in the internal degrees of freedom. For molecular ion-neutral systems e.g.(2.10) can be generalized as[22]

$$\frac{3}{2}k_B T'_{eff}\left(1+\frac{M\xi}{m}\right) = \frac{3}{2}k_B T + \frac{1}{2}Mv_d^2 \qquad -(2.16)$$

where the quantity ξ is a dimensionless ratio of the collision

integral for inelastic energy loss to that for momentum transfer. The factor $M\xi/m$ may be most readily neglected for cases of heavy ions in a light buffer gas or molecular ions moving through an atomic buffer gas.

The internal ion temperature T_i is that which results when the average ion internal energy before and after collision is the same. This average energy will depend on the relative cross sections for inelastic and elastic collisions. In the special case of molecular ions in an atomic neutral gas the internal temperature T_i equals the effective kinetic temperature T'_{eff}. This may be rationalized as follows.[19] The source of the internal energy is collision due to the translational motion of the ions. Energy is lost from both the internal and translational degrees of freedom of the ions only through the translational motion of the neutrals. Since both forms of energy have the same loss mechanism and the translational energy of the ion provides the internal energy, in the steady state T_i must equal T'_{eff}. For a mixture of buffer gases no simple relationship for T_i can be obtained even when all neutrals are atomic. In this case it is difficult to tell how on average the energy loss upon collision will be partitioned between internal and translational modes since each neutral species has a different effective kinetic temperature.

From eqs(2.10) and (2.16) it is clear the two temperature theory predicts the same interpretation of the effects of temperature and E/N as mentioned earlier for the free flight theory, namely any combination of E/N and T with the same T_{eff} gives equivalent behaviour. With the two-temperature theory similar predictions can be made for

reaction rate coefficients.

For reaction of an atomic ion swarm drifting through a buffer gas of mass M_b containing a small proportion of reactive neutral atoms of mass M_R the rate coefficient, k, is given by[23]:

$$k = \frac{1}{k_B T_R} \left(\frac{8}{\pi \mu_R k_B T_R}\right)^{\frac{1}{2}} \int_0^\infty \exp\left(\frac{-\varepsilon}{k_B T_R}\right) Q^*(\varepsilon)\, \varepsilon\, d\varepsilon \qquad -(2.17)$$

where $Q^*(\varepsilon)$ is the energy dependant cross-section for the reaction, μ_R is the ion-reactive atom reduced mass and T_R is the effective reaction temperature given by:

$$\frac{3}{2}k_B T_R = \frac{3}{2}k_B T + \frac{1}{2}M_R v_d^2 \left(\frac{m+M_b}{m+M_R}\right) \qquad -(2.18)$$

which is the mean kinetic energy in the centre-of-mass frame of the ion and reactant neutral. As was the case for mobilities, eqs.(2.17) and (2.18) predict that the rate coefficients will be the same for any combination of T and E/N that give the same T_R. Thus high temperature reaction rates may be derived from measurements of k at room temperature using high fields.

With molecular systems[22] a generalization of eq.(2.17) gives an expression which equates the experimental rate coefficient, measured as a function of E/N and T, to an equivalent thermal rate coefficient that depends on T, T_i, and the reactive translational temperature T_R. For the special case of molecular ions in an atomic buffer T_i will be equal to the effective translational temperature in the centre-of-mass frame of the ion and buffer eq.(2.16). Comparison of eqs.(2.16) (with ξ=0) and eq.(2.18) gives

$$\frac{(T_i - T)}{(T_R - T)} = \left(\frac{M_b}{M_R}\right)\left[\frac{(m+M_R)}{(m+M_b)}\right] \qquad -(2.19)$$

Thus, relative effects of internal and translational energies on reaction rates may be found by comparing measurements in two or more buffer gases. This result has been found to be consistent with experimental work.[24]

The two-temperature theory does not provide results for gaseous ion diffusion anywhere near as satisfactory as those for mobility and reaction rate coefficients. This is particularly true when the ion neutral mass ratio is greater than one; the results being essentially useless for m/M greater than about four.[1] More refined generalizations of the Einstein relation have been derived[25,26] than those of Wannier (eqs 2.7 and 2.8). These incorporate terms involving ratios of collision integrals and mass dependant parameters, however, so these expressions are not as readily applicable.

(vi) Three-Temperature Theory

The problems with diffusion in the two-temperature theory probably arise from the use of a single temperature to characterise the anisotropic velocity distribution of the ions. The three-temperature kinetic theory[27] is based on the use of two ion temperatures; one parallel and the other perpendicular to the field in addition to the neutral gas temperature. For cases involving both atomic ions and neutrals the forth term approximation of this theory provides values for mobilities and diffusion coefficients that are of comparable accuracy to experimental

data.[27,28] The physical interpretation of equations from this theory is, however, more difficult than with simpler theories.[19]

(vii) Monte Carlo Treatments

A computer simulation may be made of the fate of a single ion undergoing a very large number of collisions while drifting through a neutral buffer. The time intervals between collisions and velocity changes during collisions are chosen randomly from an appropriate distribution (hence the "Monte Carlo" label). The time averaged behaviour of the ion is taken to be representative of the ensemble averaged behaviour of the many ions in a real system.

Such simulations require large amounts of computer time but have become practicable due to improvements in hardware and software.[19] Monte Carlo studies have been implemented to verify the accuracy of equations derived by kinetic theories and to test and improve the accuracy of ion-neutral interaction potentials. The main limitation of Monte Carlo treatments is that in order to determine the effect of a change in any parameter a new calculation from the start is required.

(viii) Determination of Interaction Potentials

A direct link between mobility and interaction potential is provided, in principle at least, by eqs 2.11-2.15. The actual integrations are quite difficult to perform due to singularities and other irregularities in the integrands. However, tables of transport collision integrals are available

for (n,6,4) potentials[29] described by

$$V(r) = \frac{B}{r^n} - \frac{C_6}{r^6} - \frac{C_4}{r^4} \qquad -(2.20)$$

The inverse forth power term accounts for the attraction between the charge on the ion and the dipole it induces in the polarizable neutral. This term dominates the mobility at low temperature and fields giving the "polarization limit" as T_{eff} approaches zero. This limit, at standard gas density, is given by[5,29] the Langevin expression:

$$K_{pol} = \frac{13.876}{\alpha^{\frac{1}{2}}} \left(\frac{m+M}{mM}\right)^{\frac{1}{2}} cm^2V^{-1}s^{-1} \qquad -(2.21)$$

where α is the polarizability in $10^{-30}m^3$($\AA^3$) and the masses are in amu. The inverse sixth power term accounts for the charge induced quadrupole attraction plus the London dispersion energy. The term B/r^n is an empirical representation of the short-range repulsion energy. This type of potential (eq 2.20) cannot account for charge transfer between ion and neutral.

In the general case inversion of mobility data to yield a unique interaction potential is impossible.[29] Some assumptions must be made about the form of the potential, such as assuming an (n,6,4) model. A curve fitting procedure may then be applied to determine the values of parameters such that optimal agreement is obtained between calculated and measured mobilities.

CHAPTER 3

EXPERIMENTAL APPARATUS

(i) Requirements and drift tube types

Mobilities, diffusion coefficients and non-neutral reaction rates are studied as a function of E/N by means of devices known as drift tubes. The basic concept is very simple. A buffer gas at a pressure between about 0.01 and 10 Torr is enclosed in a region permeated by an homogeneous axial electric field. Some type of ion source is placed at one end with provision for pulsing the ion beam produced therein. At the opposite end is stationed some form of detector. To measure the range of transit times of the ions (arrival time distribution) the detector must be sensitive to the ions only for a short period a variable time after the ion source pulse. Although useful data[5] have been obtained with early instruments of this simplicity, a number of refinements enable more accurate data to be obtained and a much wider range of systems to be studied.

A mass spectrometer to identify the ions is essential where reaction of ions with the buffer gas or traces of reactant gas added to the buffer gas is important. This is almost always the case; even in a simple system like He^+ ions drifting in helium reaction occurs to produce He_2^+, let alone the possibility of reaction with unknown impurities.

Drift tube mass spectrometers utilize a wide variety of techniques to produce the desired ions. A trace of the gas from which the ion may be formed can be added to the buffer gas. Ions of the buffer gas formed by electron impact

or electrical discharge react with the trace component to form the desired secondary ions. This is the method used in the work described here. An important feature of the present instrument is that the ion source can be moved, thereby varying the drift distance. As discussed by McDaniel[5c,6] and will be explained later the ability to vary the drift distance of the ions is essential if the perturbations due to the spread of formation times of the ions by reaction are to be adequately accounted for.

Alternatively the ion source may be separate from the drift tube. A different gas to the drift tube buffer may then be present in the ionization region. The ions are then injected into the drift tube through a small orifice. A quadrupole mass analyser located between the ion source and drift tube allows selection of the ions to be injected. With this injected ion type drift tube[30] the ions must be injected against a considerable pressure gradient since the mass analyser must operate at $<1X10^{-5}$ Torr. This requires high fields and problems may then arise with subsequent "thermalization" of the ions to the drift tube field.

A flow-drift tube[4] employs a flowing afterglow apparatus to produce ions. Here primary ions are formed by electron impact of a fast flowing carrier gas. Secondary ions are then produced by reaction with other species added downstream from the carrier gas inlet but upstream from the drift tube. This apparatus is particularly useful for the determination of ion-neutral reaction rate coefficients. With a selected ion flow-drift tube (SIFT-drift)[31] the primary ions are first mass selected and then injected into the carrier gas stream which is admitted to the tube via a

venturi inlet. The single ion selected may then further react with other gases downstream as with the conventional flow-drift. This most versatile instrument allows an almost unlimited range of systems to be studied.

(ii) Description of Vacuum System

The drift tube mass spectrometer used for the work described in this thesis is depicted schematically in fig.3.1. All materials used in this apparatus are ultra-high vacuum (UHV) compatible and tolerant of moderately high temperatures; the drift tube component being routinely baked to 200^{o}C to facilitate degassing.

The vacuum chambers are both 15 cm Varian stainless steel crosses (four terminations) sealed by means of "Conflat" flanges and copper gaskets. The drift tube and mass spectrometer chambers are partitioned by a gold plated stainless steel skimmer with a 2 mm diameter orifice located about 10 mm from the end of the drift tube. The skimmer is insulated from its support by a Viton O-ring. This enables the use of an appropriate electrical bias to focus ions into the mass spectrometer chamber.

Both chambers are pumped by 2000 ℓs^{-1} (for helium) Varian 183-VHS-4 10 cm diffusion pumps, using DC705 silicone oil, fitted with liquid nitrogen traps (cryobaffles). The vacuum chambers may be sealed off from the diffusion pumps by means of Temescal hand operated straight through gate valves. The mass spectrometer chamber backing pump is an Edwards EDM20 direct drive two stage unit rated at 300 ℓmin^{-1}; the drift tube chamber is backed by a two stage belt driven Ulvac rotary pump rated at 350 ℓmin^{-1}. The chamber pressures

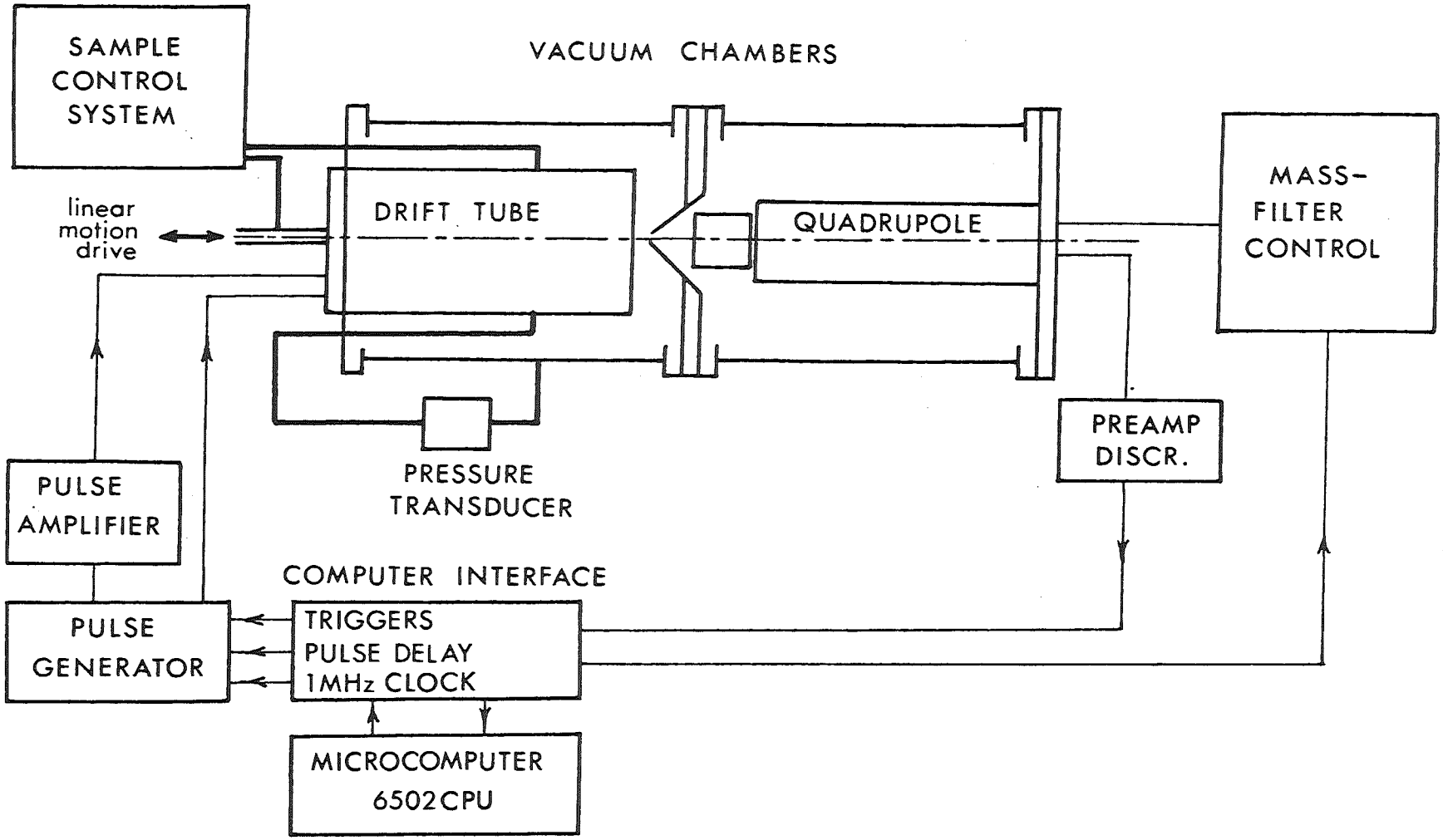

Figure 3.1 Overall schematic of the drift tube mass spectrometer

are measured with ionization gauges. Pressures in the low 10^{-7} Torr range are readily attained in both chambers with no gas in the drift tube. For a drift tube pressure of 1 Torr helium the drift tube and mass spectrometer chambers operate at $5X10^{-5}$ Torr and $4X10^{-7}$ Torr respectively. The diffusion pumps are protected by an interlock system whereby inadequate water cooling, excessive foreline pressure (determined from thermocouple gauges) or full scale deflection of the ion gauge meter constitutes vacuum failure with the subsequent shutdown of the system. Very high foreline pressure also results in shut down of the mechanical pumps, this facility also ensures that the whole system remains inactive after a power failure.

(iii) Mass Spectrometer

The mass filter is an Extranuclear model 4-270-9 ELFS quadrupole with a mass range of 1-800 amu. The quadrupole is controlled by an Extranuclear 011-15 power supply unit with 1.25 MHz High-Q head. Ions are focussed into the quadrupole with the aid of a three element Einzel lens mounted on the end of the grounded case surrounding the quadrupole rods. The quadrupole mass spectrometer allows easy conversion from positive to negative ion mode. A chosen mass range may be scanned in 50 ms or less to produce a mass spectrum on an oscilloscope.

The Extranuclear ion detection facilities are shown diagrammatically in fig.3.2. A channeltron electron multiplier type 4816 (Galileo optics) is mounted in an off axis enclosure (051-72) on a 250 mm OD Conflat flange fitted with a triaxial signal connector (062-2). The multiplier is

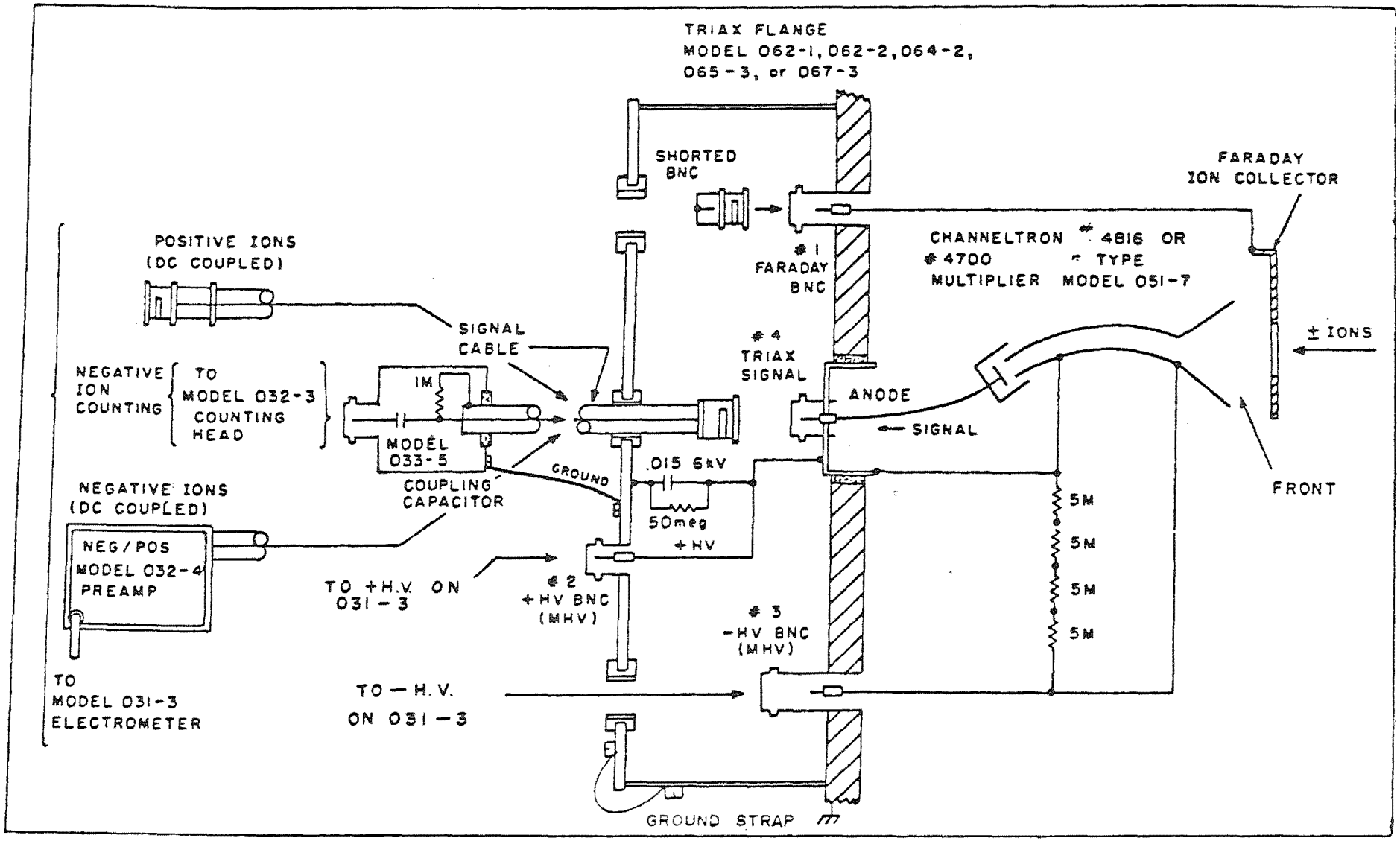

Figure 3.2 Schematic of positive and negative ion detection system

offset to avoid spurious signals due to photons and neutral particles emanating from the ion source and drift tube.

For positive ion detection a negative voltage in the range 2-2.5 kV is placed across the multiplier and the positive high voltage is set to zero. This large negative potential attracts positive ions into the multiplier and also propels the secondary electrons generated into the multiplier tube with sufficient energy to initiate an electron avalanche resulting in a signal at the anode. The pulses due to individual ions may then be passed through a coupling capacitor (033-5) into a counting preamplifier (032-3). This shapes the ion pulses into standard 5V TTL pulses and also allows noise suppression by means of a level discriminator. These pulses may then be counted by a pulse counter, a computer or converted to an instantaneous analog signal by a ratemeter (275-K2). This analog signal is input to an electrometer unit (031-3) for a meter indication. The (031-3) electrometer unit also provides the high voltage supplies for the multiplier and power supplies for the intermediate units. Alternatively, the DC current due to the electron flux at the anode can be measured directly using a preamplifier (032-4) and fed to the 031-3 electrometer.

Negative ion detection is more complicated. The front of the multiplier (cathode) must be positive relative to ground to attract negative ions and the anode of the multiplier must be positive relative to the cathode. A high positive voltage (3-3.5kV) is applied to the multiplier of which 2-2.5kV is dropped across the multiplier tube as for positive ion detection leaving a +1kV bias on the cathode. Ion signal collected at this high potential may

be input to the pulse counting circuitry as before; the coupling capacitor blocks the high DC voltage. A 032-4 preamplifier also permits direct negative ion current measurement to give a ground referenced output signal by means of internal optocoupled circuitry.

The Faraday plate surrounding the multiplier enclosure may be grounded or given a potential of ca. 70V of the same polarity as the ions to be detected to optimise the ion signal. In the case of negative ions this also serves to suppress undesirable background due to electrons which are almost invariably present.

(iv) The Drift Tube

A scale drawing of the drift tube is presented in figure 3.3. The drift tube was machined by the Physics and Engineering Laboratory of the DSIR, Petone.

The support rod (A) for the ion source is threaded; rotation of a wheel on the end of a support assembly screws the ion source in or out. A calibrated scale allows positioning to an accuracy of better than 0.1 mm. A stainless steel bellows maintains the seal between atmosphere and the drift tube interior during motion of the ion source. Unbolting of flange (E) from the main flange enables the ion source to be removed leaving the remainder of the drift tube undisturbed. The seal between flange (E) and the main flange is maintained by a gasket of 1.0 mm diameter pure tin wire. Seals between support spigot (F) and the main flange and between spigot (F) and the drift tube envelope (C) are of 0.5 mm silver wire; these seals being more susceptible to heat during bakeout of the drift tube. Although silver

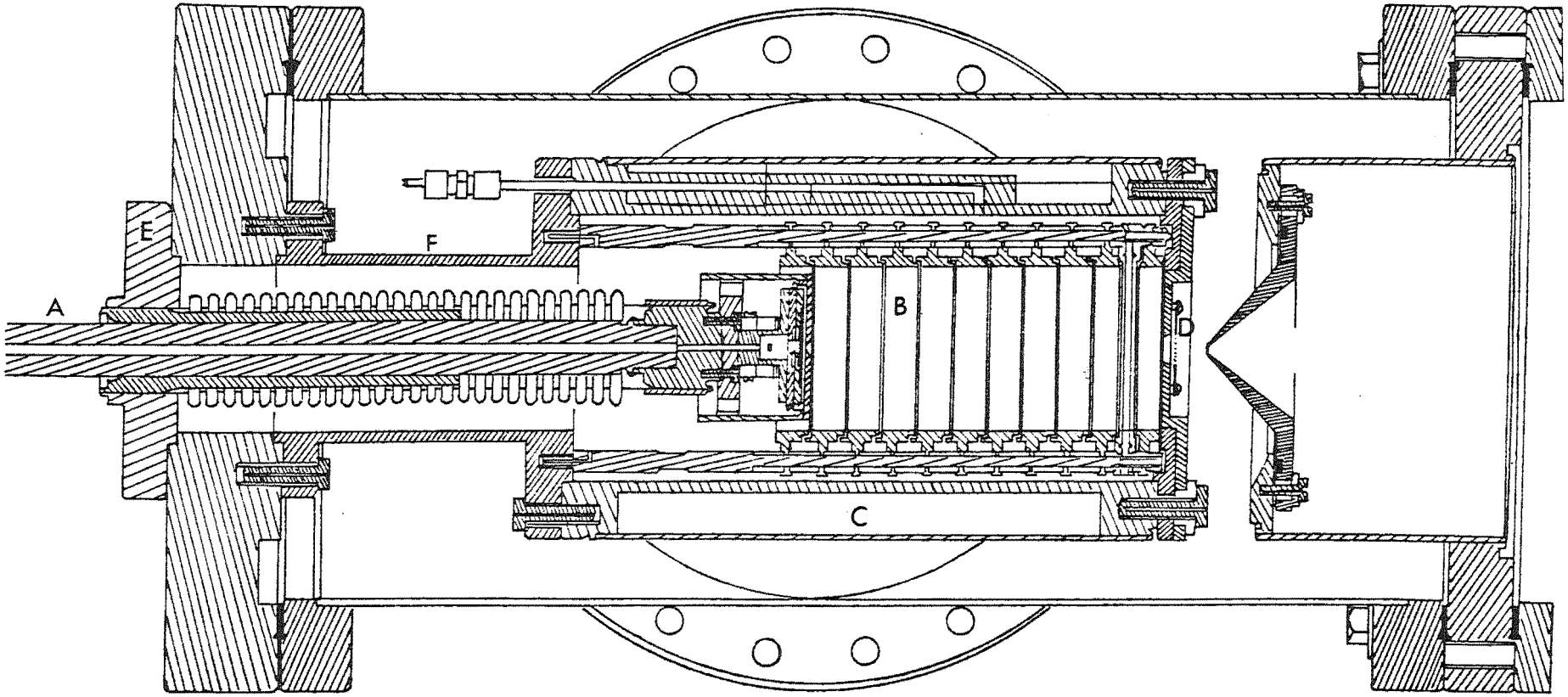

Figure 3.3 Half size scale drawing of drift tube

is harder and more difficult to join (in a circle) than gold which is customarily used for such seals it appears to be a satisfactory, more economical substitute.

The outer envelope (C) encompasses a series of channels around its entire circumference allowing the circulation of fluids for temperature control. Two embedded 145W electrical cartridge heaters enable the drift tube to be baked to 200^{o}C to outgas water vapour and other impurities. Sample admittance and pressure monitoring tubes also pass through the envelope and open into the drift tube behind the ring assembly at diametrically opposite points close to the middle drift ring. The drift tube pressure is measured using an MKS Baratron capacitance manometer (310BM-10) with a 10-Torr head. This unit has a rated accuracy of better than 0.1% and is factory calibrated against an MKS transfer standard calibrated with a CEC air deadweight tester. The pressure monitoring line provides a means of thoroughly evacuating the drift tube. The reference side of the Baratron is connected to the vacuum chamber just above the gate valve. A separate inlet channel is drilled through the support rod (A) allowing a sample to directly enter the movable ion source. This channel also provides a line-of-sight path for alignment of the whole system through to the quadrupole using a neon laser.

The ring assembly (B) is comprised of eleven 1 cm gold plated stainless steel interlocking rings of 5 cm internal diameter separated by precision ground glass ceramic insulators. The rings are interconnected by 1% tolerance 100 kΩ vacuum compatible bakeable resistors. The gold plated ion exit plate (D) is insulated from the drift tube

envelope (C) by a glass ceramic disc. The potential between the exit plate and final ring is half that between rings; this is maintained by two 100 kΩ resistors in parallel. The voltage drop (V_r) across the rings will be given by

$$V_r = 10.5\ E \qquad -(3.1)$$

where E is the electric field strength in V cm^{-1}.

Recessed into the inner side of the exit plate is a 1.5 cm diameter molybdenum disc of 0.025 cm thickness through which a conically shaped ion exit aperture of minimum diameter 0.025 cm is drilled. The exit plate is also externally fitted with a grid of 90% transmission gold plated copper electroformed mesh sandwiched between two stainless steel shims. A small bias on this grid of opposite polarity to the ions very effectively prevents passage of ions from the drift tube; by this means the ion signal can be electronically gated. The tenth and eleventh rings from the ion source end are constructed such that a similar gate may be interposed across the drift space but to date no use has been made of this facility.

Ions are formed in the movable ion source (fig.3.4) by impact of a beam of thermionically emitted electrons travelling perpendicular to the drift tube axis. The filament is spot welded onto molybdenum rods and housed in a stainless steel shield which is separated from the collision chamber by a grid and a mica heat shield. An appropriate bias on the grid enables it to be used as a control gate for the electron beam. The only filament material that proved satisfactory for use with cyanocompounds was 0.013 cm diameter iridium wire coated with barium zirconate[32] although

for other samples coated platinum ribbon was found to afford high electron emission currents. Insulation of the source from the support rod (A) is provided by a glass ceramic spacer. The ion source is equipped with an electron trap for monitoring the electron current traversing the collision chamber and a two element lens system for extracting the ions, which can also be used as an ion gate. The entire ion source is enclosed in a stainless steel sleeve which is set to a potential (V_t) which tracks its positions in the drift tube i.e.

$$V_t = Ed \qquad -(3.2)$$

where d is the distance sleeve-exit plate in cm and E the electric field strength in Vcm^{-1}.

The gas temperature in the drift tube is monitored by an iron-constantin thermocouple attached to the ninth ring (from the bellows end), a freestanding thermocouple in the space before the ring assembly and a third on the drift tube envelope. These thermocouples generally agree to within $1\text{-}2^{o}C$; this is certainly the case for temperatures close to room temperature. With the filament in operation a temperature rise of about $2^{o}C$ occurs when the ion source is positioned near the ring with a thermocouple attached although this rise rapidly reverses after repositioning of the source. The overall temperature is kept constant at ca.$20^{o}C$ by circulating water through the envelope and operating the source with the filament current as low as practicable.

The arrangement and referencing of the power supplies for the drift tube is shown in fig.3.4 for positive ions. For negative ions all voltages are reversed except those

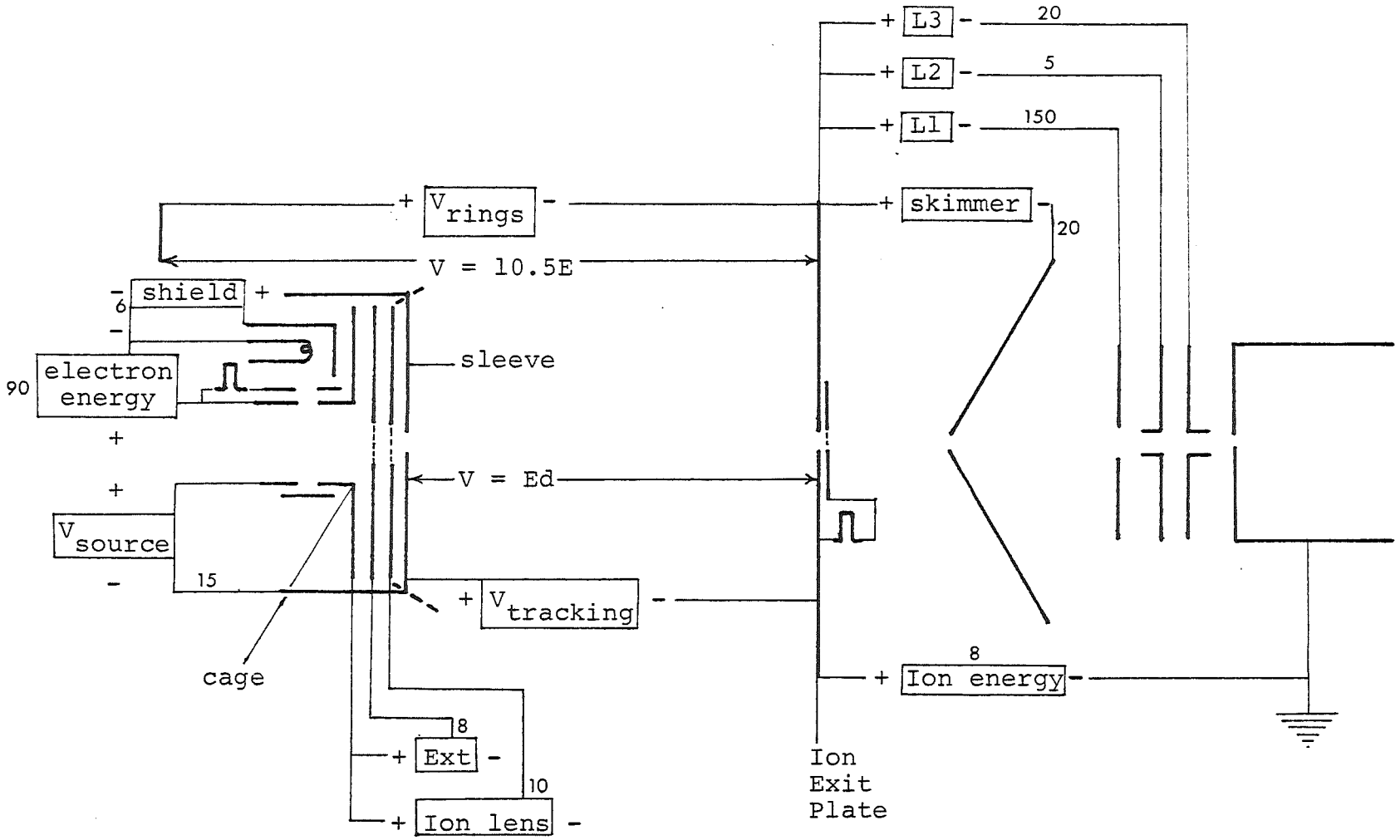

Figure 3.4 References of power supplies and schematic of ion source (for positive ions)

involved in the operation of the electron gun. Typical voltages only are given; in many experiments the actual voltages may differ considerably from those shown in fig.3.4.

The two principal voltage reference points are the ion exit plate and ion source cage. The former is held at 5-10V above ground. The ion lenses and skimmer referenced to the exit plate are then optimised for maximum ion signal. The voltage between the exit plate and ion source cage is the tracking voltage defined earlier plus an additional 10-15V across the ion source optics. The extractor and ion lens are then optimised for maximum signal; generally it is found potentials that result in a fairly uniform field along the ion source axis are best. The portion of the ion source sleeve normal to the drift tube field can be removed to release a higher flux of ions (dotted lines in fig.3.4). With this arrangement, the outer ion lens is held at the same potential as the remainder of the sleeve and the distance used to calculate the tracking voltage is taken as that between this lens element and the exit plate.

An electron energy of ca.90V proved most satisfactory; higher voltages increased the emission only marginally but resulted in a tendency to produce electrical breakdown or discharge of the sample undergoing ionization. Shield voltages slightly positive with respect to the filament resulted in optimal emission (and trap current); this presumably being due to a reduction in space charge around the filament. The referencing and operation of the pulsed gate is described later.

Voltages were measured with a Keithley 170B 3½ digit multimeter (rated accuracy 0.1% or 1 digit) or with a Datel 4½ digit panel meter. Both of these were calibrated

against a standard cell or by comparison with a Fluke 895A DC differential voltmeter. All voltages were supplied by electronically regulated power supplies with a ripple of less than 1 mV and a drift of not more than 5 mV per hour.

(v) Computer Interface

Data collection with the drift tube mass spectrometer is facilitated by interfacing to an Ohio Scientific C1P 6502 CPU based microcomputer, incorporating the factory 610 expander board, 32K of RAM and a single disk drive with OS65D V3.2 disk operating system. The basic unit has been modified using a Cegmon kit to provide a 48X32 character display and more comprehensive screen control and editing facilities. Features of the interface system relevant to drift tube experiments are shown in fig.3.5.

There are six 6821 peripheral interface adaptors (PIAs) providing twelve 8-bit I/O ports. Three of these are used to provide a 24-bit counter to register the ion pulses. Another half PIA provides two bits to reset and latch the counter and two bits to control a pulse generator described at length in the next chapter. A further two bits are combined with another half PIA to control a DAC1020 10-bit D/A converter for use as a mass programmer. The remaining two bits serve as control latches for an optocoupled 8-bit D/A converter. The interface system also incorporates two ground referenced 8-bit D/A converters, one optocoupled and one ground referenced 8-bit A/D converter and an MM58167 based real time clock interfaced via an additional PIA.

Aside from dating experiments, this real time clock is used in conjunction with two additional control bits

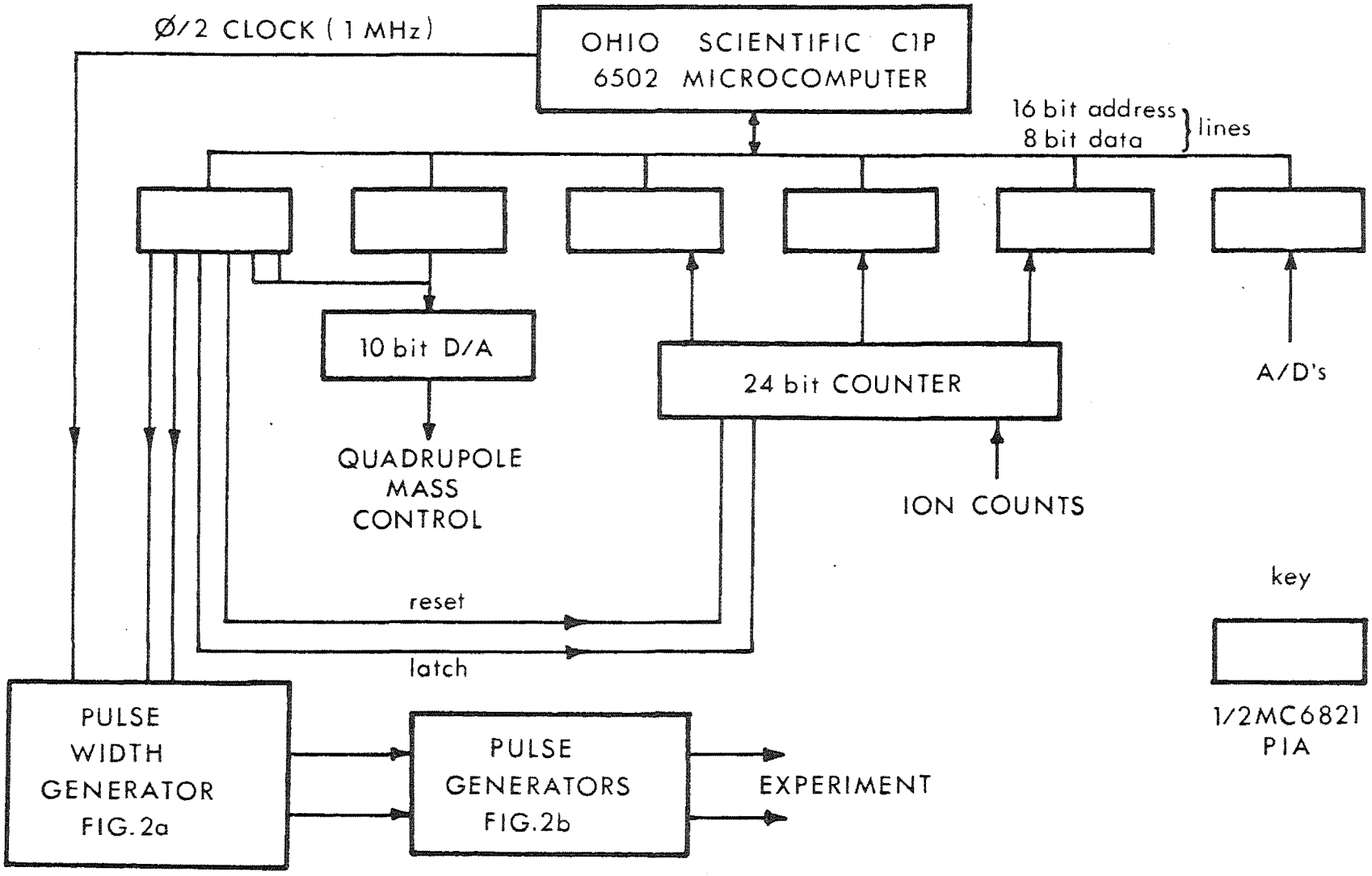

Figure 3.5 Schematic diagram of the computer interface system

supplied from PIA control registers to switch on mains powered devices via an optocoupled triac controller. This facility allows replenishment of liquid nitrogen supply to diffusion pump cold traps overnight and the shutdown of bakeout heaters to allow adequate time to recover to ambient temperature by early morning.

The linearity of the DAC1020 (rated at 0.05%) proved adequate to locate the mass peak maximum precisely with the resolution set to a more discriminating level than that required to separate individual peaks. The voltage output is converted into the 0-1 mA current required by the Extra-nuclear quadrupole control by a resistor with a 10-turn trimpot in series for very fine calibration. Three ranges may be used: a 0-200 range using the eight most significant bits, a 0-500 range employing the nine most significant bits and a 0-800 range with all ten bits specified.

(vi) Gas Handling System

A schematic diagram of the gas handling line used to transfer, purify and mix gases is given in fig.3.6. The section of the line shown as double walled is constructed from 28 mm OD glass tubing; the remainder is fabricated from 12 mm OD glass tubing. The line is evacuated by a Welch model 1402 two stage rotary pump (300 ℓmin^{-1}) aided by a CVC 2.5 cm water cooled oil diffusion pump. Liquid nitrogen traps prevent backstreaming of oil and assist removal of condensables. The ultimate pressure as measured using an ionization gauge attached to the main vacuum manifold is ca. $1X10^{-5}$ Torr. For routine applications such as the evacuation bulbs and lengths of tubing connecting

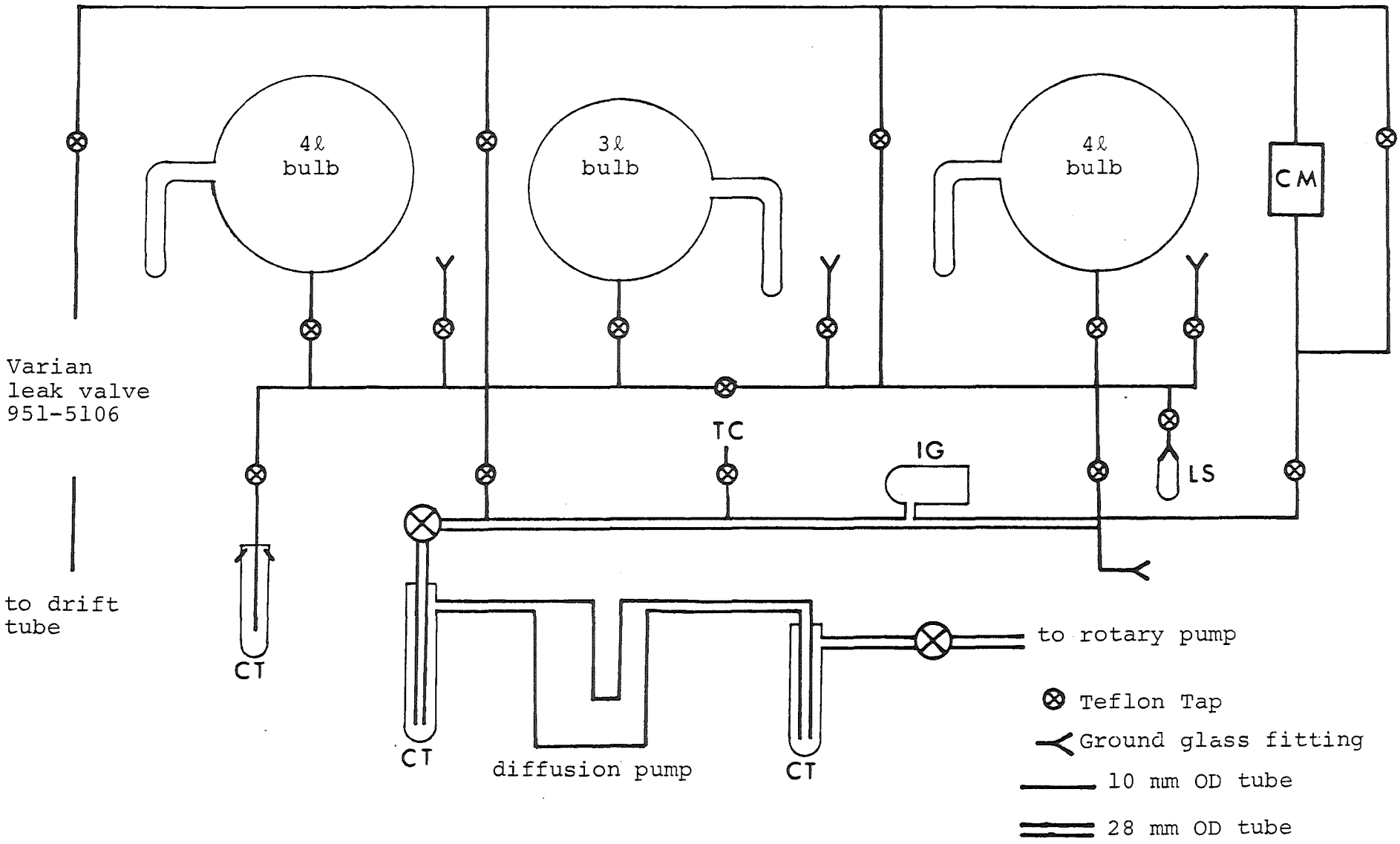

Figure 3.6 Gas handling system. IG=Ion gauge, TC=thermocouple gauge, CM=capacitance manometer, CT=cold trap, LS=Liquid sample vial.

gas cylinders to the system etc., an adequate vacuum is considered to be established when a thermocouple gauge also fitted to the main manifold returns to a zero reading ($<1X10^{-3}$ Torr).

The attached cold trap equipped bulbs and their respective connecting lines may be divided into two independant sections if desired. Each side has separate pumping lines, attachment points for additional bulbs or cylinders and a line leading to an MKS Baratron capacitance manometer for pressure measurement. This Baratron (type 221AH-A-1000) has a total pressure range of 1000 mbar and a useful resolution of ca. 0.01 mbar. One side of the system has a receptacle to which vials of liquid may be fitted so that the vapour can be obtained. A detachable cold trap forms part of the other side. This may be fitted with phosphorous pentoxide for drying or used for trap to trap distillations.

Gas mixtures are prepared as follows: the trace gas is first added to an evacuated bulb to the desired pressure (0.4-2 mbar). The bulb is then sealed and the remaining trace gas in the line is frozen back into a storage bulb or pumped away. Helium (or other buffer gas) from a cylinder is then admitted to the line to a pressure of several hundred millibars. The tap to the bulb containing the trace gas is then opened very slightly so that the helium will flow in but the trace gas is unable to diffuse out. As the helium in the line is consumed it is replenished from the cylinder. This procedure is repeated until there is no further flow of gas into the mixture bulb and the total pressure is 1000 mbar. The bulb is then sealed and the

helium remaining in the line pumped away. Mixtures are left to mix for a few hours before use to ensure homogeneity. Mass spectra were recorded to assess mixture purity.

Samples of gas mixtures are admitted to the drift tube via a Varian variable leak valve (951-5106). Throughout an experiment the leak valve must be progressively opened to compensate for the diminishing pressure of gas from the storage bulb. Small manual adjustments every few minutes readily enables the drift tube pressure to be maintained constant to within $\pm 0.05\%$.

(vii) Materials

The helium gas used for the buffer in almost all experiments was commercial scientific grade with a purity of >99.995%. No impurities could be detected using the drift tube mass spectrometer that could have unambiguously originated from this helium.

Hydrogen cyanide (HCN) was prepared by the reaction of concentrated sulphuric acid on sodium cyanide using a vacuum line. The crude product was dried over phosphorus pentoxide prior to repeated vacuum distillation.

Dicyanogen (C_2N_2) was distilled from Matheson technical grade product. Cyanogen chloride (CNCl) was prepared by the reaction of chlorine gas on sodium cyanide.[33]

Methyl cyanide (CH_3CN) and ethylene oxide ($\overline{CH_2CH_2O}$) were vacuum distilled from BDH reagent grade and ethanol (C_2H_5OH) from spectroscopic grade. Cyclopropane ($\overline{CH_2CH_2CH_2}$) was obtained from a cylinder of medical grade product.

Propene (CH_3-CH=CH_2) was prepared by dehydration of

isopropanol with concentrated phosphoric acid at 260°C. Dimethyl ether (CH_3OCH_3) was synthesised by the reaction of concentrated sulphuric acid with methanol at 135°C. Methyl isocyanide (CH_3NC) was prepared by the reaction of silver cyanide with methyl iodide.[34] No traces of isomeric CH_3CN were detected using infra-red spectroscopy.

All compounds were purged of air using freeze-thaw cycles with liquid nitrogen. Traces of water detected mass spectrometrically were removed by condensation onto phosphorus pentoxide where possible. Since these compounds were only present as <.2% of the total mixture, the presence of small amounts of impurities would not be expected to be troublesome. This was indeed the case; the major problem of contamination being outgassing within the drift tube and outgassing and small leaks into the gas handling line.

CHAPTER 4

EXPERIMENTAL PROCEDURE

(i) Experimental Requirements

All of the information required to evaluate mobilities, diffusion coefficients and reaction rate coefficients can in principle be obtained by measurement of a spectrum of ion transit times or arrival time distribution (ATD) for the ion or ions involved. Two facilities must be available to determine an ATD; the production of bursts or pulses of ions and selective temporal sensitization of the detector with respect to the ion pulses. The pulsing techniques should eliminate at least 99% of the signal during the off period to prevent the appearance of an unacceptably large background.

There are two methods of pulsing the ion beam with the present instrument; either the ion beam may be pulsed or the electron beam. There are also two methods of pulsing the detector on; the exit plate grid may be pulsed or the TTL signal pulses from the discriminator may be gated.

The ion beam leaving the ion source may be controlled by use of the two lens elements located between the collision chamber (cage) and outer sleeve of the source. These lens elements are fitted with 90% transmission gold plated electroformed copper mesh to reduce peakthrough of extraneous potentials into the source. The effects produced by either of these grids independantly or of both at the same potential are very similar. For positive ions

maximum transmission occurs for voltages about two-thirds the cage-sleeve voltage. Setting the cage-lens voltage more negative than this then reduces the signal until ca. -30V when the signal begins to rise continuously. Minimum ion transmission occurs when the cage-lens voltage is ca. +5V. This minimum, however, is still 5-10% of the maximum signal so the degree of cutoff of this gating system is inadequate. Penning ionization from metastable 2^3S He atoms which are unaffected by the grids may well contribute to this background (see later). Increasingly positive cage-lens voltages resulted in a corresponding increase in ion signal presumably due to transmission of electrons through the source and formation of ions in the drift tube. Many combinations of lens element potentials and biases were examined but none could be found that satisfactorily alleviated the above problems. With negative ions a continual background of electrons contaminated the ion signal which could not readily be suppressed.

To circumvent such difficulties with the ion beam pulsing technique, a method of pulsing the electron beam was developed. Obviously, the thermal inertia of the filament makes switching this on and off impracticable on a microsecond time scale. A stainless steel plate with an aperture slightly smaller than that of the ion source cage was interposed between cage and filament. To block electrons this plate was held at a potential 10V more negative than the filament-cage voltage (eg -100V for -90V electron energy). Switching the plate to the cage potential by the application of a positive going pulse resulted in transmission of electrons. No leakage or background was ever apparent with

this configuration.

A variable delay after the ion source pulse,the grid on the exit plate is biased to transmit ions. In the off state this grid is held at +15V above ground to block positive ion transmission. Since the exit plate is at a potential of +5 to 10V above ground the effective blocking bias is +10 to 5V; the higher bias (lower ion energy) being necessary to completely block ions drifting at high E/N (>100 Td). To transmit ions the exit grid is pulsed to ground potential. This also provides a small ion drawout voltage yielding a much larger ion signal than is obtained when the grid is simply pulsed to the exit plate potential.

Alternatively, the exit plate grid is biased to transmit ions continuously and the TTL pulses (counts) from the discriminator are then fed to a two input AND gate. The second input of this AND gate is set high a variable time after the ion source pulse. Only in this condition can pulses be transmitted. Serious disadvantages of this technique are that the exit plate to detector time can only be found by extrapolation of a plot of total ion flight times for a range of drift distances and that the ion signal may undergo an unpredictable broadening effect during transit of the quadrupole and associated ion optics. Another drawback is the increased dead time between ion source pulses and the decrease in the accumulated ion signal resulting from the reduced repetition rate of the pulsing cycle.

The criterion by which the various pulsing techniques were judged effective was that the ion signal should be linear with respect to the width of the pulse. Furthermore,

this line should pass through the origin, indicating no leakage.

(ii) The program PULSE and associated circuitry

The triggering and synchronization of the pulses and the collection of ion counts is controlled entirely by the computer using the program PULSE. The complete BASIC program and the 6502 assembler listing for the machine language subroutine are given in Appendix B. A documented source code listing useful for explaining the operation of the program is given in fig.4.1. Three computer outputs are necessary, the 1 MHz clock, a pulse to reset the system at the start of each cycle and trigger the first output pulse and a delayed pulse to enable the second output pulse.

The first computer pulse is active when high but the second is normally held high and is active when low. These pulses correspond to bits 7 and 6 respectively of the PIA located at address $E30A ($=hexadecimal; the least significant bit of the PIA is bit 0). The first part of the program (lines 50-70) initializes the cycle counter to zero. Next (lines 80-90) the ion counter is reset by setting bit 4 of the same PIA high. The PIA is then restored to the inactive condition (7lo, 6hi; lines 100-110) and this value remains in the accumulator. The X-register is next loaded with the value for the first pulse active only (7hi, 6hi; line 120). The Y-register is similarly loaded with the value for the second pulse active only (7lo, 6lo; line 130).

When first loaded from disk the object code (machine

```
 10          *= $6000
 20          P2B=$E30A      ;6821 PIA  Bit7=1st pulse
 30          CR= $E30B      ;          Bit6=2nd pulse
 40          V = $48        ;No. of cycles (16 bit)
 50 INIT     LDA #0         ;Initialize cycle count
 60          STA V
 70          STA V+1
 80          LDA #%01010000    ;Reset ion count(bit4 HI)
 90          STA P2B
100          LDA #%01000000    ;Both pulses inactive
110          STA P2B
120          LDX #%11000000    ;1st pulse active (HI)
130          LDY #%00000000    ;2nd pulse active (LO)
140 PULSE    STX P2B      ;RESET system & start 1st 4017
150          STA P2B
160          NOP          ;PHA for ODD times
170           ;
180           ;
190          NOP
200          STY P2B      ;Enable 2nd 4017 for 10us
210          NOP          ;This section of code moved
220          NOP          ;by BASIC calling program
230          NOP
240          STA P2B
250          NOP
260           ;
270           ;
280          NOP
290          JMP DLYEND     ;Maximum time (POKEd in from
300          NOP            ;               BASIC program)
310           ;
320           ;
330          NOP
340 DLYEND   PHA          ;NOP for ODD times
350          PLA
360          CLC
370          LDA V
380          ADC #1       ;Increment no. of cycles
390          STA V
400          LDA V+1
410          ADC #0
420          STA V+1
430          CMP #$FF     ;Data POKEd here from BASIC
440          BEQ NEXT
450          LDA #%01000000   ;Both OFF state
460          JMP PULSE
470 NEXT     LDA #%01100000   ;Latch ion count (bit5 HI)
480          STA P2B
490          LDA #$90
500          STA P2B
510          RTS
```

Figure 4.1 Documented 6502 assembly language listing for PULSE

language instructions) corresponding to the source code of fig.4.1 contains only 200 NOP (No Operation) instructions between lines 160-330. The opcodes (hexadecimal code values) corresponding to lines 200-240 are then POKEd into memory by the BASIC calling program at the location determined by the response to a "minimum time" input. The absolute minimum time is 6 μs since 4 μs is required for the 6502 microprocessor to execute line 200 to start the second pulse and there must be at least one NOP instruction (2 μs). Each NOP instruction between lines 150 and 200 increases the time between pulses by 2 μs. After the second pulse is disabled (line 240) another series of NOPs fills in time until a JMP instruction at line 290 enacts a jump to the cycle counting routine. This JMP instruction corresponds to the maximum time required between pulses and is inserted by the BASIC calling program.

Lines 360-420 add one to the 16-bit counter formed by V and V+1. The eight most significant bits (V+1) are then compared to a value POKEd from the BASIC program calculated from the response to a "sample time per point" request. If cycling is not completed the accumulator is restored to the both off value (line 450) and the pulsing repeated. When cycling is completed the ion counts are latched through to the counter PIAs and control returned to BASIC.

The BASIC program then overwrites lines 200-240 with NOP instructions. At the next time interval specified in the BASIC program these lines are then POKEd back into the code e.g. two memory locations later (2NOPs) for a 4 μs step. For odd times or 1 μs steps the first NOP (line 160) is replaced by a PHA (PusH Accumulator) instruction which

takes 3 μs to be executed. The PHA at line 340 is then replaced with a NOP so that the PHA instruction is not executed twice and the total time of each cycle is the same as for a cycle with an even number of microseconds between pulses. The effects of the PHA are reversed by the PLA (PulL Accumulator) instruction at line 350. This sequence of events is repeated until the maximum time between pulses is attained at which stage there are no NOP instructions between lines 240 and 290. The whole sequence from minimum to maximum time may be repeated for a preselected number of scans in order to obtain a more significant accumulation of ion counts.

The computer pulses are converted into the drift tube pulses used experimentally by the circuitry of fig.4.2. This circuitry controls the width and height of the pulses and provides isolation so that the pulses are floatable to any required reference voltage.

The pulse widths are selected in 1 μs steps by means of 4017 decade counters. These devices have ten outputs which sequentially go high in response to clock pulses at pin 14 provided the reset (pin 15) and enable (pin 13) are low. At the start of each cycle both 4017 counters are reset by bit 7 on the PIA going high. On the next clock pulse (one every microsecond) count 1 of the first (top in fig.4.2) 4017 goes high. This provides the start time for the first pulse. The other eight count outputs and the carry are connected to a thumbwheel switch which is rotated so that the stop pulse occurs after the required number of microsecond counts. After count 9 is reached the carry is set high (by the 4017) and the count returns to zero. As evident in the circuit of fig.4.2a, however, the carry is

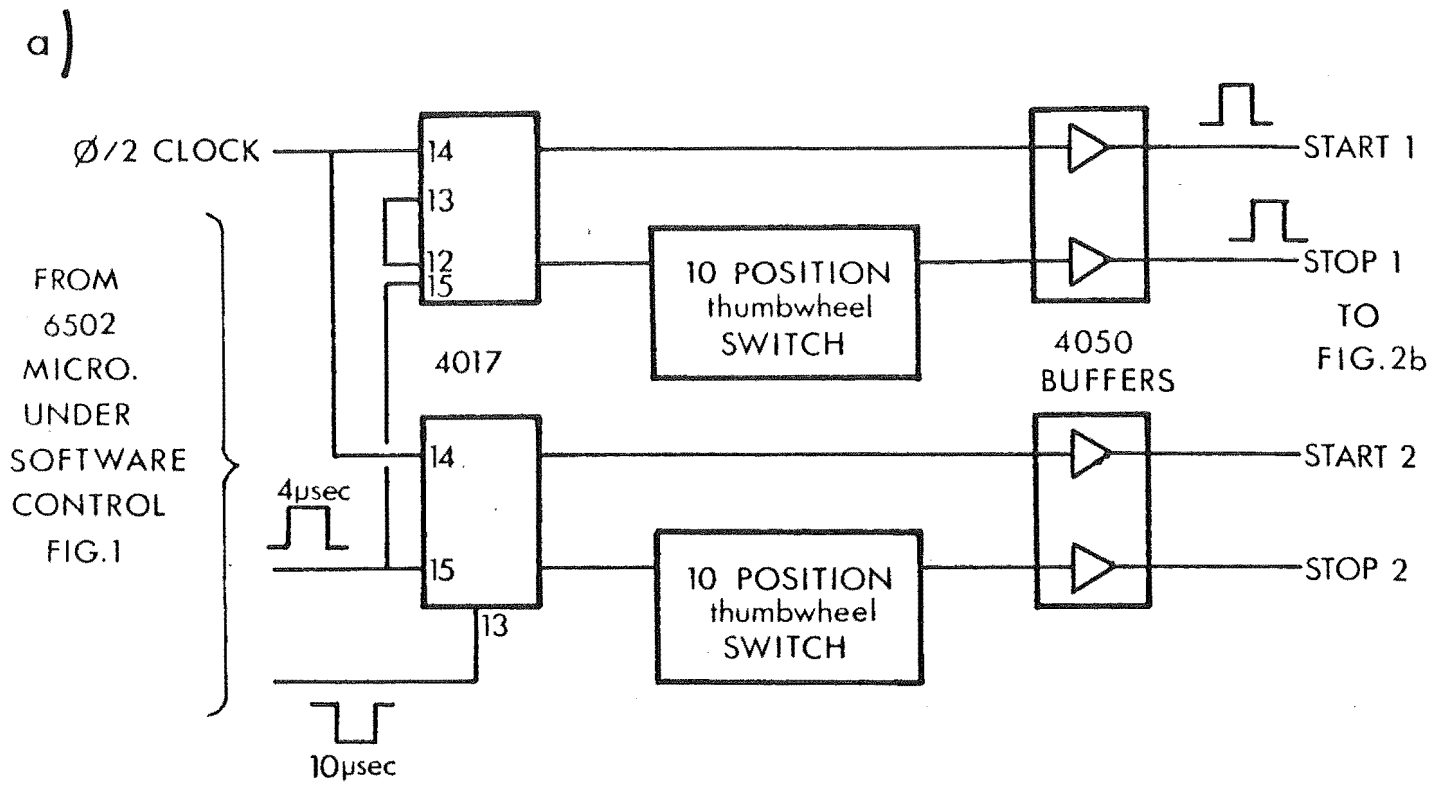

4017 DECADE COUNTER : 12 CARRY ; 13 ENABLE ; 14 CLOCK ; 15 RESET

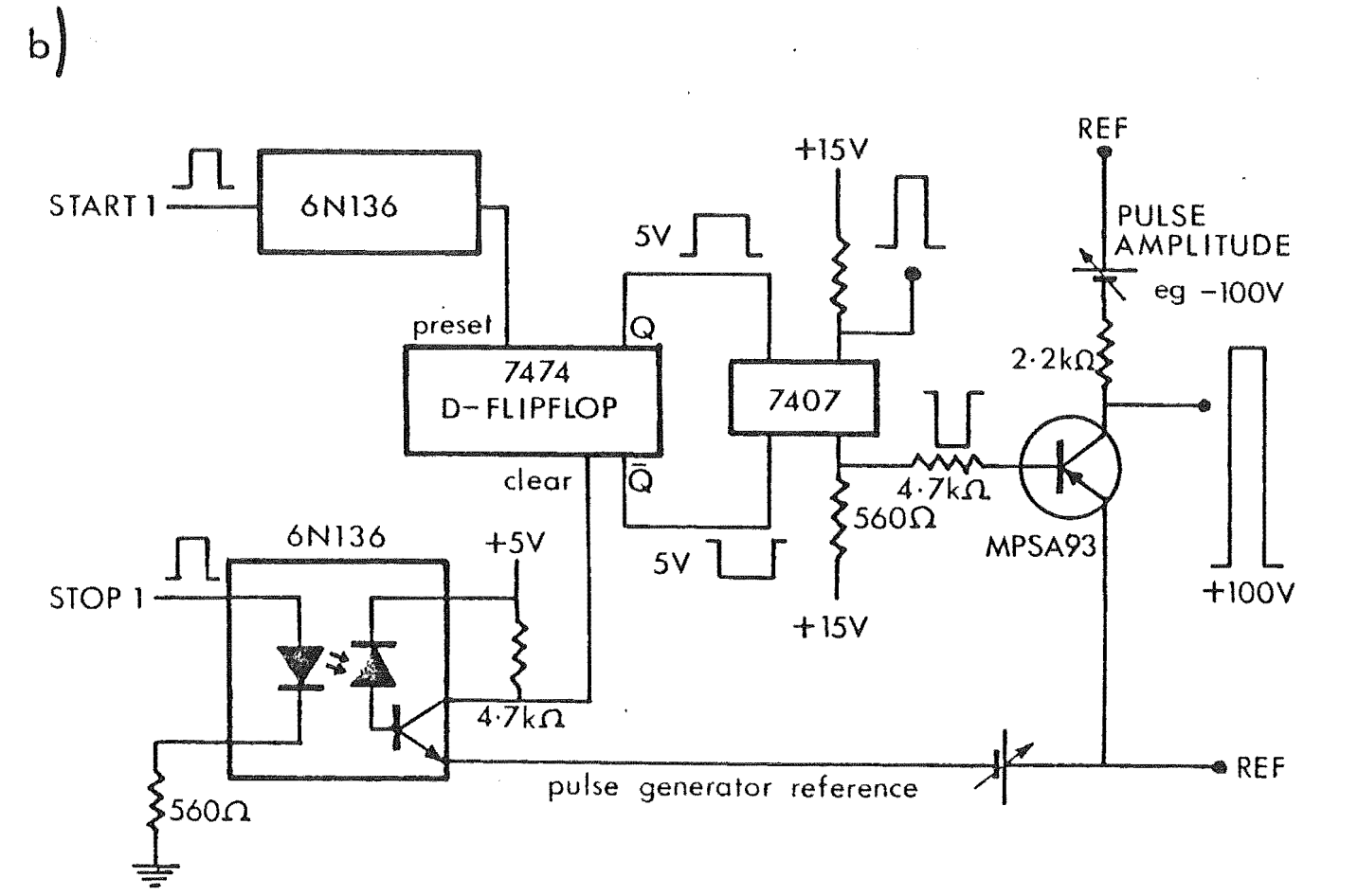

Figure 4.2 Pulse width selector and amplifier circuits

connected to the enable. The enable is therefore set high (disabled) after ten counts and no further action occurs until the 4017 is reset again. The second (lower) 4017 counter is reset simultaneously with the first but is not enabled until bit 6 of the PIA goes low. Start and stop pulses are then output as previously described; further counting is prevented by the computer disabling the 4017 after 10 μs.

The start and stop pulse from each 4017 are input through optocouplers to the preset and clear of a 7474 D-flipflop. These edge triggered devices have an output (Q) that goes high when the preset is pulsed high and remains high until the clear is pulsed high. A complementary (reverse logic) output ($\bar{Q}$) is also available. By this means either positive or negative going pulses may be produced of width equal to the time between the start and stop pulses from the 4017 circuitry. The Q and $\bar{Q}$ outputs from the 7474 flipflops are amplified to 15V by 7407 buffers. The ion source pulse is further amplified up to 200V by the circuit shown in fig.4.2b. REF is the ion source cage potential; the variable transistor (pulse generator reference) bias is necessary to produce sharp square wave pulses over a wide amplitude range.

(iii) Calculation of Arrival Time Distributions

The interpretation of an experimental arrival time distribution (ATD) is aided considerably by comparison with a calculated distribution. The equations for calculation of an ATD are obtained by solving the transport equation

relevant to the apparatus used in the experiment. For an accurate representation, the transport equation should contain terms for longitudinal and transverse diffusion and allow for reaction. Numerous solutions for primary ions are available in the literature for various types of drift tubes; some of these papers also derive expressions for secondary ions.[35,36] A general solution applicable to any type of drift tube has been derived by Woo and Whealton[3] which takes into account all the abovementioned factors and provides expressions for both primary and secondary ions. The expression for primary ions to be used here is that derived for the Georgia Institute of Technology drift tube (McDaniel et al)[37,5d] which is constructed and operated in a similar manner to the present instrument. This analysis has been extended to secondary ions by Snuggs et al.[2]

A drift velocity may be determined by treating it as a parameter that is varied until the best agreement between the experimental and calculated arrival time distributions is obtained. A simpler procedure used by many workers is simply to take the position of the arrival time maximum and consider the remainder of the distribution to be symmetrical. As will be demonstrated later this process can lead to serious errors if only data for a single drift distance is considered. Even when a drift velocity is obtained by comparison of a single experimental and a calculated ATD the result may be considerably in error due to "end effects".[5c,6] These end effects arise from perturbations to the uniform axial field of the drift tube by penetration of potentials used in the ion source and ion extraction and detection

systems. For example, a recent measurement of the mobility of NH_2^+ in helium using a drift tube with a fixed path length of 11 cm noted a 10% discrepancy from an earlier result by the same workers using a fixed drift path of 5.65 cm.[38,39] Similar discrepancies are evident for the mobility of Cl^- in nitrogen where values from a fixed drift path drift tube cell[40] and a drift-SIFT apparatus lie outside their combined uncertainties.[41]

Errors arising from end effects are readily eliminated with a movable ion source instrument measuring arrival time distributions for a series of different distances, preferably over as wide a range as possible. The drift velocity may then be taken as the slope of a plot of the mean or modal arrival time as a function of drift distance. It will invariably be found that a best-fit line through such a plot will not pass through the origin. This method of determining drift velocity as the slope of a plot of arrival time versus distance has been used for the present work. The time taken is that of maximum ion signal. This precludes the need for a detailed fit by comparison with a calculated profile for every distribution measured. An analysis of the errors expected to arise from simply using the maximum is now presented for both primary and secondary ions.

The flux of primary ions passing through the axial drift tube exit aperture of area a as a function of time t and drift distance z is given by[37,5d]

$$I_A(z,t)=\frac{sa}{4(\pi D_L t)^{\frac{1}{2}}}\left(v_d+\frac{z}{t}\right)\exp\left[-\alpha t-\frac{(z-v_d t)^2}{4D_L t}\right]\left[1-\exp\left(\frac{-r_o^2}{4D_T t}\right)\right] \qquad -(4.1)$$

All the ions are assumed to be introduced as a delta function burst with initial uniform surface density s through the ion entrance aperture of radius r_o. No ions are produced by reaction in the drift space although some are lost by reaction with frequency $\alpha (=kN_r$ where k is a second order rate coefficient and N_r is the number density of the neutral species undergoing reaction). The longitudinal and transverse diffusion coefficients, D_L and D_T may be estimated using the generalized Einstein relationships: Eq 2.7 and 2.8. Equation 4.1 is used by the program DRIFT listed in Appendix B to calculate primary ion arrival time distributions. DRIFT accurately determines the maximum of the model ATD by a bisection type iterative algorithm.

The arrival time of maximum signal was calculated for a range of distances for a primary ion of m/z=26 drifting in helium in the absence of any depleting reaction (α=0). Conditions were T=20^{o}C, E/N=80Td and K_o=13.0 $cm^2V^{-1}s^{-1}$. The results for two pressures of 0.1 Torr and 0.4 Torr are given in Table 4.1. The quantity $\Delta T/\Delta d$ is calculated as the difference between successive values of T_{max} in the table divided by the change in distance e.g. for z=7, $\Delta T/\Delta d=(24.729-21.155)/(7-6)=3.574$. For the first entry T_{max}=0 for z=0 is used. This quantity will be constant for a straight line.

It is apparent from Table 4.1 that a plot of T_{max} as a function of z would not be truly linear for the results at 0.1 Torr and for the distances less than about 3 cm at 0.4 Torr. The slope of the line from 3 cm onwards of the 0.4 Torr results corresponds to a drift velocity of $2.797X10^5$cm s^{-1} which gives the correct value for K_o of

Table 4.1 Calculated arrival time distribution maxima for primary ions not depleted by reaction. See text for details.

z(cm)	T_{max}(μs) @0.1 Torr	ΔT/Δd	T_{max}(μs) @0.4 Torr	ΔT/Δd
0.1	0.070	0.70	0.221	2.21
0.25	0.306	1.577	0.694	3.153
0.5	0.932	2.504	1.541	3.388
0.75	1.705	3.092	2.416	3.500
1	2.533	3.312	3.299	3.532
2	6.010	3.477	6.860	3.561
3	9.554	3.544	10.431	3.571
4	13.115	3.561	14.004	3.573
5	16.682	3.567	17.579	3.575
6	20.252	3.570	21.155	3.576
7	23.824	3.572	24.729	3.574
8	27.396	3.572	28.306	3.577
9	30.971	3.575	31.883	3.577
10	34.546	3.575	35.458	3.575
20	70.301	3.576	71.222	3.576

13.00 $cm^2V^{-1}s^{-1}$. The intercept of this line is -0.08 cm. Taking the single point at 9 cm (longest possible distance for the drift tube described in this thesis) yields v_d= $2.822X10^5$ cms^{-1} or K_o=13.12 $cm^2V^{-1}s^{-1}$ i.e. an error of ca.1.2%. The 0.1 Torr results give v_d=$2.801X10^5$ cms^{-1} and K_o=13.02 $cm^2V^{-1}s^{-1}$; a fairly insignificant error. Taking the 0.1 Torr value at 9 cm of 30.971 μs gives v_d=2.906 cms^{-1} or K_o=13.51 $cm^2V^{-1}s^{-1}$, a result 4% too high. Therefore, measuring the time of maximum ion signal over a range of distance should give the correct mobility provided data for the shorter distances are ignored. With a single point determination a serious error can result, particularly at low pressures but this error would probably be less significant than that due to end effects.

Consider now the case of a primary ion undergoing a depleting reaction. All conditions are the same as previously (pressure=0.4 Torr) except there is now 0.2% of a reactant gas added to the helium buffer with which the primary ions react at a rate of $3X10^{-9}$ $cm^3molec^{-1}s^{-1}$. This corresponds to a collision frequency, α=79100 s^{-1}, or a mean ion lifetime ($1/\alpha$) of 12.6 μs. Almost 90% of the primary ions will be lost during transit of the drift tube. The calculated arrival time maxima are shown in Table 4.2 for a range of distances.

Table 4.2 Calculated arrival time distribution maxima for a primary ion swarm rapidly attenuated by reaction (α= 79100 s^{-1}). See text for details.

z(cm)	T_{max}(μs)	ΔT/Δd
0.1	0.219	2.19
0.25	0.688	3.127
0.5	1.525	3.348
0.75	2.389	3.456
1	3.263	3.496
2	6.781	3.518
3	10.308	3.527
4	13.839	3.531
5	17.371	3.532
6	20.904	3.533
7	24.436	3.532
8	27.969	3.533
9	31.503	3.534
10	35.035	3.532
20	70.369	3.533
30	105.704	3.534

Comparison with Table 4.1 reveals a consistent decrease in the time of maximum signal which is proportional to

distance. This is an intuitively reasonable result since a greater proportion of the later arriving ions will be depleted by reaction. Again ignoring the values for z<4 cm, a z-t plot gives $v_d=2.831X10^5$ cms^{-1} or $K_0=13.15$ $cm^2V^{-1}s^{-1}$ with an intercept of -0.082 cm. So a fairly rapid reaction rate gives rise to an error of only 1.2% in the mobility of a primary ion.

In conclusion, by collecting data for primary ions in a relatively high pressure of uncontaminated buffer, it is possible to obtain correct mobilities from the slope of a plot of arrival time distribution maxima as a function of distance, provided some discretion is exercised over the inclusion of data for short distances.

The flux through an axial aperture of secondary ions B produced by reaction from primary ions A during transit of the drift tube is given by[2]:

$$I_B(z,t)=sa\alpha_A\int_o^t(\pi b_A)^{-\frac{1}{2}}\left[\frac{2D_{LB}(z-c_A)}{b_A}+v_{dB}\right]X$$

$$\exp\left[-dA-\frac{(z-c_A)^2}{b_A}\right]\left[1-\exp\left(\frac{-r_o^2}{a_A}\right)\right]du \qquad -(4.2)$$

where $a_A = 4D_{TA}t-4(D_{TA}-D_{TB})u$ -(4.3)

$b_A = 4D_{LA}t-4(D_{LA}-D_{LB})u$ -(4.4)

$c_A = v_{dA}t-(v_{dA}-v_{dB})u$ -(4.5)

$d_A = \alpha_A t-(\alpha_A-\alpha_B)u$ -(4.6)

All other symbols have the same meaning as for Eq(4.1). D_{TA}, D_{TB} refer to the transverse diffusion coefficients for

ion A and ion B respectively and so on. The reaction frequency α_A is that for reaction of primary ion A to secondary ion B and α_B refers to the depleting reaction of ion B to form other unspecified product ions. Secondary ion arrival time distributions were computed using the program DRIFT2 listed in Appendix B. This program is essentially an extended version of the program DRIFT for primary ions. The integration is calculated numerically using Simpson's rule with $\left[\frac{1}{4}(\text{time(T) in microseconds})+20\right]$ steps.

Simulations were performed for He^+ primary ions drifting in helium reacting to form secondary ions B^+ of m/z=26. Other conditions used were T=20^{o}C, P=0.4 Torr and E/N=80Td. The mobility of He^+ at 80Td was taken as[13] 8.12 $cm^2V^{-1}s^{-1}$ and the mobility of B^+ was set to 16.5 $cm^2V^{-1}s^{-1}$. The rate coefficient for the reaction $He^+ + B \rightarrow B^+ + He$ was set at $4X10^{-9}$ $cm^3molec^{-1}s^{-1}$. First, results were calculated assuming no additional reaction of B^+ to form tertiary ions. These are given in Table 4.3 for 0.1% and 0.2% mixtures of B in helium.

Clearly, the times of ion signal maximum for short distances are much longer than those expected by extrapolation of the times for longer distances. This reflects the fact that the B^+ ion has spent a significant proportion of the transit time as the slower moving He^+ ion. As the extent of reaction is increased, the data becomes more representative of the mobility of the faster B^+ ion. A least squares fit of the data for 4<z<10 cm gives for the 0.1% mixture: $v_d=3.439X10^5$ cms^{-1}; $K_o=15.98$ $cm^2V^{-1}s^{-1}$ and for the 0.2% mixture $v_d=3.466X10^5$ cms^{-1}; $K_o=16.10$ $cm^2V^{-1}s^{-1}$. This

Table 4.3 Arrival time maxima for secondary ions B^+ formed by reaction from He^+ and not undergoing subsequent reaction. See text for details.

z(cm)	0.1% B		0.2% B	
	T_{max}(μs)	ΔT/Δd	T_{max}(μs)	ΔT/Δd
1	4.382	4.382	4.177	4.177
2	8.568	4.186	7.353	3.176
4	14.062	2.747	13.183	2.915
6	19.867	2.903	18.98	2.899
8	25.687	2.910	24.749	2.885
10	31.492	2.903	30.497	2.874
20	60.299	2.881	59.051	2.855
40	117.414	2.856	115.803	2.838

represents an error of -3.2% for the 0.1% mixture and an error of -2.4% for the 0.2% mixture. Note that the depletion of the primary ion (He^+) swarm by reaction with impurities will have the same effect on the position of the secondary ion arrival time maximum as reaction with the added trace gas B, although of course the B^+ signal will be smaller. With reference to Eq.(4.2) the α_A value preceding the integration will be the frequency of formation of B^+ but the value of α_A used to compute d_A(Eq.4.6) will be that for depletion of He^+.

Further calculations were performed for a system identical to that described earlier for the calculation of Table 4.3 except that now the secondary ion swarm (B^+) reacts further with trace neutral B to form unspecified tertiary products. The rate coefficient used for this second reaction is $2.5X10^{-9}cm^3molec^{-1}s^{-1}$ and the results are shown in Table 4.4

Table 4.4 Arrival time maxima for secondary ions undergoing further reaction. See text for details.

z(cm)	0.1% B		0.2% B	
	T_{max}	$\Delta T/\Delta d$	T_{max}	$\Delta T/\Delta d$
1	4.424	4.424	4.273	4.273
2	9.121	4.697	7.722	3.449
4	14.676	2.778	13.440	2.859
6	20.322	2.823	19.196	2.878
8	26.099	2.889	24.930	2.867
10	31.882	2.892	30.641	2.840
20	60.640	2.876	58.992	2.835
40	117.617	2.849	115.244	2.813

Comparison with Table 4.3 reveals that the arrival time maxima appear at later times. This result is to be expected since the earlier formed secondary ions will suffer more severe attenuation by reaction. Table 4.5 lists mobilities derived from linear regression of selected ranges

Table 4.5 Mobilities calculated from data of Table 4.4.

z range (cm)	% mixture	intercept (cm)	v_d $X10^5 cms^{-1}$	K_o $cm^2V^{-1}s^{-1}$	error %
4-10	0.1	-1.100	3.485	16.19	-1.9
4-10	0.2	-0.692	3.488	16.21	-1.8
10-40	0.1	-1.188	3.500	16.27	-1.4
10-40	0.2	-0.892	3.547	16.48	-0.1

of data. Again, the mobilities found are too low but by a lesser amount than was found with no further reaction; the error now is unlikely to exceed 2%. It is evident from the intercepts that determination of a mobility from the maximum of a single arrival time distribution would lead to a result very seriously in error.

(iv) Consideration of further sources of error

In view of the above analysis, it might be naively suggested that the mole fraction of the trace reactant gas be increased somewhat in order to minimize the error of the secondary ion mobility. Another error of greater magnitude soon becomes apparent, however. The mobilities measured will be those characteristic of the mixture of trace gas and helium, not of pure helium, and should be reported as such. The deviation of mixture mobility from mobility in pure helium may be estimated at low field using Blanc's Law (Eq.2.9) reformulated here for the case of a two-component buffer:

$$K_{mix} = \frac{K_{He}K_B}{(1-x)K_B+xK_{He}} \qquad -(4.7)$$

where x is the mole fraction of reactant gas B and K_{He} and K_B are the mobilities of an ion in pure helium and pure B respectively. Figure 4.3 depicts the deviation of K_{mix} from K_{He} calculated by Eq.(4.7) for three different systems. The extent of deviation for a small mole fraction of reactant gas is larger than might be intuitively anticipated. The mobilities used[13,14] are listed in the accompanying table. Mobilities of ions in their parent gases are generally lower than expected by comparison with other ions of equivalent mass, perhaps the most notable example being the low mobility of He^+ in helium. This is due to the predominance of resonant charge transfer as the ion-neutral interaction mechanism. From fig.4.3 it is apparent that a mole fraction of reactant gas exceeding 0.2% could well result in a mobility error greater than that predicted above.

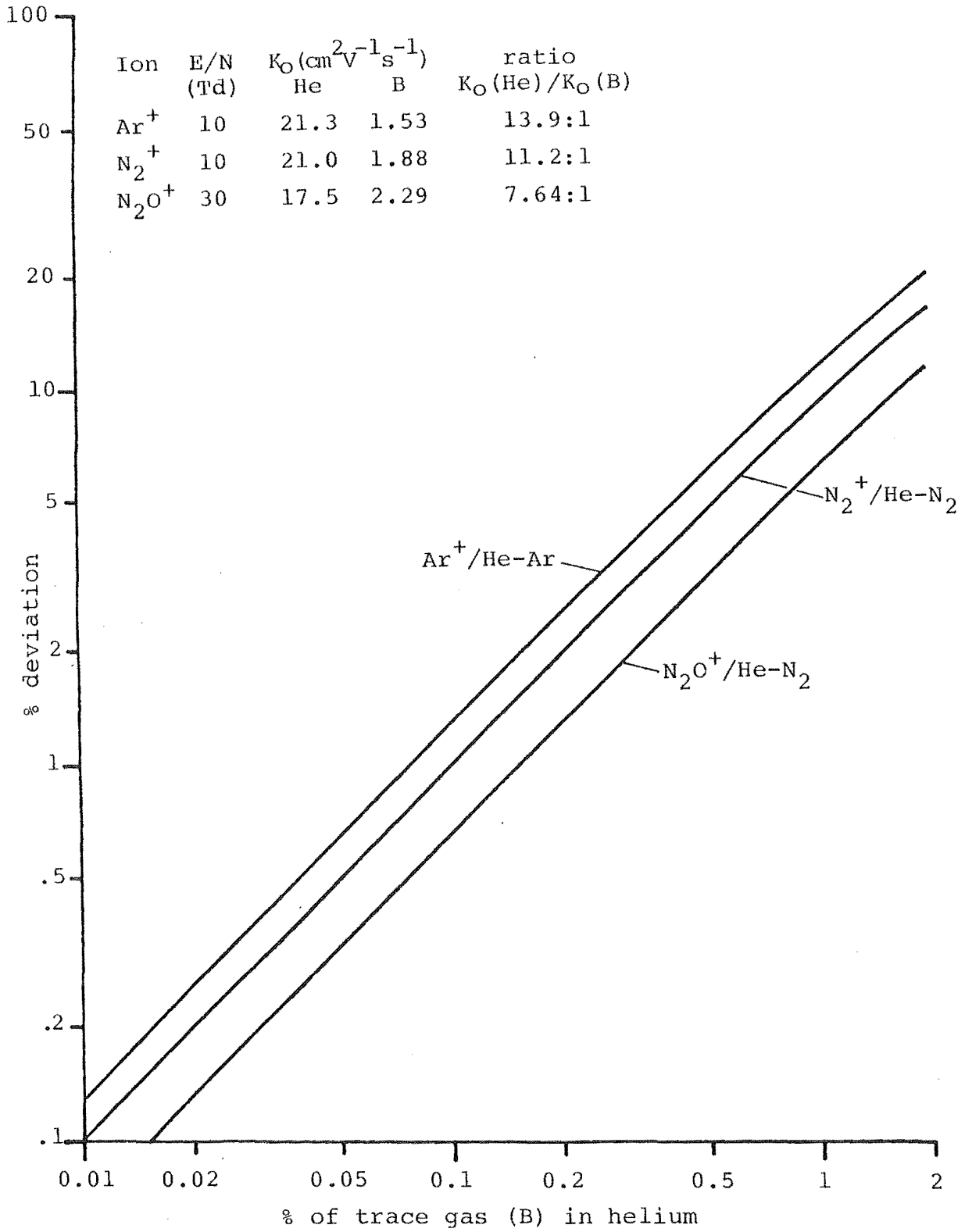

Figure 4.3 Mobility deviations in mixtures according to Blanc's Law

An assumption implicit in the derivation of equations 4.1 and 4.2 used above to calculate arrival time distributions is that the ions are produced in a delta function burst. That is, the ion pulse consists of ions created instantaneously in an infinitesimally thin area, a difficult condition to approximate experimentally; the shortest possible pulse is 1 μs for the apparatus described here. The effects of the finite widths of both the ion source and exit grid pulses were determined by comparison of arrival time spectra collected for a range of gate widths. Arrival time distributions were recorded for the tertiary ion H_2CN^+ formed in a 0.1% HCN in helium mixture for E/N= 100Td, drift distance (z)=6.87 cm and pressure = 0.4 Torr. First, the exit gate was fixed at 1 μs duration and the ion source gate stepped from 1 μs to 4 μs. The four ATDs obtained were almost superimposable; a barely perceptible broadening occurred with the ATD corresponding to a gate width of 4 μs. The procedure was then repeated with a source gate of 1 μs width and the exit gate varied from 1 μs to 4 μs. No significant difference existed between the four ATDs measured in this experiment. Further ATDs recorded for various combinations of source and exit gate widths gave similar results eg. the ATD for both gate widths equal to 3 μs could be superimposed over the ATD for both gates of 1 μs width. For all measurements reported in the succeeding chapters both gates are opened for a 2 μs period except where the total drift time exceeds 50 μs in which case the gates are both opened for 3 μs or 4 μs for drift times exceeding 100 μs. Clearly then, the finite widths of the source and exit gates will have a negligible effect on the

shape of an ATD and the assumption of ion production as a δ-function burst is indeed reasonable.

Also inherent in the derivation of equations (4.1) and (4.2) is the assumption that the drift tube is of infinite radial extent of equivalently that the loss of ions by collision with the outer sections of the drift tube is negligible. Solution of the time independent diffusion equation for a drift tube of cylindrical geometry[5e] provides an estimate of the average lifetime τ against collision with the walls:

$$\tau = \frac{1}{D_T}\left(\frac{r_o}{2.405}\right)^2 \qquad -(4.8)$$

Setting the radius of the drift tube r_o=2.5 cm and taking the transverse diffusion coefficient D_T=4000 cm^2s^{-1} (a typical value at 0.4 Torr and E/N=80Td), τ is found to be about 270 μs. This is considerably longer than most drift times except those for very low E/N but under these conditions the diffusion coefficient would be lower. Besides, the ions are sampled on axis for all experiments discussed here, so the only ions of interest lost are those that would have diffused out to the distance of the walls and then diffused back onto axis - a very small proportion indeed. No errors could be expected to arise due to the finite radial extent of the drift tube.

Various theoretical approaches all treat the ions as acting independantly i.e. there is no Coulomb repulsion between ions. This will not be true if the ion number density is too high; under these conditions space charge expansion of the ion swarm will occur as it moves along the drift tube. Expansion transverse to the drift field

decreases the efficiency of ion sampling through the exit aperture and expansion parallel to the field distorts the shape of the ATD. The parallel expansion results in longitudinal diffusion coefficients derived from ATD widths being considerably larger than the true values.[6,35] Since the expansion will be symmetrical about the midplane of the drifting ion swarm perpendicular to the drift tube axis, a negligible effect on drift velocity may be expected. If several ions of different identity are present, however, the space charge from an abundant species may push forward or hinder other ions; such an effect has been observed for the case of H^+ ions drifting in the presence of the much more abundant H_3^+ ions.[42] To determine the influence of space charge on the present results arrival time distributions were collected for He^+ ions drifting in helium and compared with spectra calculated by Eq.4.1. Results for two distances are given in fig.4.4, indicating that space charge effects are not particularly apparent. (Actually, the validity of the generalised Einstein equations 2.7 and 2.8 for calculation of diffusion coefficients is of some doubt when the ion-neutral interaction is dominated by charge transfer). Another test is to reduce the filament current (and consequently the emission current) until there is no decrease in the width of the measured arrival time distribution.

Operating with the filament current as low as practicable offers other advantages. At very high currents electrical breakdown or discharges may occur in the filament region of the ion source causing rapid deterioration and failure of the filament. With arrival time spectra recorded

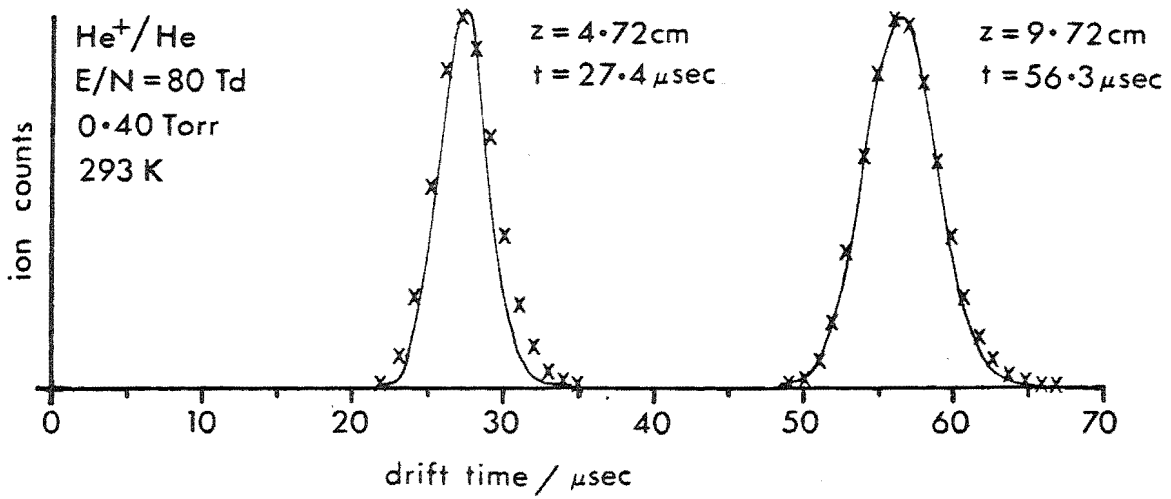

Figure 4.4 Experimental and calculated arrival time distributions for He^+ in helium

while the filament current is excessively high the signal takes a very long time to decay back to zero after the maximum, producing a long tail sometimes extending for three or four times the period of maximum signal. This is thought to be due to the presence of excited helium atoms in the metastable 2^3S state 19.82 eV above the ground state.[43] These metastable helium atoms have enough energy to ionize any species except neon. Being uncharged, the metastables diffuse out of the ion source some time after the He^+ ions and by reaction with the trace reactant gas produce the ions observed at very long times in the ATD. Where the time between successive ion source pulses is small (<50 μs), as would be the case for ions studied at high E/N (>100Td), all the helium metastables have not been lost by quenching or reaction before the next ion source pulse occurs. The ATD then exhibits a high background count before the true position due to ions arriving that were formed from metastables of the previous pulse.

Bearing in mind the conclusions of these last two subchapters, particular attention was paid to the following points in order to minimize errors with mobility measurements.

1. A graph of arrival time maxima as a function of distance was usually plotted to detect anomolous points, particularly those prevalent for short drift distances. Generally, the collection of data for distances less than 3 cm was not found to be worthwhile. If the correlation coefficient of the line fitted to the data by linear regression (least squares) was less than 0.999 the data was considered suspect.

2. Data were collected at more than one total pressure, or partial pressure of reactant gas, or for differing degrees of contamination of the drift tube. When the mobility was found to no longer increase with conditions leading to a higher reaction frequency the reaction rate was considered adequate.

3. The filament current was kept as low as was compatible with reasonable ion signal intensity.

Finally, some consideration must be given to uncertainties in the measurement of pressure, temperature and voltages. Assuming the calibration of the MKS Baratron to be reliable, the uncertainty of the pressure measurement will be that of fluctuation due to manually adjusting the leak valve to maintain a constant pressure i.e. ca.1%. The maximum temperature variation during a run is no more than $2^{o}C$; an uncertainty of 0.7% for temperatures around 293K. Voltage measurements are taken as close as possible to the drift tube terminals. The rated accuracy of the Keithley meter of $\pm$ 1 digit gives a maximum uncertainty of 0.5% (for 20.0V). The sum of uncertainties in measurements of the experimental parameters is thus ca.2.2%.

The total error in a mobility measured using the apparatus and techniques described here would thus be less than $\pm$ 5%. This allows ca.3% for errors due to the spread of formation times of reaction produced ions, Blanc's Law deviations due to the addition of trace reagents to the helium buffer and spurious contributions to the actual ion signal. In view of the fact that the first two factors both tend to reduce the ion mobility the uncertainty would possibly be better expressed as $^{+3}_{-7}$%. The reproducibility

between repeated mobility measurements is generally found to be within 2-3%.

CHAPTER 5

RESULTS I: MOBILITIES OF IONS CONTAINING THE -CN GROUP

(i) Introduction

Results for ions formed by electron impact of helium gas containing trace (0.04-0.2%) quantities of HCN, C_2N_2, CH_3CN, CH_3NC and CNCl are presented and discussed in this chapter. Where more than one structure is possible for an ion of a given empirical formula, this ion has been produced from more than one precursor in an attempt to detect possible structural differences by corresponding differences in mobility. Larger ions should exhibit a larger momentum transfer collision integral $\Omega^{(1,1)}$ and consequently a lower mobility. Data are also presented for some ions of which mobilities have previously been measured to provide an indication of the reliability of the present results and the methods used for their determination.

To determine a mobility at a particular value of E/N, arrival time distributions (ATDs) were measured for a range of distances from 2-9 cm as indicated on an external scale attached to the ion source linear motion assembly. In most cases it proved possible to conduct the experiment under conditions of pressure and mixture composition that produced a sharp maximum in the arrival time distribution. Under these circumstances only the top portion of the ATD from about half maximum to half maximum was collected. When it was necessary or of interest to compare the experimental ATD with one computed using Eq.(4.1) or (4.2) data were collected

over the entire time range for which the ion signal significantly exceeded the background noise. The experimental data were smoothed using a five point smoothing polynomial:[44]

$$y'_i = \frac{1}{35}(-3y_{i-2}+12y_{i-1}+17y_i+12y_{i+1}-3y_{i+2}) \qquad -(5.1)$$

where y_i denotes any experimental data point and y_{i+n} is the nth data point relative to the first. The data point corresponding to the largest signal was located. A five point Lagrange interpolating polynomial was then fitted to this point and the two points on either side. The expressions used were:

$$p(t) = \sum_{k=o}^{4} y_k \ell_k(t) \qquad -(5.2)$$

$$\text{with} \quad \ell_k(t) = \prod_{\substack{i=o \\ i\neq k}}^{4} \frac{t-t_i}{t_k-t_i} \qquad -(5.3)$$

where y_k are the smoothed data points at times t_k. The value of the quartic polynomial p(t) was then computed for times ranging from the time of the data point before the maximum to the time of the data point after the maximum in steps of one quarter the time interval between points. The maximum value of p(t) was then found and the corresponding time taken as the position of the arrival time maximum. These maxima were then plotted as a function of distance. Figure 5.1 presents a range of typical t-z plots obtained in this manner.

In order to assess the reliability of this technique mobilities have been measured for He^+ in helium and some secondary ions of known mobility under a range of conditions.

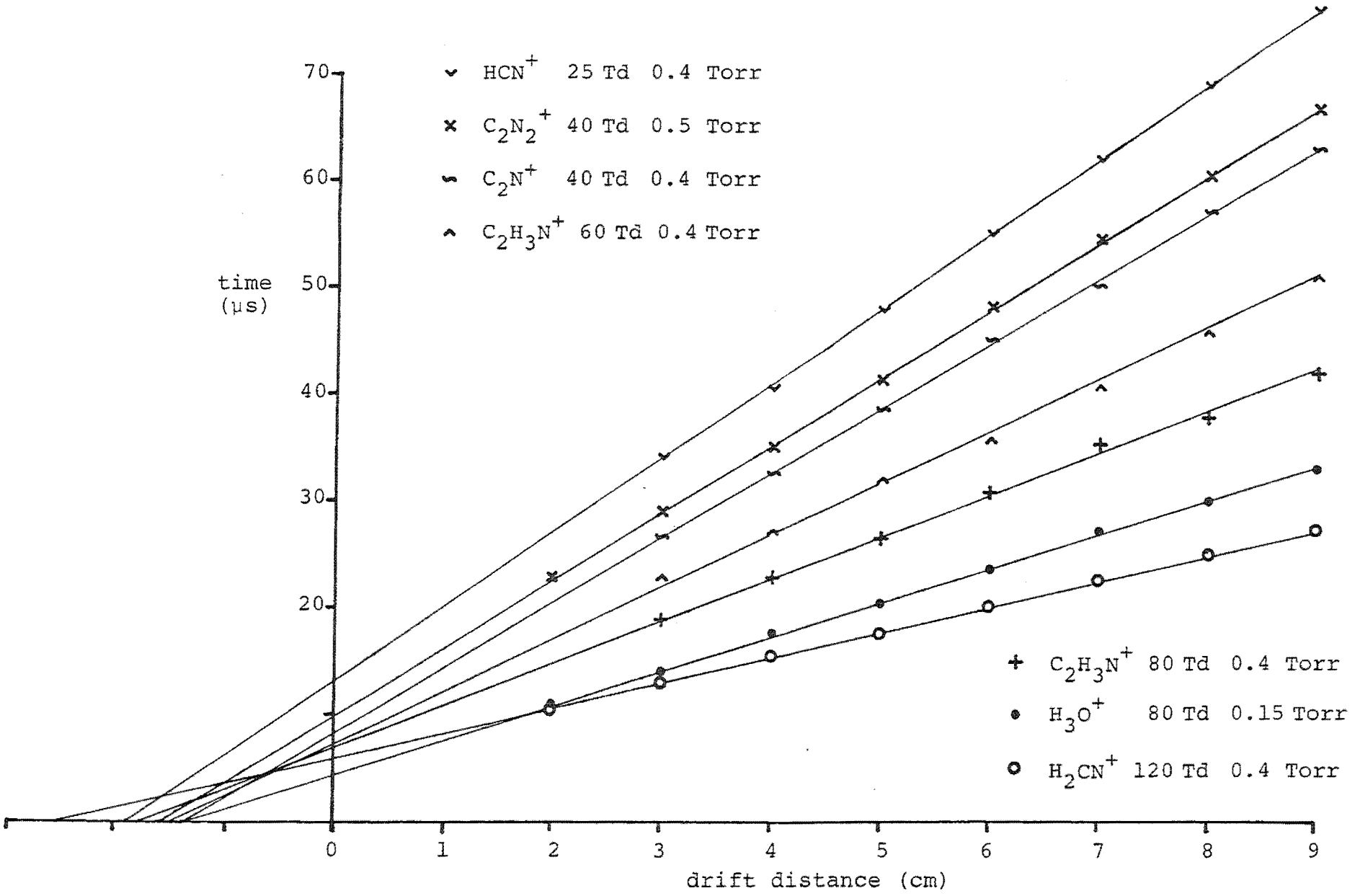

Figure 5.1 Representative t-z plots

Table 5.1 compares a compilation of such data for He^+ in helium with previously reported values.[13,35,45]

Table 5.1 Experimentally determined mobilities of He^+ in helium.

E/N (Td)	P (Torr)	K_o(exp) $cm^2V^{-1}s^{-1}$	K_o(lit,±3%) $cm^2V^{-1}s^{-1}$	deviation %
60	0.15	8.26	8.67	-4.7
80	0.10	8.02	8.12	-1.2
80	0.15	7.93	8.12	-2.3
80	0.40	8.04	8.12	-1.0
100	0.15	7.43	7.67	-3.1
100	0.40	7.64	7.67	-0.4
150	0.10	6.50	6.78	-4.1
150	0.15	6.45	6.78	-4.9
300	0.15	4.96	5.19	-4.4

It is evident that the values measured are in all cases slightly less than the literature results. All deviations are well within the combined uncertainty of the two sets of measurements, however.

Some mobility results for secondary and tertiary ions measured at 0.4 Torr and 100 Td are compiled in Table 5.2 together with previously reported values. With these ions

Table 5.2 Experimental mobilities in helium of ion produced by reaction

Ion	Buffer (trace in He)	K_o(exp) $cm^2V^{-1}s^{-1}$ (±5%)	K_o(lit) $cm^2V^{-1}s^{-1}$	Ref. (also 13,14)	Deviation %
H_2O^+	b/g*H_2O	18.3	17.6(±4%)	46	+3.8
H_3O^+	b/g H_2O	16.8	16.4(±4%)	46	+2.4
N_2O^+	0.11% N_2O	12.97	12.7(±2%)	47	+2.1
NO^+	0.11% N_2O	15.02	15.0(±7%)	48	+0.1
N_2^+	0.11% N_2O	15.49	15.2(±7%)	4	+1.9

* b/g = background impurity

produced by reaction it is apparent that agreement with previous work is well within combined uncertainties.

(ii) HCN: Mobilities of HCN^+ and H_2CN^+

Mixtures containing from 0.04% to 0.2% hydrogen cyanide (HCN) in helium were studied. Electron impact of these mixtures produced almost exclusively He^+ which forms other ions by reaction; this was ascertained by reducing the electron energy below the ionization potential of helium whereupon almost no signal due to other ions was detected. The reaction of He^+ with HCN has been examined previously both by ion cyclotron resonance (ICR)[49] and flowing afterglow (FA)[8]. The ICR study found a rate coefficient of $3.1\pm.6X10^{-9}cm^3molec^{-1}s^{-1}$ and the following product distribution:

$$He^+ + HCN \rightarrow HCN^+ + He \qquad <0.01 \qquad -(5.1a)$$

$$\rightarrow CN^+ + H + He \qquad 0.47 \qquad -(5.1b)$$

$$\rightarrow CH^+ + N + He \qquad 0.21 \qquad -(5.1c)$$

$$\rightarrow C^+ + N + H + He \qquad 0.25 \qquad -(5.1d)$$

$$\rightarrow N^+ + C + H + He \qquad 0.07 \qquad -(5.1e)$$

The FA study[8] measured a rate coefficient of $3.9X10^{-9}$ $cm^3molec^{-1}s^{-1}$ and found CN^+ to be the major product with a small proportion of CH^+ and C^+. The parent HCN^+ was also observed but could not be positively identified as a primary product because of spurious production from the reaction of metastable $He(2^3S)$ and HCN.

Further reaction of the primary reaction products gives HCN^+:

$$CN^+ + HCN \rightarrow HCN^+ + CN \qquad -(5.2)$$

at a rate measured by FA[50] of $9.8X10^{-10}cm^3molec^{-1}s^{-1}$.

The proportion of each ion present relative to the sum of all ions measured as a function of distance is shown in fig.5.2 for a 0.07% HCN in helium mixture at 0.4 Torr and 120 Td. Note that the true distance will be longer since reaction will also occur while the ions are traversing the ion source. This system was then modelled by calculations using the rate coefficients quoted above.

Program DRIFT (listed in Appendix B) was used to calculate the total He^+ flux at each distance z which is given by:[2,5]

$$I(z) = \frac{sa}{4D_L^{\frac{1}{2}}} \exp\left(\frac{zv_d}{2D_L}\right)\left\{\left[2D_L^{\frac{1}{2}}+\frac{v_d}{(\alpha+v_d^2/4D_L)^{\frac{1}{2}}}\right]\right.$$

$$X \exp\left[\frac{-z}{D_L^{\frac{1}{2}}}\left(\frac{v_d^2}{4D_L}+\alpha\right)^{\frac{1}{2}}\right]-\left[\frac{z}{(z^2/4D_L+r_o^2/4D_T)^{\frac{1}{2}}}+\frac{v_d}{(\alpha+v_d^2/4D_L)^{\frac{1}{2}}}\right]$$

$$\left.X \exp\left[-2\left(\frac{z^2}{4D_L}+\frac{r_o^2}{4D_T}\right)^{\frac{1}{2}}\left(\frac{v_d^2}{4D_L}+\alpha\right)^{\frac{1}{2}}\right]\right\} \qquad -(5.4)$$

where all symbols take the same meaning as for Eq.(4.2) of the previous chapter. Ions of planar source density s emanate from the source aperture of radius r_o and leave the drift tube via the exit aperture of area a. The longitudinal and transverse diffusion coefficients are represented by D_L and D_T, respectively, v_d is the primary ion drift velocity and α the reaction frequency.

Program DRIFT2 (also listed in Appendix B) was used to calculate an arrival time distribution for the secondary ion CN^+. The total ion flux defined analytically by an infinite time integral was approximated by summing the points

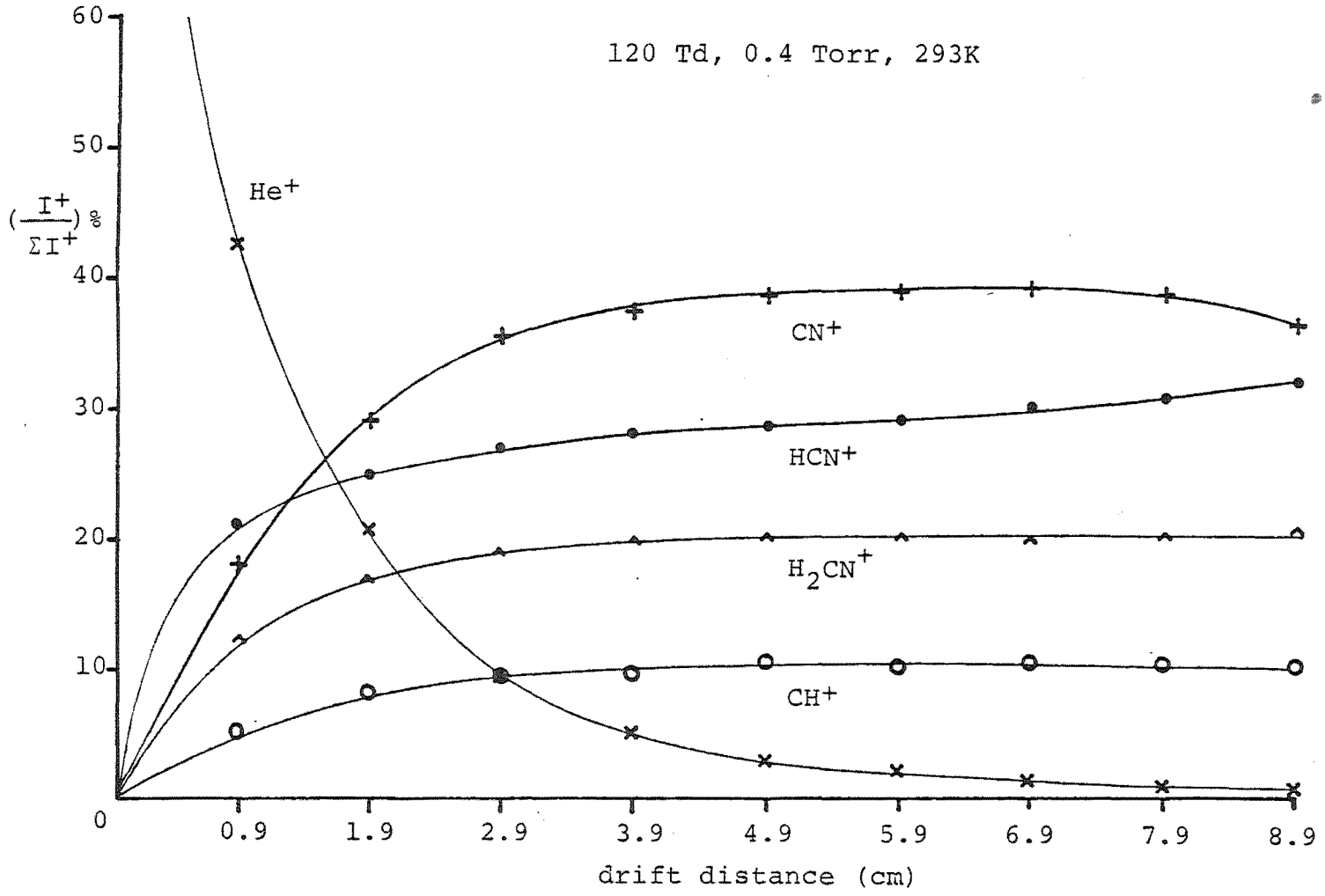

Figure 5.2 Experimental ion intensities as proportion of total ions for 0.07% HCN in helium

of the arrival time distribution i.e.:

$$I(z) = \int_0^\infty I(z,t)dt \cong \sum_{t_1}^{t_2} I(z,t)\Delta t \qquad -(5.5)$$

where t_2 and t_1 are the values over which $I(z,t)$ is significantly large and Δt the time interval between calculated values of $I(z,t)$. An analogous summation procedure to Eq.(5.5) was used to estimate the He^+ flux from arrival time distributions calculated by DRIFT and was found to give precise agreement with the analytic expression Eq.(5.4).

Firstly, $I(z)$ for CN^+ was computed assuming no further reaction of the CN^+ ions (i.e. $\alpha_B=0$ in Eq.4.3), then the calculations were repeated with reaction included. The HCN^+ intensity was then set equal to the difference of the two CN^+ intensities. Since the mobilities (and diffusion coefficients) of CN^+ and HCN^+ are not very different this provides a good approximation to the true HCN^+ signal as a function of distance. The results of these calculations are presented in fig.5.3a for a 0.07% mixture of HCN in helium at 120 Td and 0.4 Torr.

From comparison with fig.5.2 it appears that reaction has progressed at a far faster rate than expected during the experiment. Plausible explanations for this include (1) there is extensive reaction with background impurities, (2) there is a large contribution to HCN^+ signal from ionization of HCN by metastable 2^3S He atoms and (3) the mixture concentration has become enriched due to differential effusion. This latter effect where the helium buffer is lost faster than the trace gas has been found to result in mixture enrichments of up to 50% under some conditions.[51]

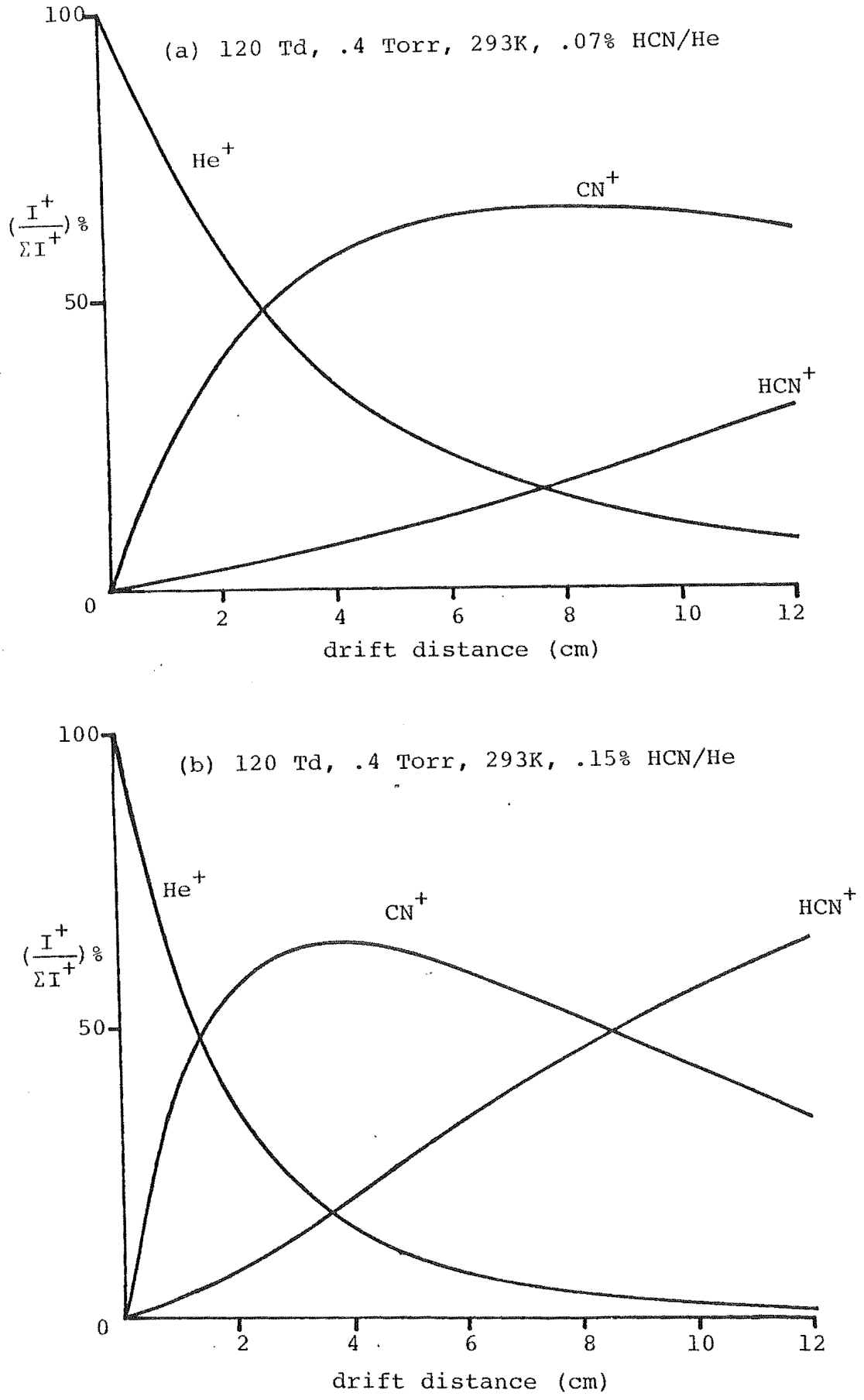

Figure 5.3 Calculated ion intensities as proportion of total for (a) 0.07% HCN and (b) 0.15% HCN in helium

This enrichment effect is particularly important when the exit aperture is of the same order as the mean free path (molecular flow regime). This is not the case with the present instrument where the exit aperture of diameter 0.25 mm is far larger than the mean free path of ca.$1X10^{-3}$mm. Also, close examination of figs.5.2 and 5.3a reveals that although the rate of removal of He^+ and the rates of formation of HCN^+ and H_2CN^+ are much faster than expected, the rate of formation of CN^+ appears to be in good accord. The calculations were repeated for a 0.15% HCN in helium mixture and the results are shown in fig.5.3b. The agreement with the experimental results is no better; HCN^+ still rises much later and CN^+ is now depleted too early. Thus, it may be concluded that mixture enrichment cannot account for the early appearance of HCN^+ and H_2CN^+ and is not a problem with the present instrument as operated here.

The only impurity detected during the data collection for fig.5.2 was a small quantity of air resulting in peaks at m/e=14,16,28,32. Some of the m/e=28 signal in fig.5.2 labelled H_2CN^+ would in fact be due to N_2^+. Reaction with these impurities would diminish the He^+ signal but not contribute to early HCN^+ formation. The rapid rise of HCN^+ must, therefore, be the result of either formation by direct charge transfer (reaction 5.1a) or a product of reaction of metastable (^3S) helium atoms with HCN. The former reaction appears unlikely since the exothermicity as determined by differences in ionization potentials[52] is 10.8 eV which would tend to cause fragmentation as observed with the ICR study.[49] Formation by Penning ionization from 2^3S He atoms is therefore considered the most reasonable explanation

for the early appearance of HCN^+.

It has been concluded from scrutiny of charge exchange mass spectra,[53] collisional activation (CA) mass spectra[54] and predicted by theoretical calculations[55] that the ion structure HNC^+ is more stable than HCN^+ by about $87kJmol^{-1}$.[55] The CA study[54] concluded that HNC^+ was formed from all H,C and N containing precursors except HCN. Formation by reaction (5.2) could occur by either charge or H atom transfer. From differences in ionization potentials,[52] the exothermicity of reaction (5.2) is ca.$70kJmol^{-1}$. The barrier for the isomerization $HCN^+ \rightarrow HNC^+$ has been calculated[55] to be $45kJmol^{-1}$ so according to these results it is energetically feasible for charge transfer to result in isomerization. This would also be true for HCN^+ formed by Penning ionization from 2^3S He metastables. H atom transfer would require the positively charged CN^+ ion to approach the positive end of the HCN molecule (dipole moment of ca.3 debyes[56]) so this mechanism would not be expected to contribute significantly. It is not possible to be sure which structure HCN^+ or HNC^+ (or a mixture) is the ion of m/z=27 here. Attempts to measure the mobility of the m/z=27 ion from methylamine (CH_3NH_2) which has been shown to be HNC^+[53,54] were precluded by the very low cross section for the formation of this ion. Other sources of the HNC^+ ion also produce the $C_2H_3^+$ ion of the same nominal mass which could not be distinguished from HNC^+/HCN^+ by the quadrupole mass spectrometer used with the present instrument.

There are three possibilities for the structure of the H_2CN^+ ion and they have been the subject of numerous ab initio calculations.[56-60] Structure B is least stable and there

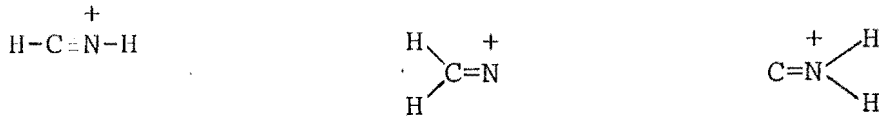

(A) (B) (C)

is no barrier to conversion from structure B to structure A.[59] Structure C is higher in energy than A by between 160kJmol^{-1}[60] and 290kJmol^{-1}[57,59] but there is an interconversion barrier of ca.125kJmol^{-1}. A collisional activation study[54] found evidence only for the existence of the $HCNH^+$ structure A regardless of precursor. The H_2CN^+ ion formed by proton transfer of hydrogen cyanide in the drift tube is therefore assumed to exist only as structure A which is isoelectronic with acetylene (C_2H_2).

The mobilities of HCN^+ and H_2CN^+ are graphed in figs.5.4 and 5.5 as a function of E/N and effective temperature calculated using Eq.(2.10) with the correction factor β=0. Narrow arrival time distributions and linear t-z plots could only be obtained for HCN^+ by using a series of mixture compositions to span the range of E/N from 20 to 140 Td. For the low E/N range (20-50 Td) a very dilute mixture, 0.05% HCN in helium restricted reactive attenuation of the HCN^+ signal and resulted in linear t-z plots. Mixtures of composition 0.1% HCN in helium were used to overlap this range of E/N and to extend the data to E/N=140 Td where there is less time available for reaction. At the higher values of E/N the HCN^+ ion was formed too slowly at 0.4 Torr total pressure and the resulting t-z plots were non-linear. The excellent agreement between mobilities determined for a range of mixture compositions verifies the assertion that the data is representative of ion transport in pure helium

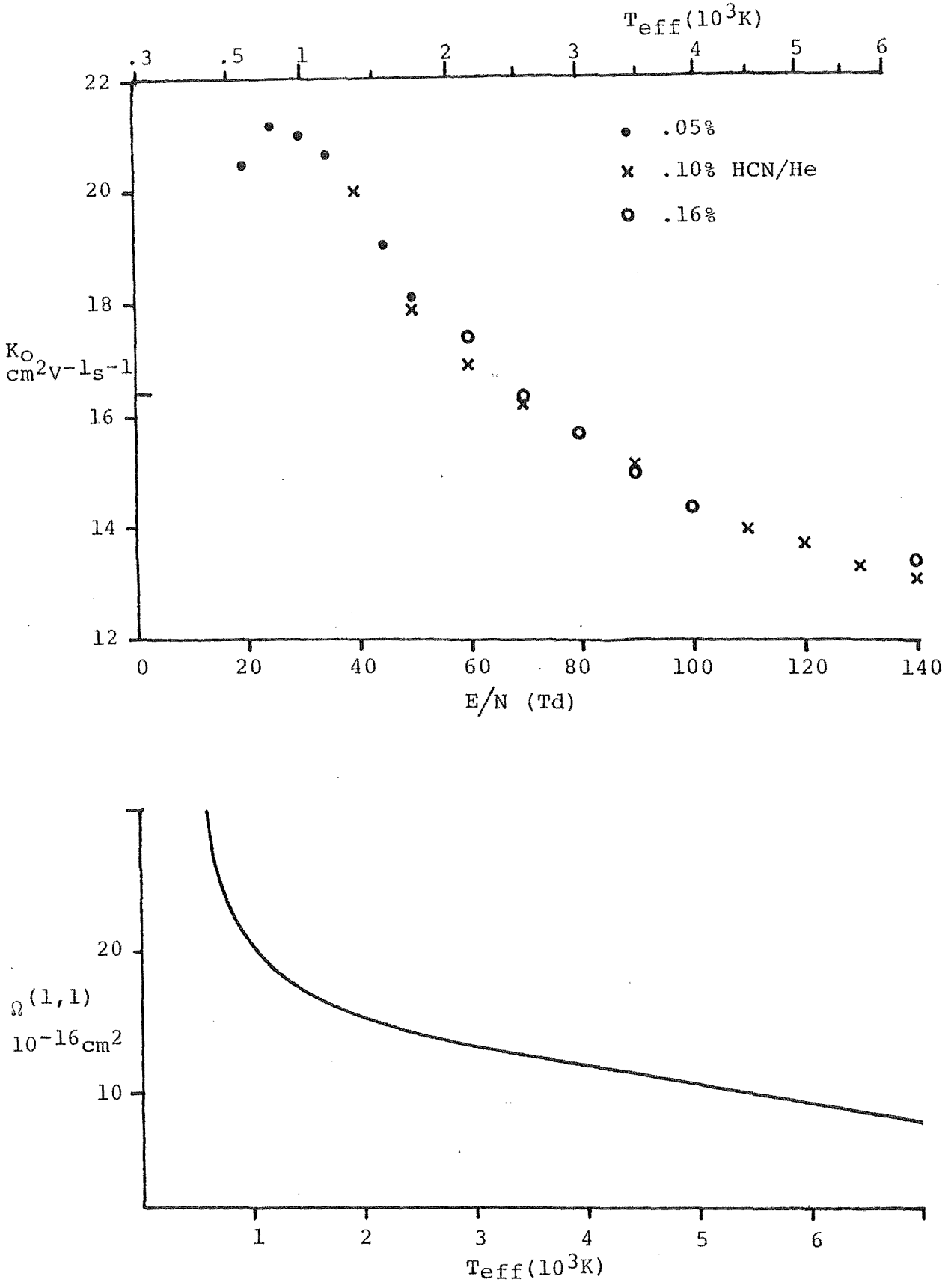

Figure 5.4 Mobilities and momentum transfer collision integrals for HCN^+

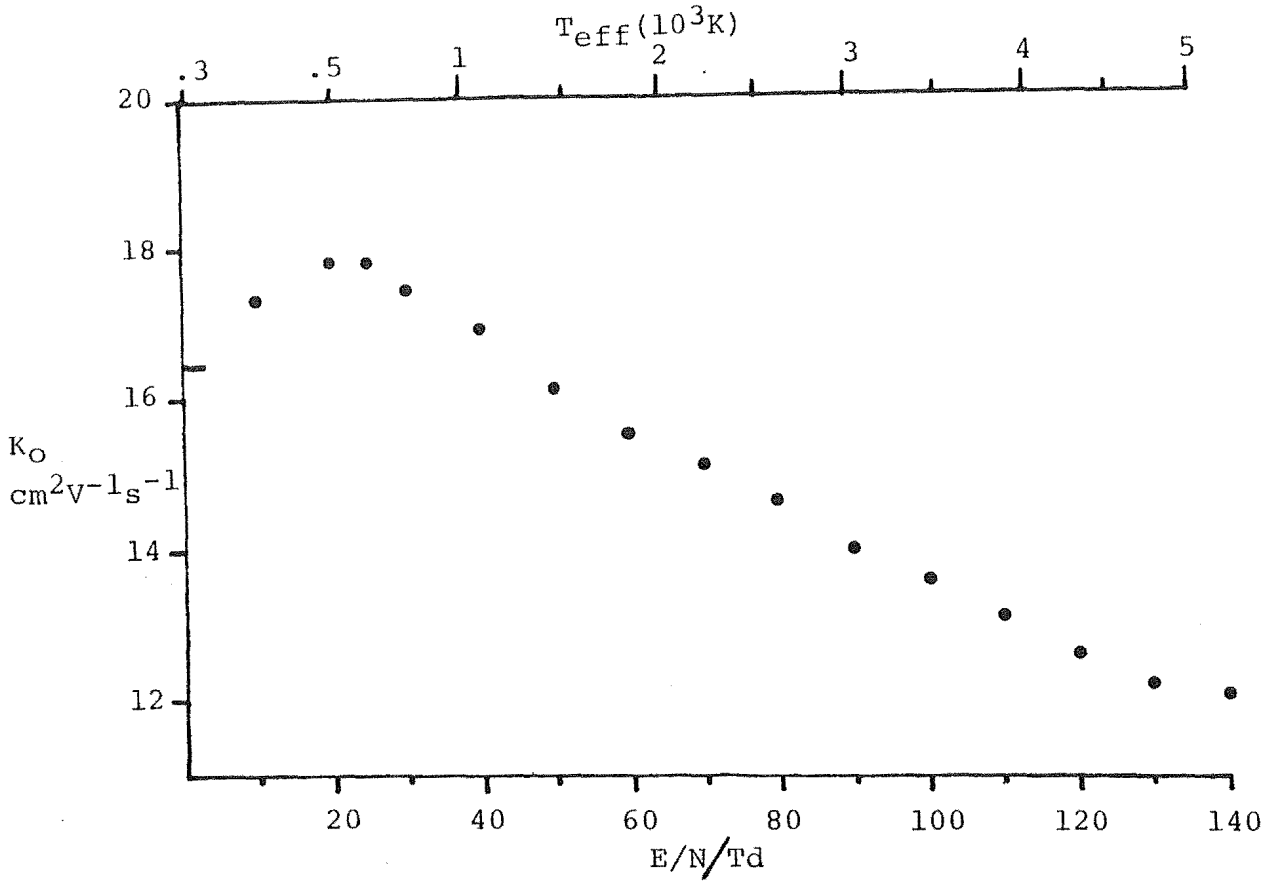

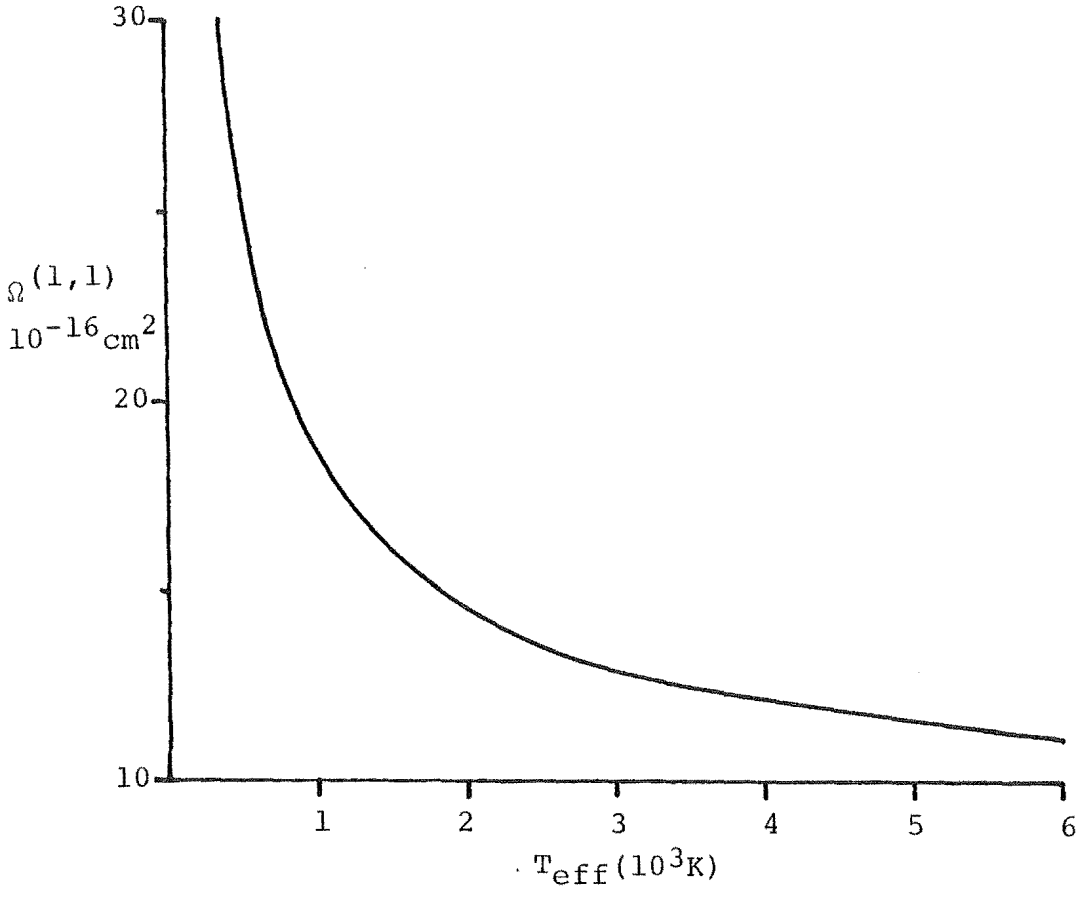

Figure 5.5 Mobilities and momentum transfer collision integrals for H_2CN^+

and that Blanc's Law deviations (see previous chapter) are negligible. Mixtures of 0.16% to 0.20% HCN in helium were employed for the H_2CN^+ mobility measurements. These less dilute mixtures were necessary to provide a sufficiently high reaction frequency to form H_2CN^+, particularly at higher values of E/N.

The drift velocity, v_d, may be calculated (in cms^{-1}) from the data presented and the relationship:

$$v_d = 269K_o(E/N) \qquad -(5.6)$$

where K_o is in $cm^2V^{-1}s^{-1}$ and E/N is in Td. Also presented in figs.5.4 and 5.5 are the momentum transfer collision integrals, $\Omega^{(1,1)}$, calculated by use of the two-temperature theory Eq.(2.11) with the correction term $\alpha=0$. The effective hard sphere collision diameter (d) may be calculated from the relationship:[29]

$$\Omega^{(1,1)} = \pi d^2 \qquad -(5.7)$$

(iii) $\underline{C_2N_2}$: Mobilities of $\underline{C_2N_2^+}$ and $\underline{C_2N^+}$

Mixtures from 0.05% to 0.1% C_2N_2 in helium were studied at 0.4 Torr. Primary He^+ ions react with C_2N_2 at a rate of $3.5X10^{-9}cm^3molec^{-1}s^{-1}$[61] to produce a variety of products:

$$He^+ + C_2N_2 \rightarrow CN^+ + CN + He \qquad -(5.8a)$$

$$\rightarrow C_2N^+ + N + He \qquad -(5.8b)$$

$$\rightarrow C_2^+ + N_2 + He \qquad -(5.8c)$$

$$\rightarrow C_2N_2^+ + He \qquad -(5.8d)$$

where the reaction channels are listed in order of decreasing frequency as observed in the present work. Mass spectra normalized to the largest signal (CN^+, m/z=26) are presented

for three distances in fig.5.6 (ions less than 1% of the largest are omitted). The C_2N^+ and C_2^+ ions appear to undergo no further reaction but CN^+ is removed by charge transfer:

$$CN^+ + C_2N_2 \rightarrow C_2N_2^+ + CN \qquad -(5.9)$$

at a rate measured by ICR[7] of $2.1\pm0.4X10^{-9}cm^3molec^{-1}s^{-1}$.

The mobility and momentum transfer collision integral of the $C_2N_2^+$ ion is presented in fig.5.7 as a function of E/N and T_{eff} respectively. It is presumed that the $C_2N_2^+$ ion retains the linear dicyanogen structure.

The structure of the C_2N^+ ion has been the subject of two recent theoretical studies[62,63] which find the CNC^+ structure to be more stable than the CCN^+ structure by[62] $195kJmol^{-1}$ or[63] $125kJmol^{-1}$. The interconversion barrier is estimated to be ca.$270kJmol^{-1}$. Taking the appearance potential of C_2N^+ from C_2N_2 as 19.5eV[64,65] the exothermicity of reaction (5.8b) is 5.1eV or $490kJmol^{-1}$ which is more than adequate to overcome the barrier to isomerization.

The C_2N^+ ion is also produced by dissociative charge transfer of He^+ with methylcyanide, CH_3CN and methyl isocyanide, CH_3NC. (See fig.5.9). In the absence of rearrangement both C_2N_2 and CH_3CN would produce CCN^+ and CH_3NC would produce CNC^+. The mobilities of C_2N^+ from all three sources were determined in an effort to detect possible differences related to structure. The results of all mobility determinations are given in fig.5.8. Rapid reaction of C_2N^+ with CH_3CN and CH_3NC prevented the measurement of mobilities for lower E/N. The solid line represents an estimated fit to the data. The momentum transfer collision integral is also presented as a function

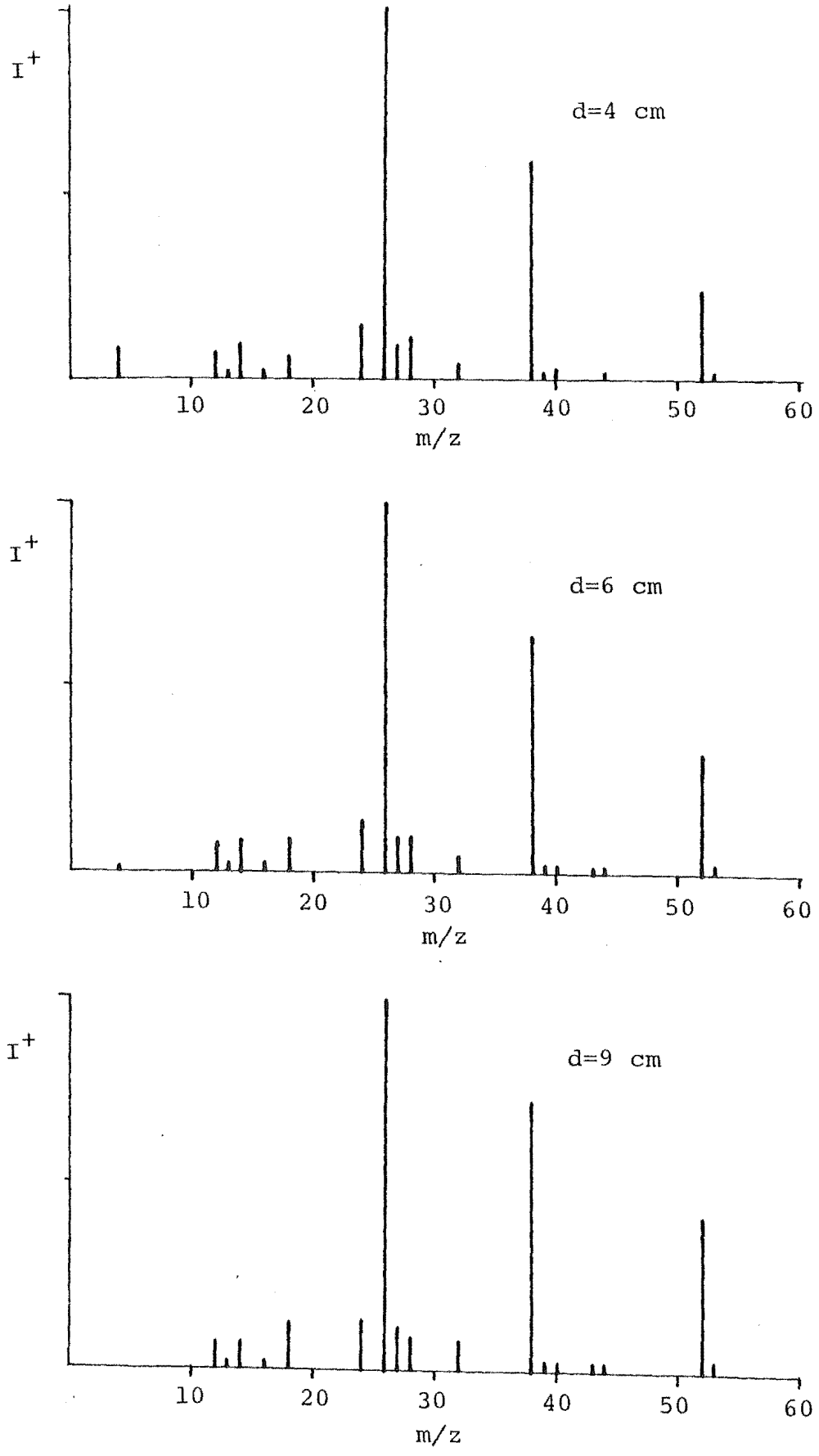

Figure 5.6 Mass spectra at three source distances for 0.05% C_2N_2 in helium (120 Td, .4 Torr, 293K)

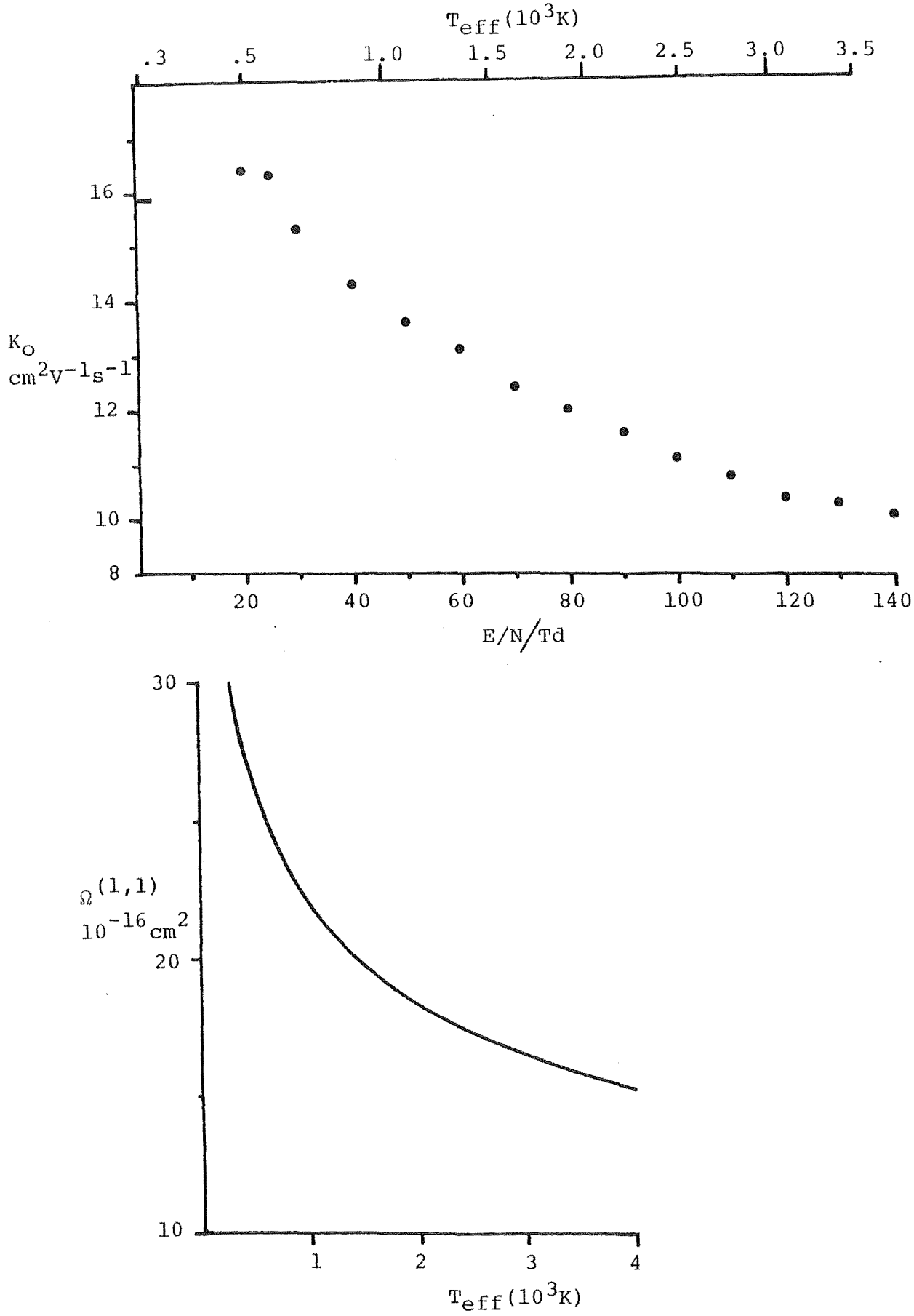

Figure 5.7 Mobilities and momentum transfer collision integrals for $C_2N_2^+$

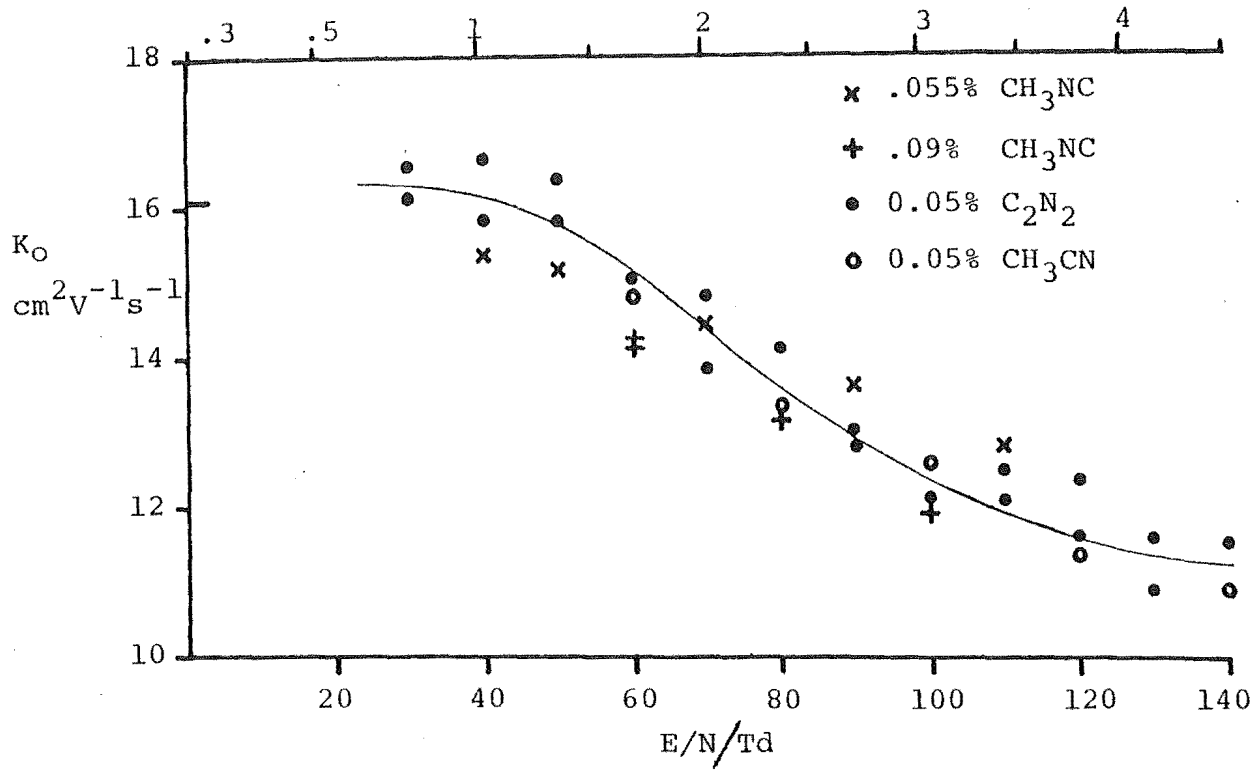

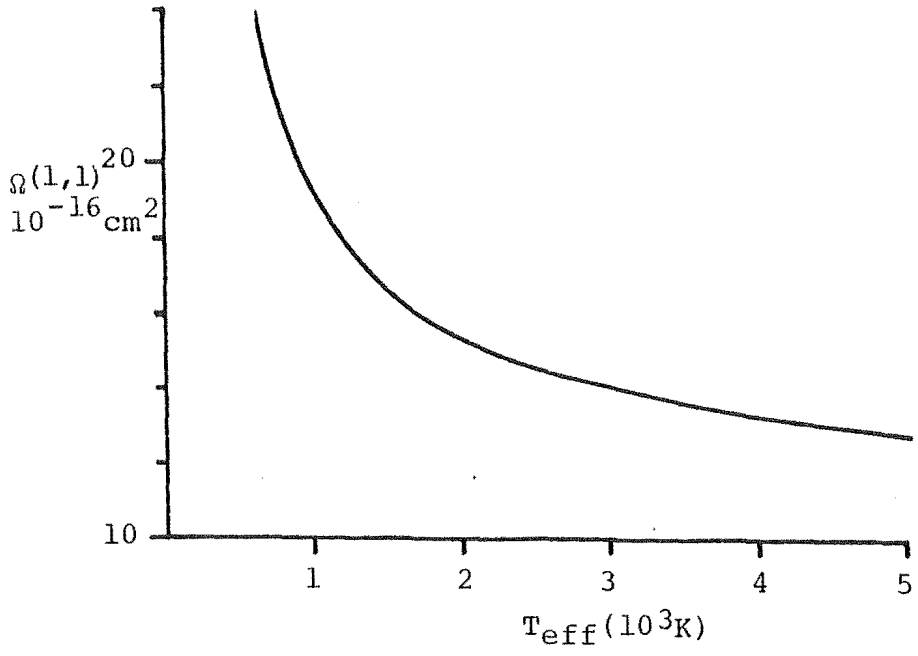

Table 5.8 Mobilities and momentum transfer collision integrals for C_2N^+

of T_{eff} calculated using drift velocities determined from the best fit mobilities.

From fig.5.8 there are evidently no consistent differences between the mobilities of C_2N^+ derived from any of the three precursors within the accuracy of these measurements. This does not necessarily preclude the possibility of differing structure. In fact, important factors influencing mobility such as mass, ion size and charge distribution are identical or very similar, therefore the absence of significant structure related differences in mobility is not too surprising.

(iv) CH_3CN and CH_3NC: mobilities of $C_2H_3N^+$ and HC_2N^+

Mixtures ranging from 0.05% to 0.1% methyl cyanide or methyl isocyanide in helium were studied in the drift tube. Mass spectra recorded at short distances (little time for reaction) are presented as the spectra on the left of fig.5.9. Qualitatively, there are many similarities between the mass spectra of the two isomers. The high exothermicity (>12eV[43,52]) of primary ionization from He^+ causes extensive fragmentation to produce predominantly C_2N^+ and HC_2N^+ (m/z=38,39). These ions then react by charge and proton transfer to form $C_2H_2N^+$, the parent ion $C_2H_3N^+$ and the protonated molecule $C_2H_4N^+$ (m/z=40,41,42). The latter two ions account for almost all the ion signal at longer distances.

The above mass spectral similarities have also been observed with 70eV electron impact (EI) spectra.[66,67] A consideration of the intensities of metastable peaks[67] has shown that this is not due to some degree of isomerization

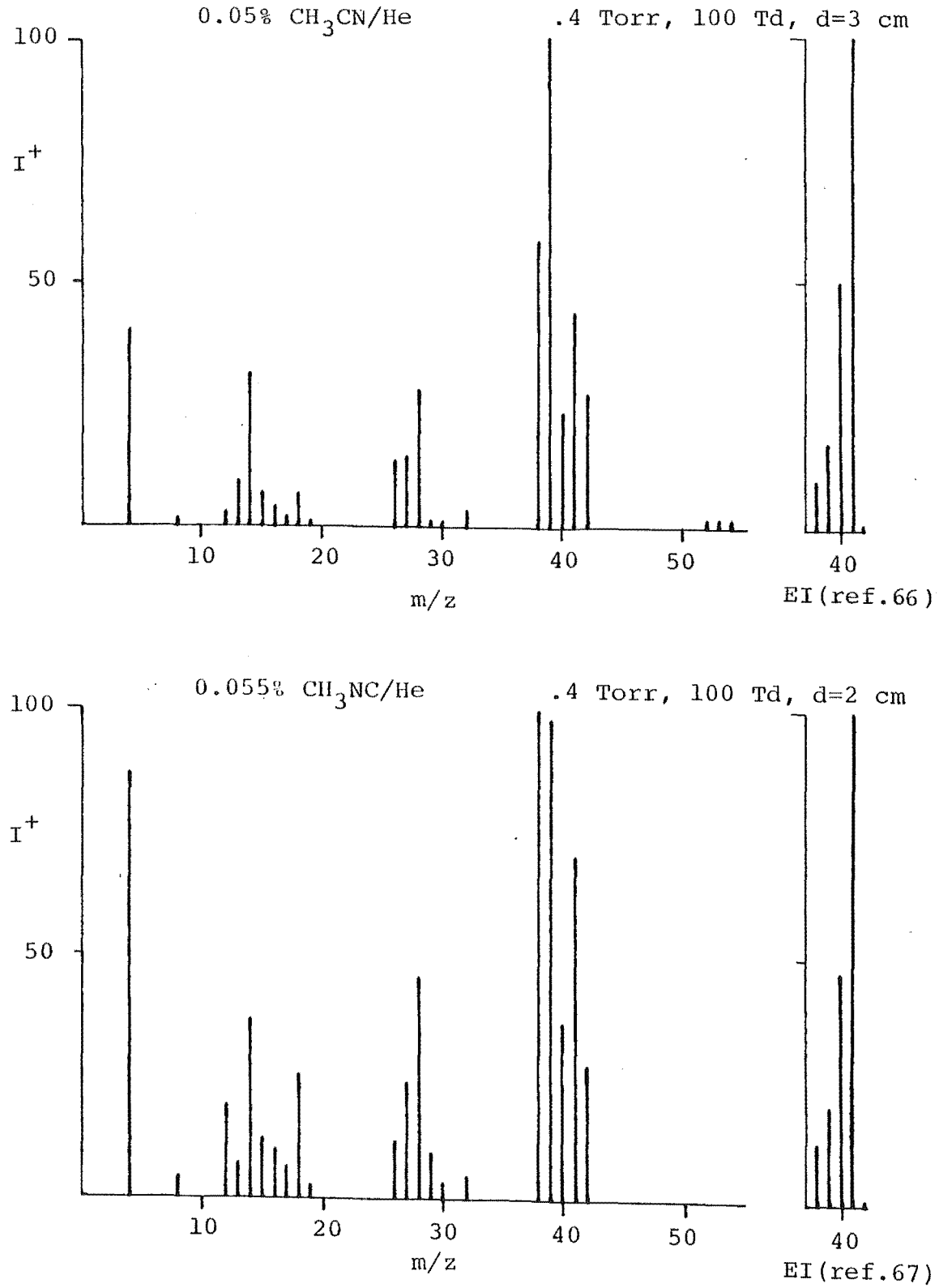

Figure 5.9 Mass spectra of CH_3CN and CH_3NC mixtures in helium at short source distances

of isocyanide to cyanide during ionization. A collision induced dissociation (CID) study of ions of empirical formula $C_2H_3N^+$ derived from a range of compounds[68] also concluded that both methyl cyanide and methyl isocyanide retain their original configuration under 70eV electron impact ionization. Another CID study[69] provided further confirmation of this and also concluded that the tautomeric enol forms of CH_3CN^+ and CH_3NC^+, i.e. $CH_2{=}C{=}NH^+$ and $CH_2{=}N{=}CH^+$ are more stable than the original structures by $155kJmol^{-1}$ and $71kJmol^{-1}$ respectively. However, the barrier to keto-enol rearrangement was estimated to be $163kJmol^{-1}$ for the methyl cyanide cation and $75\text{-}96kJmol^{-1}$ for the methyl isocyanide cation. Comparison of the drift tube mass spectra with the reported electron impact results[66,67] (fig.5.9) reveals a greater degree of fragmentation by He^+ ion charge transfer. The possibility that considerable rearrangement may occur during the more disruptive charge transfer reaction with He^+ or subsequent products cannot therefore be precluded and the structure of $C_2H_3N^+$ formed in these experiments cannot be unequivocally assigned.

The mobility and momentum transfer collision integral, $\Omega^{(1,1)}$, for $C_2H_3N^+$ from CH_3CN is presented in fig.5.10. The collision integrals were calculated using Eq.2.10 and Eq.2.11 with α and β set to zero. Also included amongst the mobility data are some measurements for $C_2H_3N^+$ formed from CH_3NC. The excellent agreement with the data from CH_3CN is apparent. Again, this cannot be interpreted as being necessarily indicative of structural equality, since very little difference would be expected between the mobility of CH_3CN^+ and CH_3NC^+, (or between $CH_2{=}C{=}NH^+$ and $CH_2{=}N{=}CH^+$), as

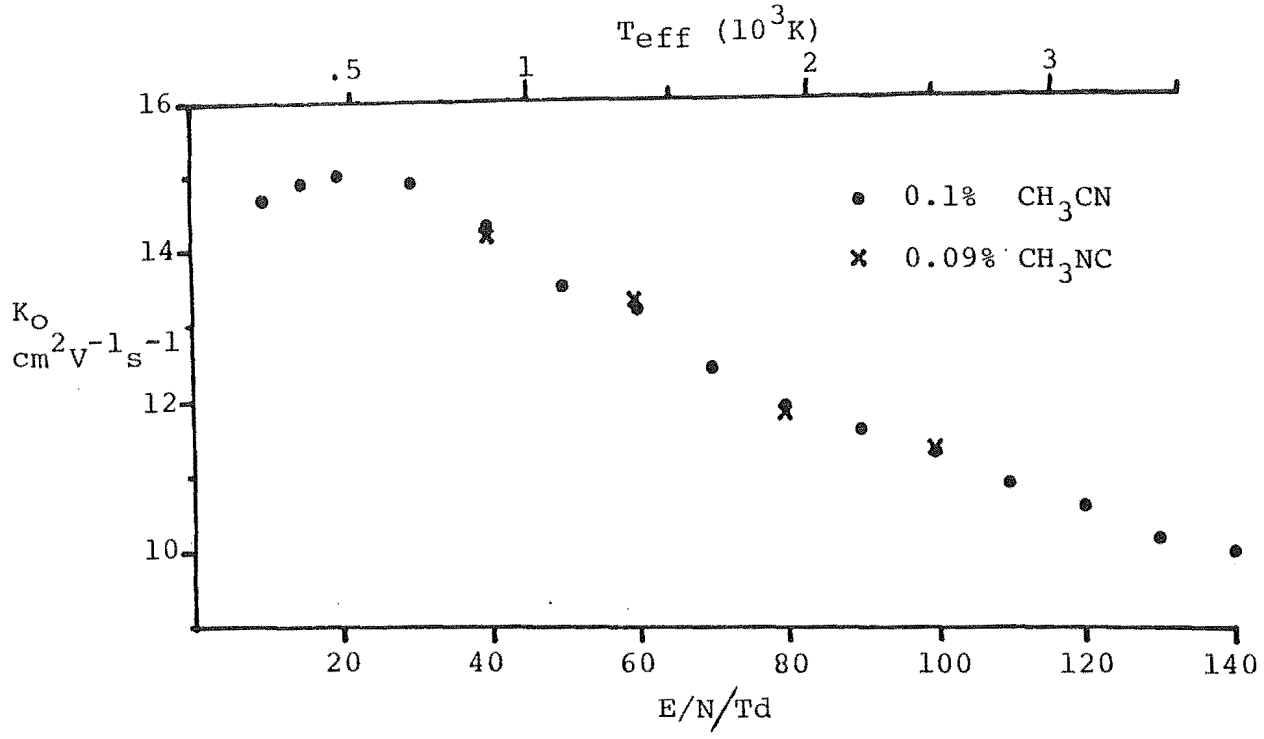

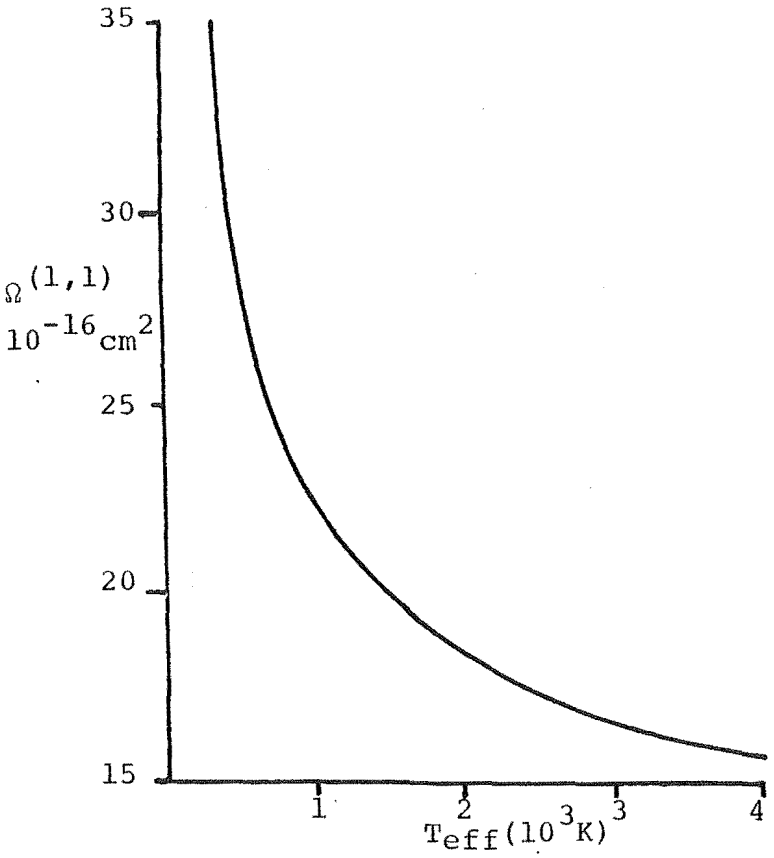

Figure 5.10 Mobilities and momentum transfer collision integrals for $C_2H_3N^+$

discussed previously for the analogous case of C_2N^+.

Experimental and derived data for the ion HC_2N^+ (m/e=39) from CH_3CN are presented in fig.5.11. As for the C_2N^+ ion excessive loss of ions by reaction precluded determination of mobilities at low E/N. Two measurements for the mobility of the HC_2N^+ ion from CH_3NC are also included; again no significant different to the m/z=39 ion from CH_3CN was found. Presumably ions of structure $HCCN^+$ and $HCNC^+$ would be produced from CH_3CN and CH_3NC respectively, although other structures are possible. Since no theoretical or experimental results are available relating to the structure of HC_2N^+ little comment is possible. However, the suggestion applied to C_2N^+ and $C_2H_3N^+$ that only a small difference in mobility would be expected between closely related structures would also apply to $HCCN^+$ and $HCNC^+$.

(v) Mobility of CN^+.

Determination of the mobility of CN^+ proved especially difficult due to the fast reaction of this ion with the corresponding precursor neutral relative to its rate of formation by dissociative charge transfer from He^+. Low mole fractions of reactant neutral (ca.0.05%) resulted in the arrival time distributions (ATDs) extending out to the time taken by the precursor He^+ ions to transit the drift tube (see figs.5.14,5.15). Higher mole fractions (ca.0.1%) resulted in further reaction with the trace neutral (HCN or C_2N_2) to rapidly deplete the ion signal. The proportion of CN^+ initially formed from CH_3CN was too small to be useful.

Mixtures of cyanogen chloride (CNCl) in helium (0.04-0.1%) were investigated as an alternative source of CN^+. No

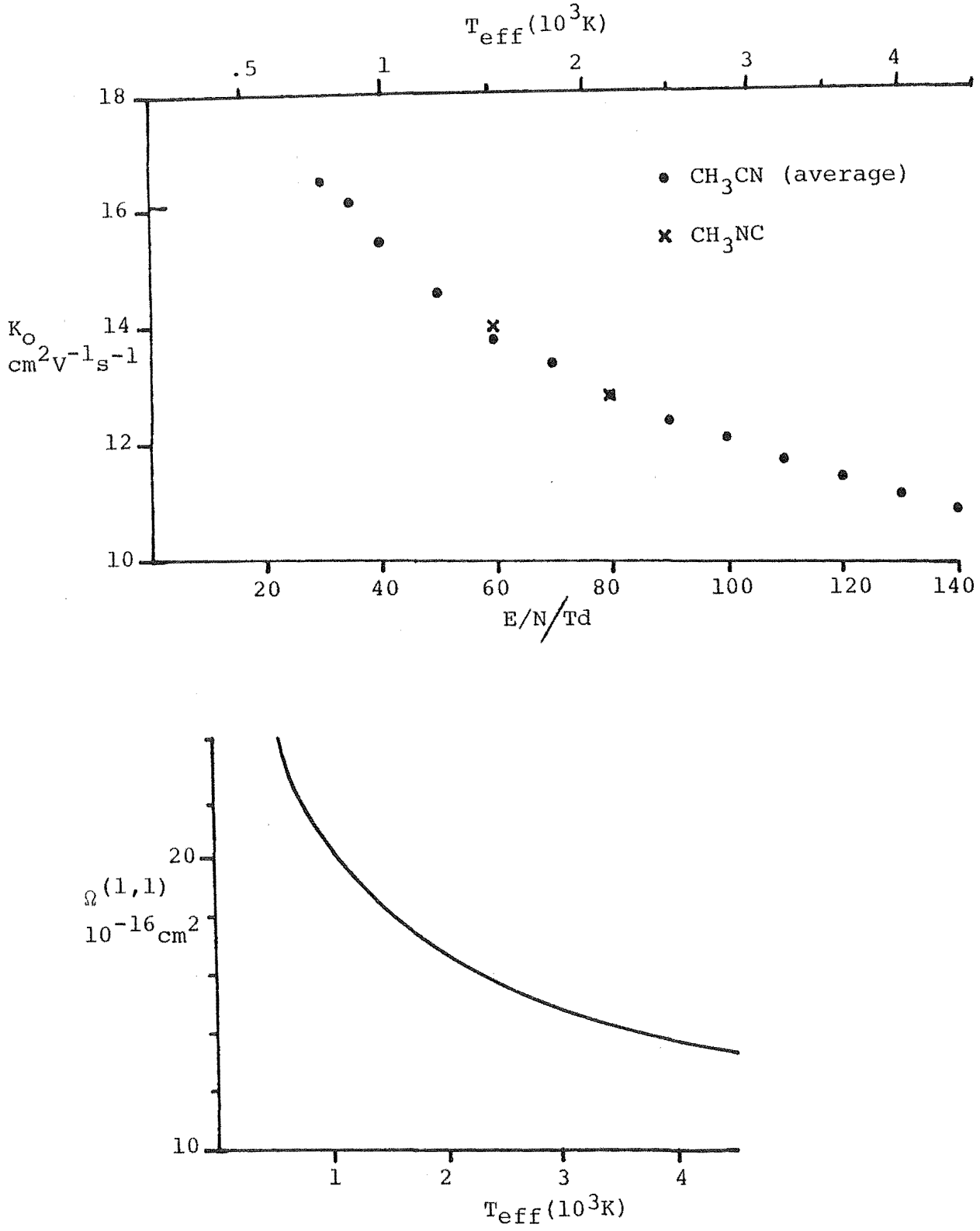

Figure 5.11 Mobilities and momentum transfer collision integrals for HC_2N^+

previous studies of the ion-molecule chemistry of CNCl have been reported. All fragment ions rapidly reacted to form $CNCl^+$, the species of lowest ionization potential.[52] Figure 5.2 depicts the observed ion populations as a proportion of the total ion signal for a 0.045% mixture over a range of distances at 80 Td and 0.4 Torr total pressure.

The complexity of the CN^+ ATDs precluded a determination of the mobility from the slopes of t-z plots and a curve fitting procedure was adopted. The smoothed experimental ATD for a dilute mixture of HCN (0.04-0.07%) was compared with ATDs calculated by the program DRIFT2 (see chapter 4(iii) and Appendix B) employing estimated values for the mobility of CN^+ and literature values for the mobility of He^+ and the relevant rate coefficients.[7,8] The mobility of CN^+ was then adjusted in the necessary direction to improve agreement; by this iterative method an optimum value of mobility could be found to within ± 0.2 $cm^2V^{-1}s^{-1}$.

The geometric distance between the ion source sleeve and ion exit plate was not the distance appropriate for these calculations since some adjustment was necessary for the extra distance traversed by the ions through the ion source. The "effective distance" for use in calculating an ATD was taken as the distance which gave a good fit to the trailing edge of the experimental distribution. The trailing edge (see fig.5.14) of the CN^+ distribution results from those ions formed from He^+ ions that have survived virtually the entire length of the drift tube and would almost be coincident with the trailing edge of an ATD for He^+ in helium recorded under identical conditions. When the distance that satisfied the above criterion was

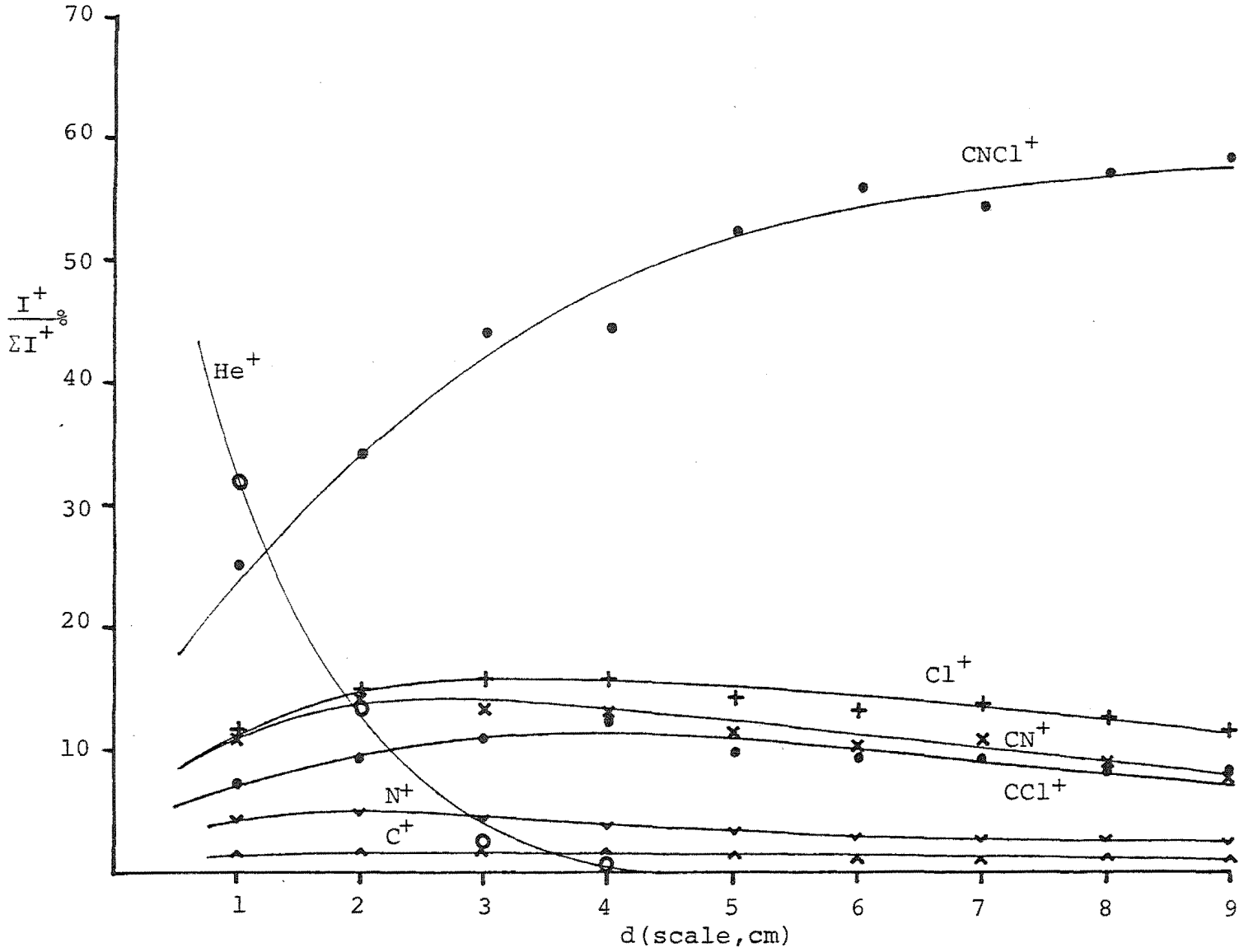

Figure 5.12 Ion intensities as proportion of total ions for 0.045% CNCl in helium (80 Td, 0.4 Torr, 293K)

found (usually 1.63 cm longer than the geometric distance) the mobility of CN^+ was varied to provide close agreement between the position of the leading edge of the smoothed experimental and calculated arrival time distributions.

The calculations were then repeated for other experimental drift distances at the same E/N using the ion source correction factor giving the best fit in the first calculation. Slight adjustments were often necessary to both the optimal distance correction and mobility of CN^+ of the first calculation in order to obtain a close fit between experimental and calculated ATDs over the entire range of experimental drift distances.

The validity of this procedure was first tested by fitting a calculated ATD to data collected for O^+ drifting through a 0.1% O_2 in helium buffer at 0.4 Torr and 100 Td. The literature values for the mobilities of O^+[13,69] and He^+ were used and the only variable was the effective distance. The results are shown in fig.5.13. Very good agreement could be achieved using the same distance correction of 1.63 cm over the full range of experimental drift distances. A rate coefficient of $9X10^{-10}cm^3molec^{-1}s^{-1}$ at 100 Td reported from a previous drift tube study[51] was used. The value of the rate coefficient chosen affects mainly the relative height of the early and late portions of the ATD and not the position of these sections; the value of mobility found to give optimum agreement is therefore fairly insensitive to the choice of rate coefficient.

Following validification of this technique it was applied to the CN^+ data for the full range of E/N studied i.e. from 40-120 Td. The distance correction of 1.63 cm was

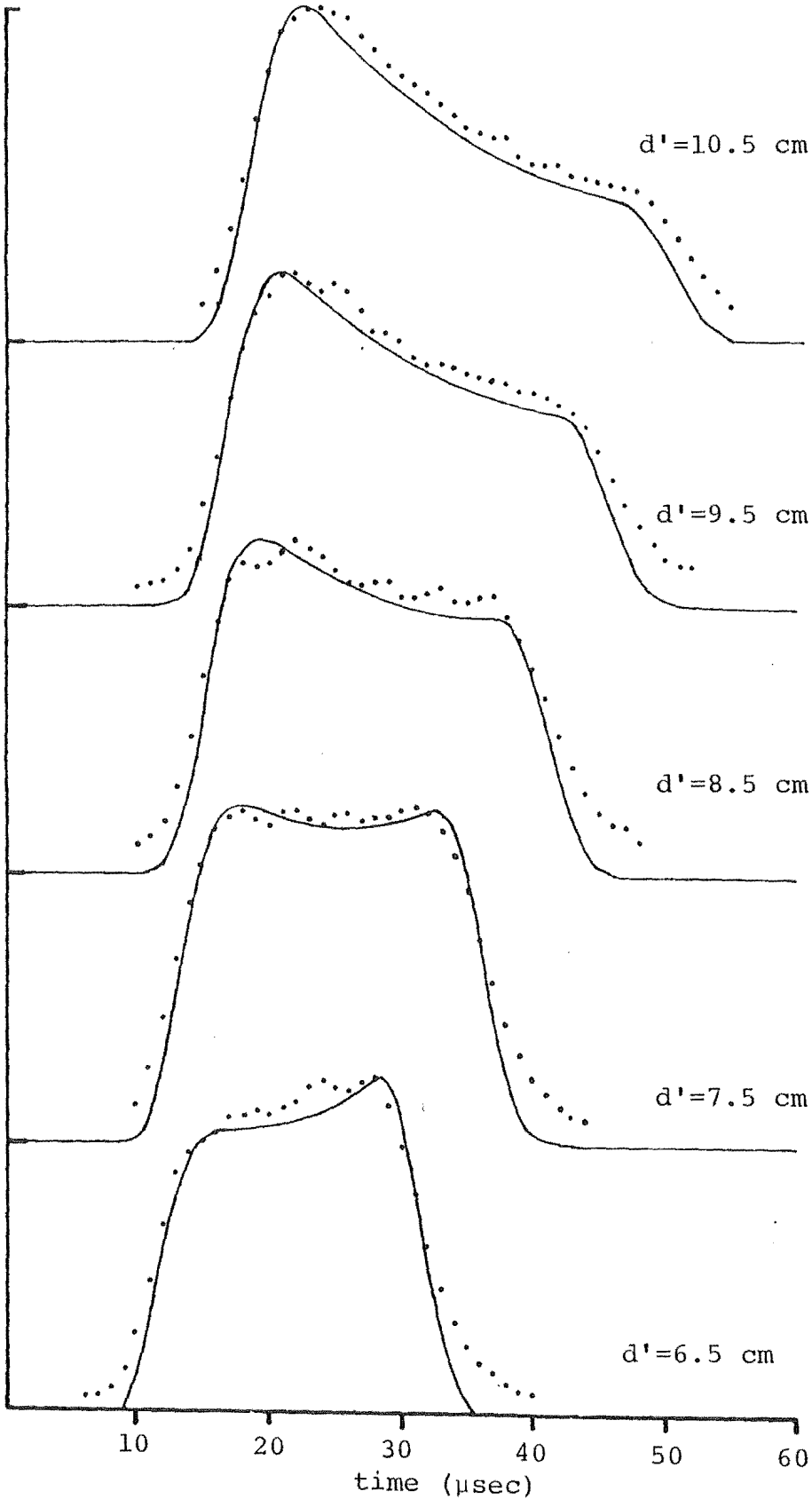

Figure 5.13 Calculated and experimental ATDs for O^+ in 0.045% O_2/He for a range of short distances (100 Td, 0.4 Torr; $K_O(O^+)=20.5$ $cm^2V^{-1}s^{-1}$; $K_O(He^+)=7.67$ $cm^2V^{-1}s^{-1}$)

optimal in almost all cases. The calculated and experimental ATDs for a 0.04% mixture of HCN in helium at 0.4 Torr and 80 Td are presented in fig.5.14 for a range of effective distances (d′) from 5.5 to 10.5 cm (geometric distances from 3.87 to 8.87 cm). The mobility for CN^+ of 16.3 $cm^2V^{-1}s^{-1}$ and distance correction of 1.63 cm remain unchanged throughout. Literature rate coefficients[7,8] of $3.9X10^{-9}$ $cm^3molec^{-1}s^{-1}$ for reaction 5.1 and $3.1X10^{-9}cm^3molec^{-1}s^{-1}$ for reaction 5.2 were used.

To further assess the reliability of this curve fitting procedure a series of experiments were conducted where the total pressure was varied with the drift distance remaining constant. For a 0.07% mixture of HCN in helium at 100 Td and an effective distance (d′) of 10.5 cm (geometric distance of 8.87 cm) the pressure was increased from 0.1 to 0.5 Torr in 0.1 Torr steps and ATDs collected. These were then compared with ATDs calculated using $K_o(CN^+)$= 15.3 $cm^2V^{-1}s^{-1}$ and rate coefficients as above. The results are presented in fig.5.15, a close fit is obtained for all but the lowest pressure of 0.1 Torr. At this pressure the electric field strength required to maintain an E/N of 100 Td was only 3.33 Vcm^{-1} so the drift tube field would be more sensitive to perturbations arising from intruding source and exit component fields and contact potentials than at the higher pressures normally used. The disparity is therefore believed to be of little significance.

The mobilities of CN^+ derived with this curve fitting procedure are shown graphically in fig.5.16. The uncertainty of 5% estimated for the results extracted from t-z plots appears to be reasonable for this curve fitted

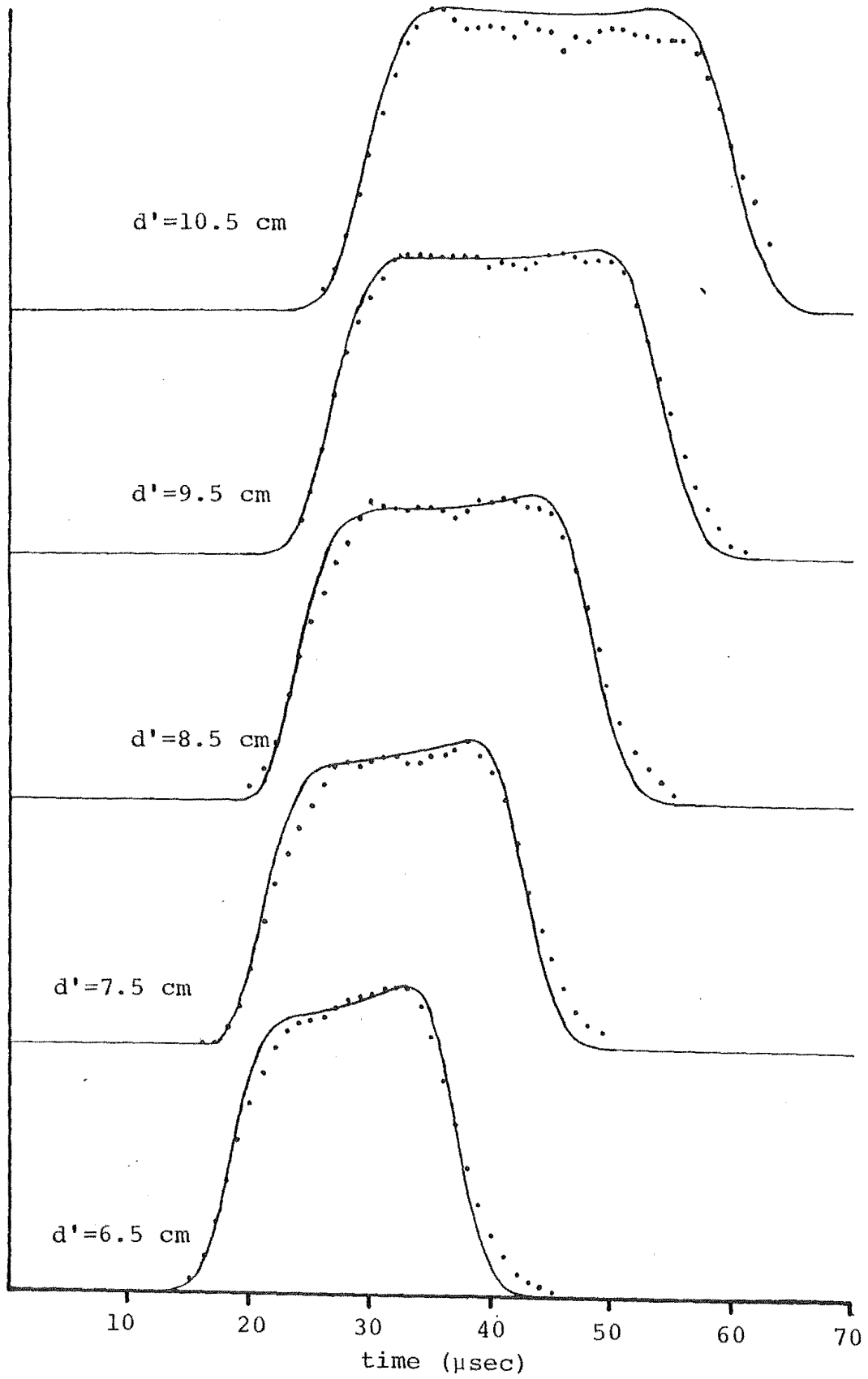

Figure 5.14 Calculated and experimental ATDs for CN^+ in 0.04% HCN/He for a range of source distances (80 Td, 0.4 Torr, 293K; $K_o(He^+)=8.12\ cm^2V^{-1}s^{-1}$, $K_o(CN^+)=16.3\ cm^2V^{-1}s^{-1}$)

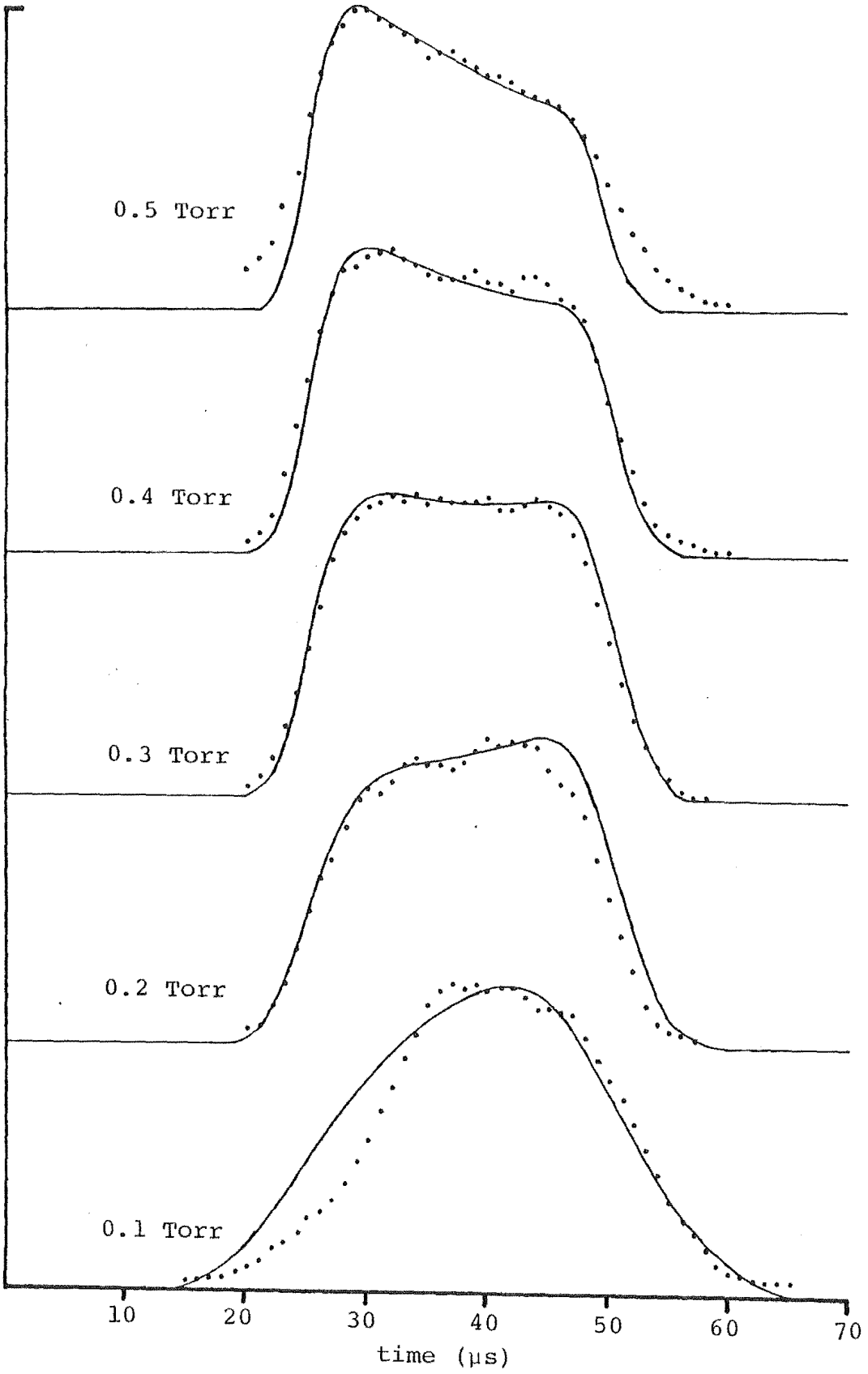

Figure 5.15 Calculated and experimental ATDs for CN^+ in 0.07% HCN/He for a range of drift tube pressures (100 Td, d'=10.5 cm, 290K; $K_o(He^+)$= 7.67 $cm^2V^{-1}s^{-1}$, $K_o(CN^+)$=15.3 $cm^2V^{-1}s^{-1}$)

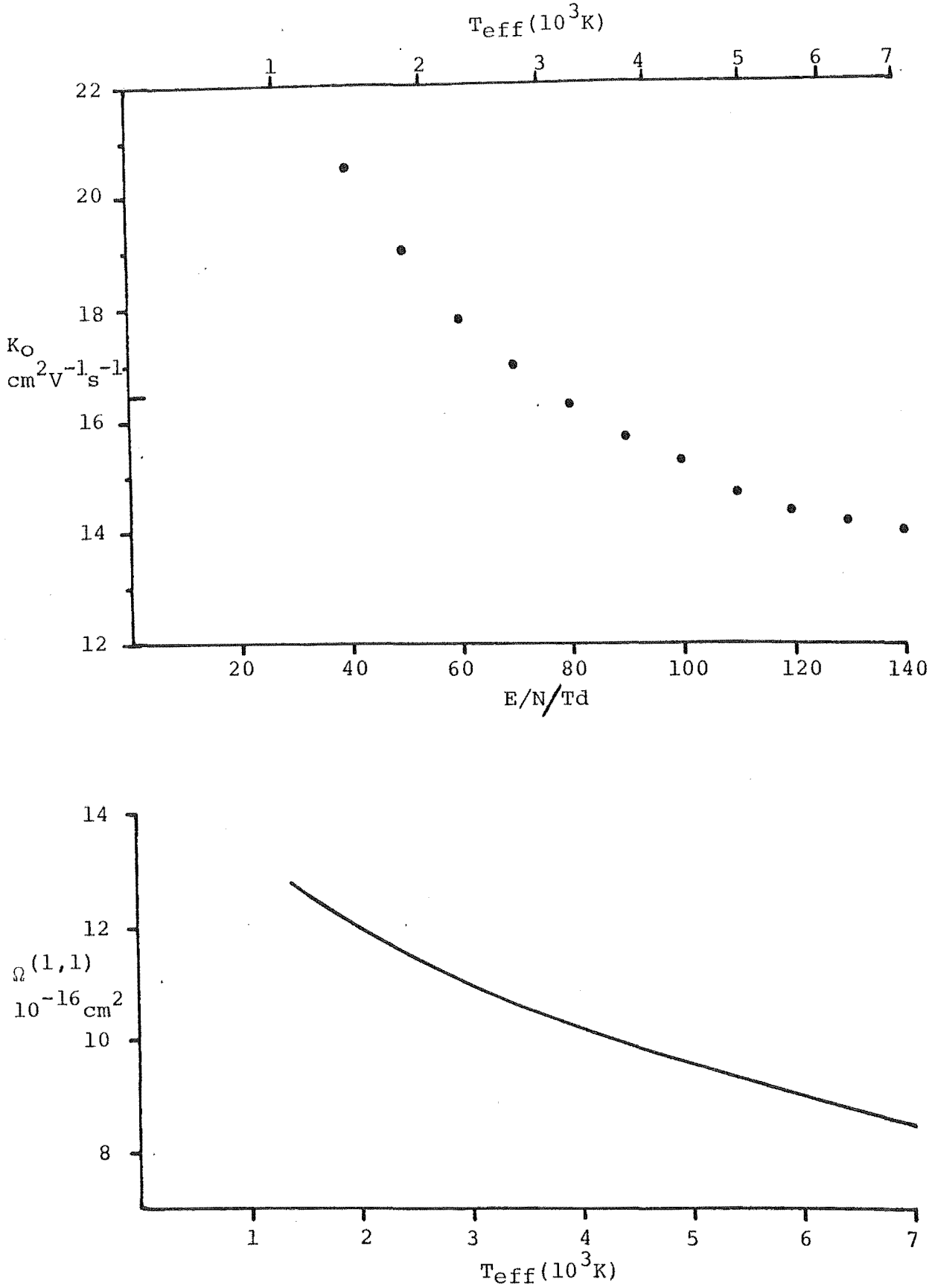

Figure 5.16 Mobilities and momentum transfer collision integrals for CN^+

data too. The momentum transfer collision integral calculated as a function of T_{eff} is also presented.

(vi) Measurement of Negative Ion Mobilities: CN^-

Reversal of the polarity of all power supplies (except those involved with the electron impact source) within the drift tube mass spectrometer allows negative ion signals to be detected. However, in practice determination of negative ion mobilities is somewhat more difficult than for positive ions.

Primary negative ion formation occurs by two main processes: associative and dissociative electron attachment. Associative attachment involves the capture of a near thermal electron to form a molecular negative ion:

$$AB + e^-(\sim 0eV) \rightleftharpoons (AB^-)^* \qquad -(5.10)$$

The resulting AB^- anion contains all the exothermicity of its formation; if the pressure is sufficiently high for this to be rapidly dissipated by collision as is possible in the drift tube then this ion will be stabilised. Dissociative attachment involves the capture of low energy electrons with subsequent fragmentation of AB^-:

$$AB + e^-(\text{low eV}) \rightarrow A^- + B \qquad -(5.11)$$

The electron energy must be within a narrow resonance range (typically 1-3 eV) for the dissociative attachment cross section to be significant. Both of these attachment processes typically have cross sections two or three orders of magnitude lower than the corresponding positive ion formation processes. Electrons of ca.90eV energy are emitted

in the drift tube in order to penetrate the buffer gas and formation of negative ions under these circumstances relies on the low energy electrons generated by inelastic scattering or secondary electrons from positive ion formation.

Most positive ions of interest are formed in the drift tube primarily by chemical ionization i.e. reaction of buffer gas (helium) ions with the appropriate trace additive. Only a very small proportion result from direct electron impact. On the other hand, with a buffer that does not have a positive electron affinity and therefore cannot form stable negative ions itself, all the desired negative ions must be produced directly from electron impact of the trace neutral. This was the case for the present experiments performed in a helium buffer.

Mixtures of 0.1% HCN in helium were studied in the negative ion mode in an attempt to observe CN^-. The ion signals detected were close to the background level and were noisier than positive ion signals due to the presence of electrons. The signal level was raised by increasing the HCN mixture composition to 1% for experiments conducted at a total drift tube pressure of 0.15 Torr. The lower total pressure was necessary with the higher partial pressure of HCN to prevent rapid deterioration of the electron gun filament. When a corresponding experiment was attempted with cyanogen the emission was extremely low and the filament expired after several minutes.

The CN^- ion, formed by dissociative electron attachment to HCN;

$$HCN + e^- \rightarrow CN^- + H \qquad -(5.12)$$

and an ion of m/z=42 presumed to be CNO^- formed by reaction of CN^- with background traces of H_2O and O_2 were the only ions detected. Mobilities of CN^- were measured over the range of E/N from 30 to 160 Td with 1% mixtures of HCN in helium at 0.15 Torr. As shown in fig.5.17 the results are far more scattered than for any of the positive ions studied. Low ion signals and interference from the background of electrons are thought to be largely responsible for the poor reproducibility between measurements. The t-z plots exhibited a high degree of linearity, however, and data points recorded at short distances (2-3 cm) did not show the deviation from the overall slope evident with positive ions formed by charge transfer reactions.

The graph of fig.4.3 predicts a systematic error of 6-12% due to interaction of the CN^- with neutral HCN in accordance with Blanc's Law. A correction of 10% has been added to the experimental mobilities as an estimated compensation for the Blanc's Law deviation. Effective temperatures have been calculated using drift velocities derived from these "corrected" mobilities and momentum transfer collision integrals derived from these values of T_{eff} are presented in the lower graph of fig.5.17. Even with the addition of an extra 10% the mobility of CN^- is notably less than of CN^+ at a given E/N and the momentum transfer collisions integrals are correspondingly larger. Perusal of tables of ion mobilities[13,14] reveals that this is a fairly typical result for ion transport in helium e.g. $K_o(0^+)=24.5\ cm^2V^{-1}s^{-1}$, $K_o(0^-)=19.8\ cm^2V^{-1}s^{-1}$ in helium at 50 Td. Another difference is that negative ion mobilities continue to rise as E/N tends to zero whereas positive ions

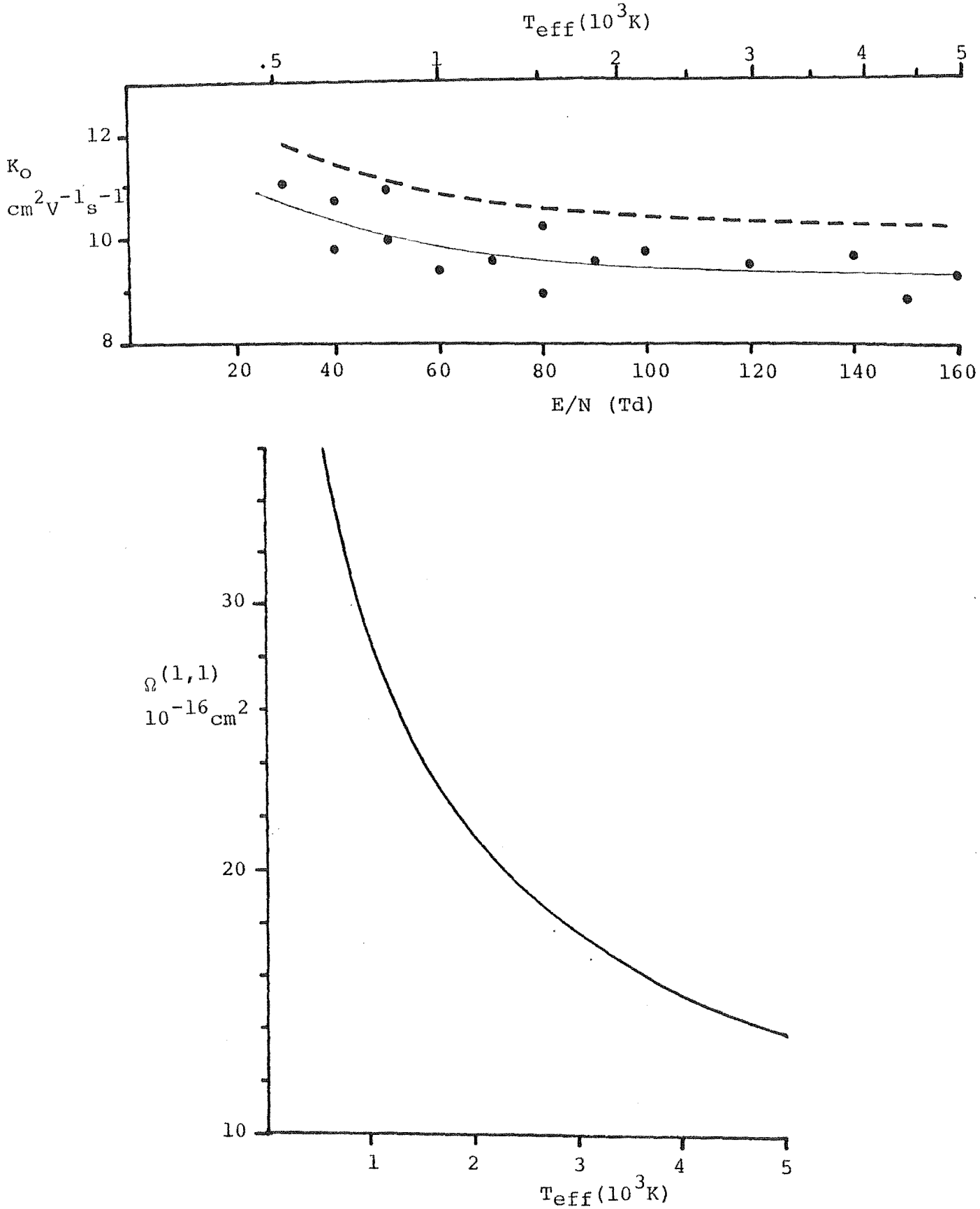

Figure 5.17 Mobilities and momentum transfer collision integrals for CN^-

normally exhibit a maximum between 10-30 Td. The mobility of CN^- in helium is less than that of all the larger and more massive positive ions studied. The differences between positive and negative ions in the behaviour of mobility as a function of E/N reflects differences in the ion-neutral interaction potential. Although the long range attractive potentials would be similar (same "polarization limit"), the short range interelectronic repulsion energy (B/r^n in Eq.2.20) would be more significant with negative ions.

More refinement in technique is required before negative ion mobilities can be as routinely measured as those of positive ions. The ability to contain a gas in the ion source separate from the buffer in the remainder of the drift tube, a facility for which some provision has been made with the present instrument, would be a considerable advantage. A high concentration of negative ion precursor neutral could then be ionized in the source without the consequent reduction in mobility due to interaction of ions with this neutral during transit of the drift tube. The formation of ions by electrons drifting through the buffer might be controlled by the application of a blocking pulse on the source optics during and for 1-2 μs following the operation of the electron gun. During the additional period electrons would be lost by contact with the source extremities but most of the far slower moving ions would remain.

(vii) Discussion

The mobilities of several ions containing the -CN group have been determined. Derivation of the mobility from the slope of a plot of arrival time maxima against distance has been demonstrated to yield reproducible and reliable results using the drift tube described in this thesis. For CN^+ where this method could not be readily applied an alternative technique of matching calculated and experimental ATDs by treating the mobility as a variable parameter yields results of comparable accuracy.

The calculated "polarization limits" (Eq.2.21) of the mobility for the ions studied is marked along the vertical mobility axes. The mobilities of most of the ions studied tend to a value close to this limit at low E/N. The mobility variation with E/N is in all cases, typical of positive ions drifting in helium with a maximum between 10-40 Td followed by a decrease in mobility with increasing E/N. As evident from Table 5.3 at a given E/N or effective temperature the mobilities are inversely related to the order of mass and size of the ions.

Table 5.3 Reduced mobilities of ions at 50 Td and 1500K ($cm^2V^{-1}s^{-1}$)

Ion m/z	26	27	28	38	39	41	52
K_o(E/N=50Td)	19.0	18.0	16.1	15.7	14.6	13.6	13.6
$K_o(T_{eff}=1500K)$	20.5	19.4	16.1	15.5	14.0	12.9	12.8

Marked mobility decreases are seen when the size of an ion increases due to additional protons e.g. compare HCN^+, m/z=27, and H_2CN^+, m/z=28, or $C_2H_3N^+$, m/z=41, which has the

same mobility as heavier ion $C_2N_2^+$, m/z=52. That the mobility variations with E/N of all ions exhibit such predictable behaviour is an indication that a similar type of interaction determines the mobility throughout.

The extension of the t-z plot technique to buffers other than helium would not necessarily be straightforward. Rate coefficients for charge transfer from He^+ are very fast due to the large exothermicity involved; with other buffers lower rates could result in all ATDs having to be analysed by the fitting procedure adopted above for CN^+ in helium. However, mobilities are much lower in heavier buffers than in helium so the total time involved would be correspondingly longer. Preliminary investigations of ArH^+ (produced by reaction of Ar^+ with background water) in argon showed a very broad arrival time distribution. The ion signals were lower in argon and very much smaller in neon compared to helium. As was suggested for negative ion studies, mobility measurements in these buffers might be facilitated by the ability to maintain different gas compositions in the ion source and drift regions.

CHAPTER 6

RESULT II: MOBILITIES OF ISOMERIC IONS

(i) Introduction

The use of mobility measurements to detect structural differences between ions of equal mass and empirical formula was mentioned in the previous chapter. It might well be expected that each isomeric structure has a characteristic mobility; determination of the mobility for an isomer of unknown structure could then lead to its identification by comparison with the mobilities for isomers of known structure. Rearrangements could be inferred from the observation of identical mobilities.

Three main groups of techniques are currently employed for the discrimination of isomeric ion structures: collision induced dissociation (CID), appearance potential measurements and studies of ion-molecule reactions.

Collision induced dissociation or collisional activation (CA) spectra[11] are recorded using a double focussing mass spectrometer with reverse geometry. Ions of chosen m/z are selectively transmitted using the magnetic analyser into the field free region between analysers. A collision cell maintained at a pressure of $\sim 10^{-4}$ Torr of inert buffer gas in this region results in ion-neutral collisions in which some of the ion kinetic energy is converted into internal energy. The resulting ion decomposition products are then identified by scanning the electrostatic analyser. The interpretation is similar to that developed for unimolecular metastable

ion spectra. Normally CID spectra are insensitive to the previous internal energy of the mass analysed ion[11] but this is not always the case.[70] Also, the collisionally activated ion may isomerize prior to decomposition.

Appearance potential measurements[12] attempt to determine the lowest energy for which an ion formation process can occur. The heat of formation of the ion may then be deduced from thermodynamic considerations. Problems with these techniques include the possibility of the ion being formed with excess kinetic energy, the need to know the heats of formation of all other species involved in the ion formation process and lack of monoenergicity where ionization is by electron impact.

Scrutiny of ion-molecule reaction data can provide structural information. Isomeric ions may react at different rates, produce different product ratios or a selected reaction may be thermodynamically unfavourable for some isomers. Variation of the internal energy of an ion can produce similar changes in reaction parameters however, so inferences must be made cautiously.

Comparison of mobilities of isomeric ions could usefully supplement the above techniques. Since the ions are "thermalised" to the effective temperature of the drift field no ambiguities arise due to variations in internal energy. This method could be most readily applied to a flow drift tube apparatus[4] which may be used to study ion-molecule reactions and to perform mobility measurements. Ions produced by selected reactions upstream of the drift region could be "mobility analysed" to provide structural information.

An obvious complication with this proposed technique is that mobilities for different isomers may appear the same, either fortuitously or because factors influencing mobility such as ion size and charge distribution differ insufficiently to provide a mobility difference measurable within the resolution of the drift apparatus. To explore these possibilities ions from a variety of isomeric organic compounds were studied in the drift tube.

(ii) Mobilities of $C_3H_6^+$ and $C_3H_3^+$

The drift tube was charged with mixtures of 0.1% propene, $CH_3-CH=CH_2$, or cyclopropane, $\overbrace{CH_2CH_2CH_2}$, in helium to a total pressure of 0.4 Torr at 293K. Charge transfer from He^+ produced predominantly ions of m/z=38,39 ($C_3H_2^+$, $C_3H_3^+$) with both precursors and, in addition, m/z=37 (C_3H^+) with propene. Subsequent reaction gave ions of m/z=41 ($C_3H_5^+$) and the parent ion, m/z=42 ($C_3H_6^+$), with both hydrocarbon neutrals.

Mobilities of $C_3H_6^+$ and $C_3H_3^+$ were determined from the slopes of t-z plots. The results are presented in figs.6.1 and 6.2 respectively, where different symbols indicate the corresponding precursor neutrals. No significant differences are discernable between the mobilities of the $C_3H_3^+$ ions from either precursor or of the $C_3H_6^+$ ions from either precursor. This is perhaps surprising since the spatial properties would differ considerably for ions formed from these respective neutrals in the absence of rearrangement. A reasonable conclusion would be, therefore, that rearrangement does in fact occur during ionization to form the linear $CH_3-CH=CH_2^+$ structure for $C_3H_6^+$ and the cyclic

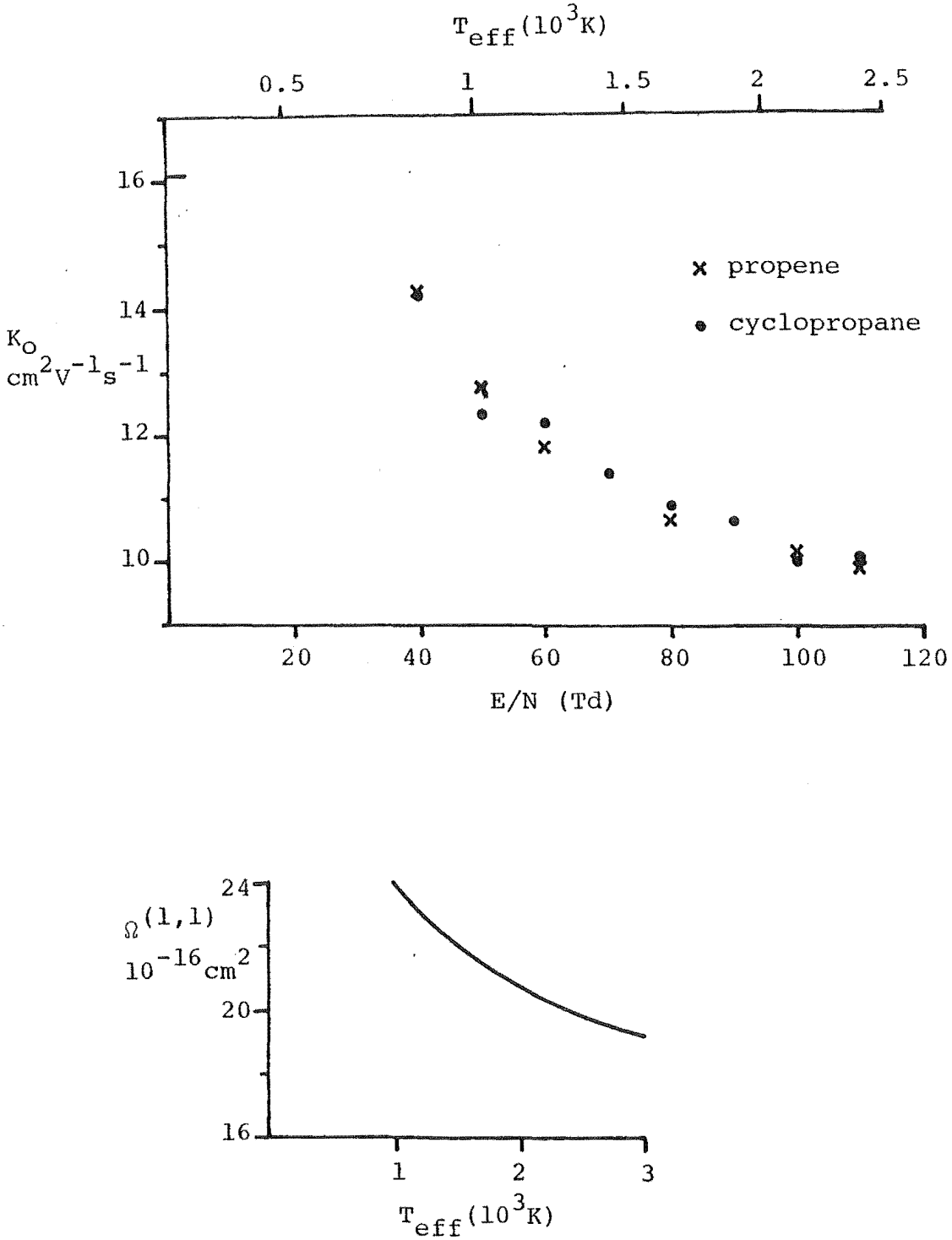

Figure 6.1 Mobilities and momentum transfer collision integrals for $C_3H_6^+$ ions from propene and cyclopropane

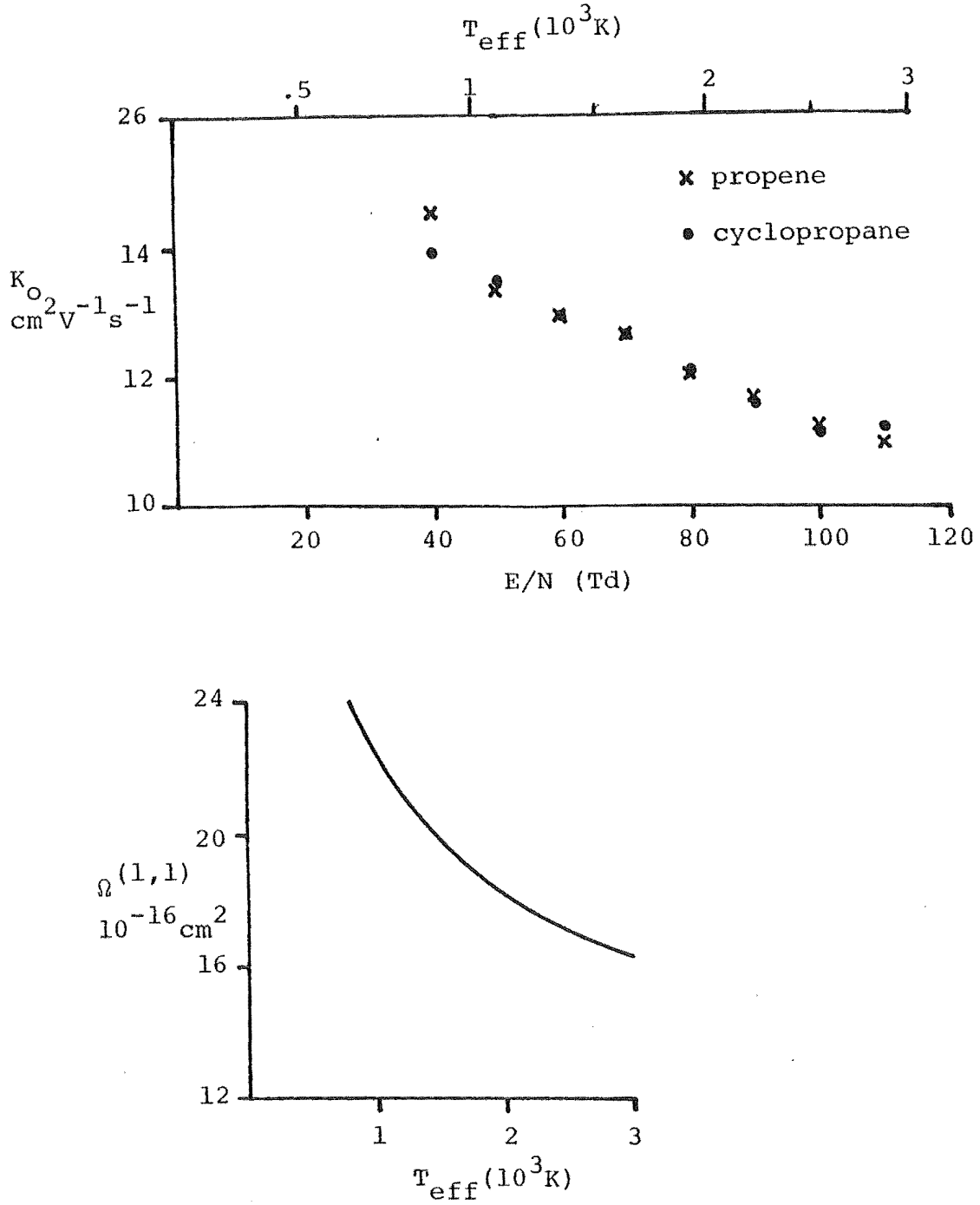

Figure 6.2 Mobilities and momentum transfer collision integrals for $C_3H_3^+$ ions from propene and cyclopropane

structure with $C_3H_3^+$ irrespective of the precursor molecule. These inferences are supported by a variety of experimental and theoretical evidence.

Appearance potential measurements[52] indicate that the linear propene structure for $C_3H_6^+$ is approximately 40 $kJmol^{-1}$ lower in energy than the cyclic structure and it has been established from ion-molecule reaction studies that these two types of $C_3H_6^+$ ions can be distinguished on the basis of their reactivity with NH_3.[71] The cyclo-$C_3H_6^+$ ion reacts to produce predominantly $CH_3NH_2^+$ product whereas $CH_3CHCH_2^+$ reacts exclusively by proton transfer to form NH_4^+. This method of distinction has been employed in ion cyclotron resonance (ICR) studies.[72,73] Approximately 60% of the $C_3H_6^+$ ions formed from cyclopropane were found to have the linear propene structure for electron impact ionization above 13eV.[72] Formation of $C_3H_6^+$ from cyclopropane by charge transfer reactions produced an increasing proportion of CH_3-CH=CH_2^+ as the recombination energy of the precursor ion was increased.[73] The barrier to isomerisation was estimated to be in the range 1.3-1.7eV from these results. It is therefore likely that charge transfer from He^+ produces mainly the lower energy linear CH_3-CH=CH_2^+ ion irrespective of the precursor neutral molecule.

The heat of formation of the $C_3H_3^+$ ion produced from a range of three and four carbon unsaturated hydrocarbon molecules and radicals was determined from appearance potentials measured using a monoenergetic electron source.[74] A value of 1075±15 $kJmol^{-1}$ ascribed to the cyclopropenyl structure (A) was obtained for all precursors except the propargyl radical ($\cdot CH_2$-C≡CH) for which a value of

1175 $kJmol^{-1}$ was obtained. The ion produced in the latter case is believed to retain the propargyl structure (B)

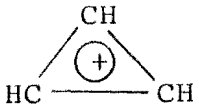

(A)

$$H_2C{=}{=}C{\equiv}CH^+$$

(B)

which theoretical calculations[75] estimate to be 130 $kJmol^{-1}$ higher in energy than structure (A). The greater stability of the cyclopropenyl structure (A) is not unexpected since (A) is the simplest case (n=0) of a Hückel (4n+2) π-electron system. Subsequent work[76,77] has demonstrated that the propargyl structure (B) may be formed only from 1-iodopropyne and propargyl iodide by electron impact close to threshold[76] or in conjunction with (A) (up to 60% of total $C_3H_3^+$) from propargyl chloride and propargyl bromide by charge transfer provided the reaction is not too exothermic.[77] Therefore, the $C_3H_3^+$ ion formed from propene by He^+ charge transfer almost certainly adopts the cyclopropenyl structure (A).

(iii) Mobilities of $C_2H_4O^+$ and $C_2H_5O^+$

Ethylene oxide (oxirane, $\overbrace{CH_2\text{-}CH_2\text{-}O}$), ethanol ($C_2H_5OH$) and dimethyl ether ($CH_3OCH_3$) were used as trace additives to produce ions of m/z=44 and 45 of empirical formula $C_2H_4O^+$ and $C_2H_5O^+$, respectively. Mixtures of 0.1% in helium (0.2% for ethanol) were admitted to the drift tube to a total pressure of 0.4 Torr at 293K. Ionization and subsequent reaction produced a prominent peak at m/z=45 ($C_2H_5O^+$) for all precursor neutrals, corresponding to the parent ion minus one H for ethanol and dimethyl ether and

the protonated parent ion for ethylene oxide. The signal at m/z=44 ($C_2H_4O^+$) corresponded to the largest peak from ethylene oxide (parent ion). The m/z=44 peak from ethanol was of lower cross-section but still of sufficient intensity for mobility measurements. The m/z=44 signal from dimethyl ether proved to be too low to afford reliable mobility measurements.

The mobilities of $C_2H_4O^+$ ions from both ethylene oxide and ethanol are presented in fig.6.3 and a 10-15% difference is evident between ions formed from these precursors. The data represent the amalgamation of results collected over several months using different gas mixtures so the possibility of systematic error between measurements for different precursors is eliminated. The upper T_{eff} scale applies to the ions from ethanol and the lower to those from ethylene oxide. Momentum transfer cross sections for each ion are displayed in the lower graph calculated as a function of the appropriate effective temperature.

A considerable amount of effort has been employed both experimentally and theoretically to determine the structure of $C_2H_4O^+$ ions. Four structures are presented for discussion corresponding to the molecular ions of vinyl alcohol (A), acetaldehyde (B) and ethylene oxide (C) and a C-C ring opened ethylene oxide (D). The first three structures have been distinguished as non-interconverting

$CH_2=CH-OH^+$ (A)

$CH_3-CH=O^+$ (B)

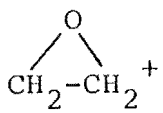
(C)

$CH_2-O-CH_2^+$ (D)

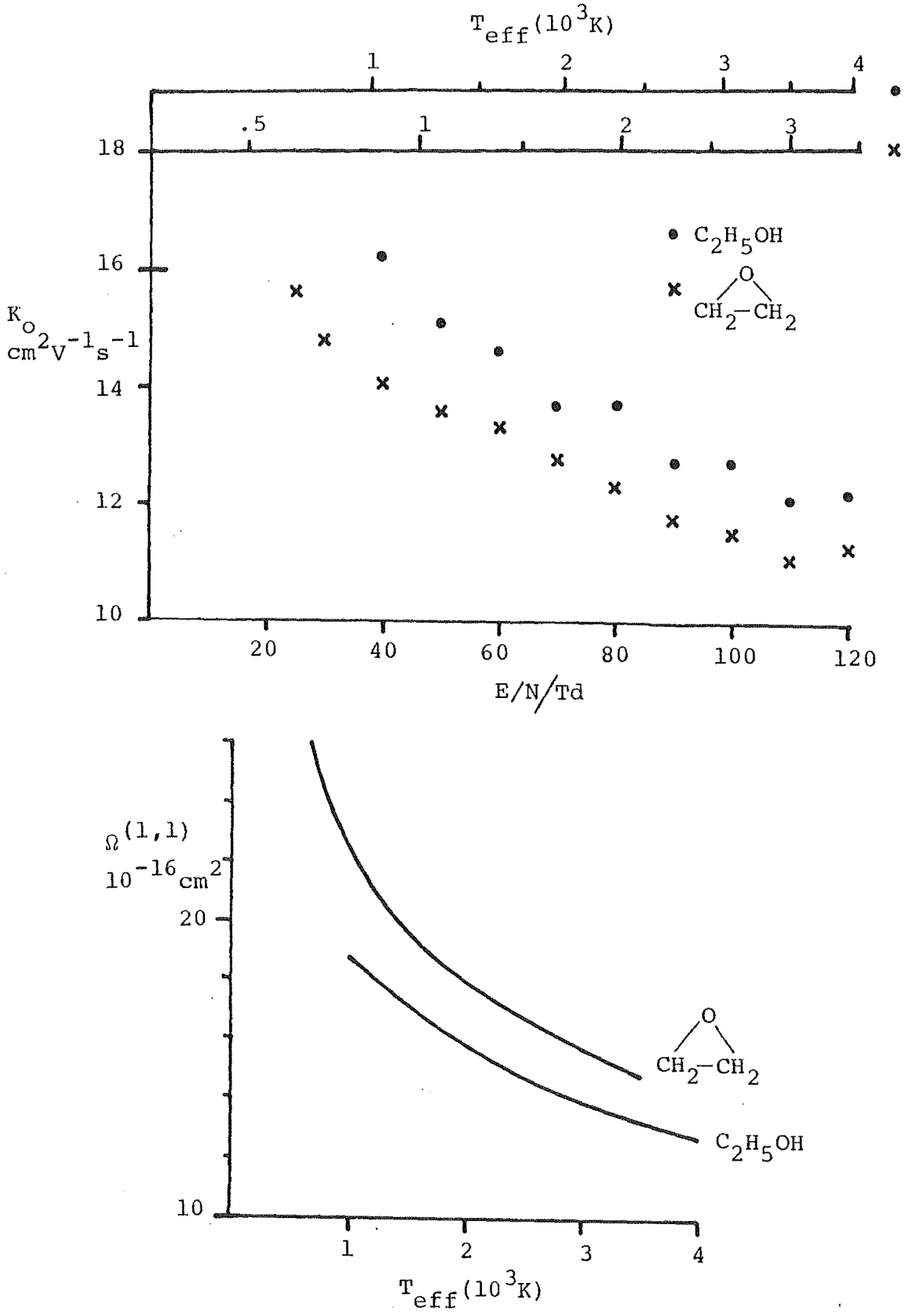

Figure 6.3 Mobilities and momentum transfer collision integrals for $C_2H_4O^+$ ions from ethanol and ethylene oxide

species by a collisional activation study.[78] A metastable ion study[79] reported the observation of transitions corresponding to decompositions of these three isomers and suggested that the m/z=44 ion from 1,2-dimethoxyethane ($CH_3OCH_2CH_2OCH_3$) might be a forth isomer. The heats of formation of (A), (B), (C) and (D) were determined by appearance potential measurements of a range of carboxy compounds using a monoenergetic ion source.[80] The heat of formation of the $C_2H_4O^+$ ion from ethanol was consistent with the vinyl alcohol structure (A). An ion-molecule reaction study[81] reported reactions of an "activated" ethylene oxide ion derived from the ethylene oxide molecular ion. Two ICR studies[82,83] both proposed that this reactive $C_2H_4O^+$ isomer from ethylene oxide is the C-C ring opened structure (D). Finally, an ab initio molecular orbital study[84] calculated total and relative energies of structures (A)-(D) and several other alternative $C_2H_4O^+$ structures. The barrier to conversion of the closed ethylene oxide structure (C) to the more stable C-C ring opened form (D) was estimated to be 105-120 $kJmol^{-1}$. The results of some of these studies are summarised in Table 6.1.

Table 6.1 Experimental and theoretical energies ($kJmol^{-1}$) for $C_2H_4O^+$ isomers

Isomer	Experimental Energies[80] ΔH_f	Relative	Relative ab initio energy[84]
A	757	0	0
B	820	63	52.3
C	967	209	182.6
D	858	101	124.9

On the basis of the above results the $C_2H_4O^+$ isomer from ethanol would be expected to exist as the vinyl alcohol structure (A) and that from ethylene oxide would be the C-C ring opened structure (D). The exothermicity of the reaction of He^+ with ethylene oxide of 1460 $kJmol^{-1}$ calculated as the difference in ionization potentials[43,80] is vastly in excess of the energy estimated for ring opening. Structure (D) has also been generated from 1,3-dioxolane,[80] which has a prominent fragment at m/z=44; the measurement of mobilities for this ion would therefore be of interest in relation to the above assignment.

Mobilities and momentum transfer collision integrals of $C_2H_5O^+$ ions from both ethanol and dimethyl ether are presented in fig.6.4. The upper T_{eff} scale applies to ions from ethanol and the lower to ions from dimethyl ether. A consistent and reproducible 3-6% difference is discernible between the mobility data determined for the $C_2H_5O^+$ ion produced from dilute mixtures of ethanol in He and from dimethyl ether in He.

Four possible structures for the $C_2H_5O^+$ ion are given below. Results of experimental and theoretical[85]

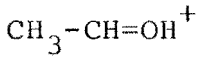

(A)

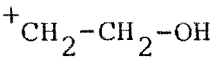

(B)

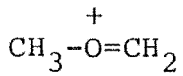

(C)

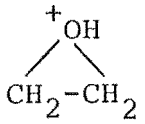

(D)

investigations are presented in Table 6.2. On the basis of

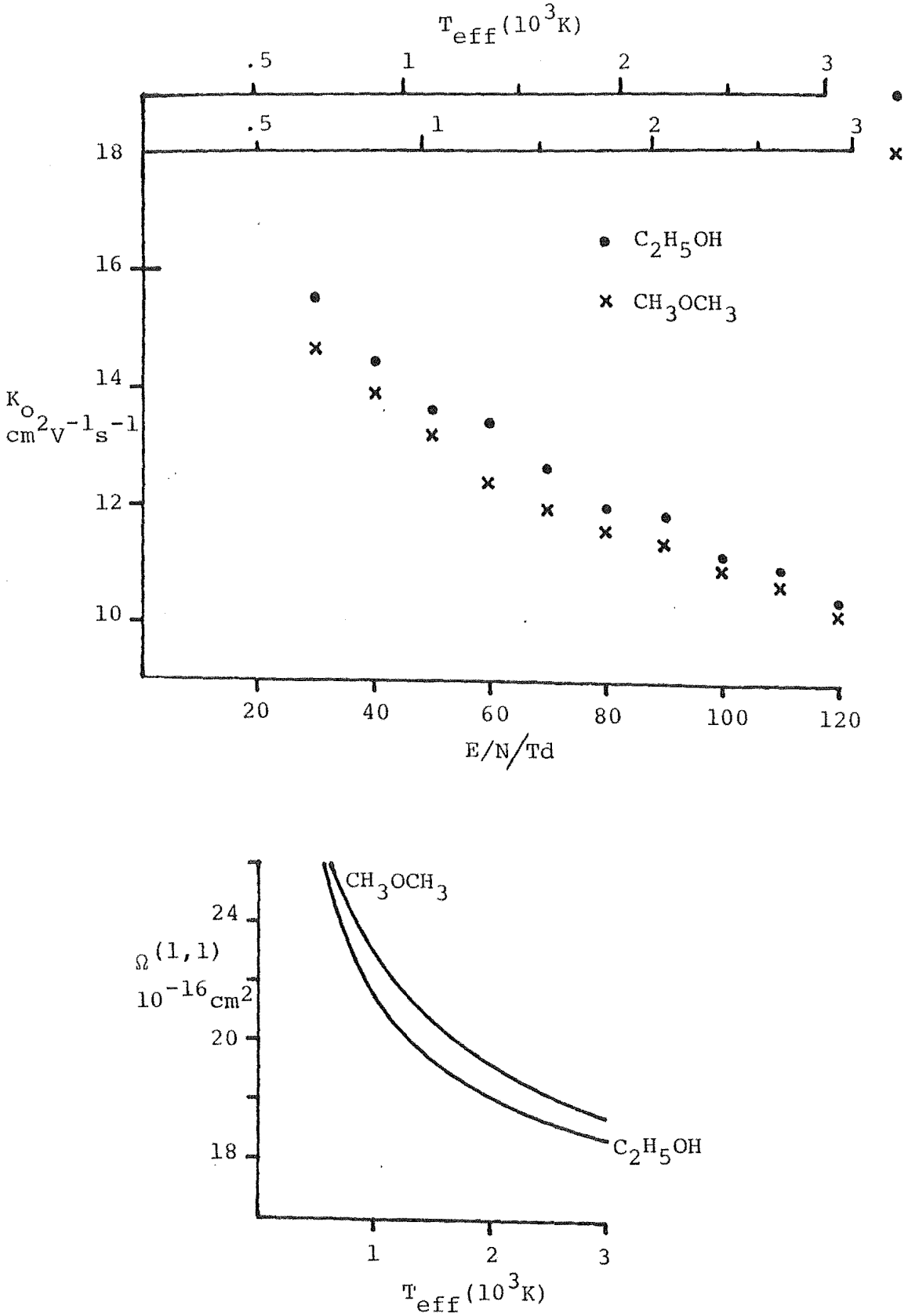

Figure 6.4 Mobilities and momentum transfer collision integrals for $C_2H_5O^+$ ions from ethanol and dimethyl ether

Table 6.2 Experimental and theoretical energies for $C_2H_5O^+$ ions ($kJmol^{-1}$)

Structure	Experimental Energies ΔH_f^o	Relative	Ref.	Calculated Energy (Relative)
A	598	0	(86)	0
B	-	-	-	182
C	661	63	(87)	-
D	707	109	(88)	132

the above results the protonated acetaldehyde structure (A) has been assigned to the $C_2H_5O^+$ ion derived from ethanol and structure (C) is believed to represent the isomer from dimethyl ether. The measurement of the mobilities of protonated ethylene oxide would be of interest to see if the ring structure is preserved and a third set of mobilities are obtained.

Note that a similar trend in mobilities exists for both $C_2H_4O^+$ and $C_2H_5O^+$; in both cases the C-O-C structure has a higher momentum transfer collision integral ($\Omega^{1,1}$) than the C-C-O structure. This may be rationalized by recognizing that each terminal carbon atom has at least two hydrogen atoms projecting outward from each end whereas there is only one for a terminal oxygen. Thus the magnitude of $\Omega^{(1,1)}$ merely reflects the spatial volume and hence the collision cross section of the ions.

(iv) Conclusion

It has been demonstrated that comparison of ion mobilities is a viable technique for the discrimination of isomeric ion structures. Differences of 5% may readily be

observed with the present apparatus. Alternatively, evidence may be obtained for suspected rearrangements to give equivalent structures.

The formation of ions by charge transfer from He^+ with its high exothermicity can result in isomerization of product ions to yield only the most thermodynamically stable structures. Formation of ion by less energetic processes would be expected to provide a means of characterizing a wider selection of ion structures. Buffers of lower ionization potential or separation of source and drift regions as discussed in the conclusion to Chapter 5 would prove useful in this respect.

ACKNOWLEDGEMENTS

First and foremost I wish to express my sincere thanks to my supervisor Dr P.W. Harland for his continual direction and motivation throughout the course of this work. I would also like to thank Mr N.R. Thomas for preparation of compounds and assistance with data collection for the work described in Chapter 6.

Acknowledgement is also due to the Physics and Engineering Laboratory of the DSIR for the machining of the drift tube. Furthermore, I would like to express my appreciation of the extensive technical assistance provided by Chemistry Department staff. In particular, I wish to thank Mr K.M. Gillard for his assistance with modifications to the drift tube and Mr G. Collins and Mr R.A. Loeffen for construction and maintenance of electronic equipment and the computer interface, respectively.

REFERENCES

(1) L.A. Viehland and E.A. Mason, Ann.Phys. (N.Y.) 91, 499 (1975); Ann.Phys. (N.Y.) 110, 287 (1978).

(2) R.M. Snuggs, D.J. Volz, I.R. Gatland, J.H. Schummers, D.W. Martin and E.W. McDaniel, Phys.Rev. A 3, 487 (1971).

(3) S.B. Woo and J.H. Whealton, Phys.Rev. 180, 314 (1969); Phys.Rev. A 1, 1558.

(4) M. McFarland, D.L. Albritton, F.C. Fehsenfeld, E.E. Ferguson and A.L. Schmeltekopf, J.Chem.Phys. 59, 6610,6620,6629 (1973).

(5) E.W. McDaniel and E.A. Mason, "The Mobility and Diffusion of Ions in Gases", Wiley, New York (1973). (5a) p.118; (5b) p.315; (5c) p.36; (5d) p.76; (5e) p.12.

(6) E.W. McDaniel, J.Chem.Phys., 52, 3931 (1970).

(7) M.J. McEwan, V.G. Anicich, W.T. Huntress Jr., P.R. Kemper and M.T. Bowers, Int.J.Mass Spectrom. Ion Phys., 50, 179 (1983).

(8) J.P. Liddy, C.G. Freeman and M.J. McEwan, Mon.Not.R.Astr. Soc., 180, 683 (1977).

(9) E. Herbst and W. Klemperer, Astrophys.J., 185, 505 (1973).

(10) W.T. Huntress and V.G. Anicich, Astrophys.J., 208, 237 (1976).

(11) F.W. McLafferty, R. Kornfeld, W.F. Haddon, K. Levsen, I. Sakai, P.F. Bente III, S.C. Tsai and H.D.R. Schuddemage, J.Am.Chem.Soc., 95, 3886 (1973).

(12) H.M. Rosenstock, Int.J.Mass Spectrom.Ion Phys., 20, 139 (1976).

(13) H.W. Ellis, R.Y. Pai, E.W. McDaniel, E.A. Mason and L.A. Viehland, At.Data Nucl.Data Tables, 17, 177-210 (1976).

(14) H.W. Ellis, E.W. McDaniel, D.L. Albritton, L.A. Viehland, S.L. Lin and E.A. Mason, At.Data Nucl.Data Tables, 22, 179-217 (1978).

(15) L.G.H. Huxley, R.W. Compton and M.T. Elford, Bull.Inst. Phys.Physical Soc., 17, 251 (1966).

(16) G.H. Wannier, Bell System Tech.J., 32, 170 (1953); Phys.Rev., 83, 281 (1951); Phys.Rev., 87, 795 (1952).

(17) R.D. Present, "Kinetic Theory of Gases", McGraw Hill, New York (1958).

(18) E.A. Mason and H. Hahn, Phys.Rev., A5, 438 (1972).

(19) L.A. Viehland, Spec.Per.Rep., 6, 84 Royal Soc.Chem. (London) (1981).

(20) T. Kihara, Rev.Mod.Phys., 25, 844 (1953).

(21) E.A. Mason and H.W. Schamp, Ann.Phys. (N.Y.) 4, 233 (1958).

(22) L.A. Viehland, S.L. Lin and E.A. Mason, Chem.Phys., 54, 341 (1981).

(23) L.A. Viehland and E.A. Mason, J.Chem.Phys., 66, 422 (1977).

(24) D.L. Albritton in "Kinetics of Ion-Molecule Reactions" ed. P. Ausloos, Plenum Press, New York (1979).

(25) L.A. Viehland and E.A. Mason, J.Chem.Phys., 63, 2913 (1975).

(26) H.R. Skullerud, J.Phys. B 9, 535 (1976).

(27) S.L. Lin, L.A. Viehland and E.A. Mason, Chem.Phys., 37, 411 (1979).

(28) L.A. Viehland and S.L. Lin, Chem.Phys., 43, 135 (1979).

(29) L.A. Viehland, E.A. Mason, W.F. Morrison and M.R. Flannery, At.Data Nucl.Data Tables, 16, 495-514 (1975).

(30) Y. Kaneko, L.R. Megill and J.B. Hasted, J.Chem.Phys., 45, 3741 (1966).

(31) F. Howorka, F.C. Fehsenfeld and D.L. Albritton, J.Phys. B 12, 4189 (1979).

(32) D. MacNair, Rev.Sci.Instrum. 38, 124 (1967).

(33) G.H. Coleman, R.W. Leeper and C.C. Schulze, Inorganic Syntheses, 2, 90 (1946).

(34) H.L. Jackson and B.C. McKusick, Organic Syntheses Coll. Vol.IV ed. N. Rabjohn. Wiley (1963).

(35) E.C. Beaty and P.L. Patterson, Phys.Rev., 137, 346 (1965).

(36) D. Edelson, J.A. Morrison, L.G. McKnight and D.P. Sipler, Phys.Rev., 164, 71 (1967).

(37) J.T. Moseley, I.R. Gatland, D.W. Martin and E.W. McDaniel, Phys.Rev., 178, 234 (1969).

(38) R. Thomas, J. Barassin and A. Barassin, Int.J.Mass Spectrom.Ion Phys. 41, 95 (1981).

(39) J. Barassin, A. Barassin and R. Thomas, Int.J.Mass Spectrom.Ion Phys. 49, 51 (1983).

(40) T. Fujii and G.G. Meisels, J.Chem.Phys., 75, 5067 (1981).

(41) L.A. Viehland and D.W. Fahey, J.Chem.Phys., 78, 435 (1983).

(42) T.M. Miller, J.T. Moseley, D.W. Martin and E.W. McDaniel, Phys.Rev., 173, 115 (1968).

(43) C.E. Moore "Atomic Energy Levels" NBS Cir 467, Vol.1 (1949).

(44) L.G. Kelly "Handbook of Numerical Methods and Applications", Addison-Wesley Pub.Co. (1967) p.84.

(45) J.A. Hornbeck, Phys.Rev., 84, 615 (1951).

(46) I. Dotan, W. Lindinger and D.L. Albritton, J.Chem.Phys., 67, 5968 (1977).

(47) Y. Kaneko, T. Koizumi and N. Kobayashi, J.Phys.Soc. Japan, 40, 605 (1976).

(48) W. Lindinger and D.L. Albritton, J.Chem.Phys., 62, 3517 (1975).

(49) W.T. Huntress and V.G. Anicich, Astrophys.J., 208, 237 (1976).

(50) C.G. Freeman, P.W. Harland, J.P. Liddy and M.J. McEwan, Aust.J.Chem., 31, 963 (1978).

(51) J. Heimerl, R. Johnsen and M.A. Biondi, J.Chem.Phys., 51, 5041 (1969).

(52) H.M. Rosenstock, K. Draxl, B.W. Steiner and J.T. Herron, J.Phys.Chem.Ref.Data 6, Suppl.1 (1977).

(53) G. Bieri and B. Jonsson, Chem.Phys.Lett. 56, 446 (1978).

(54) F.W. McLafferty and D.C. McGilvery, J.Am.Chem.Soc., 102, 6189 (1980).

(55) J.N. Murrell and A.Al. Derzi, J.C.S. Faraday II 76, 319 (1980).

(56) N.N. Haese and R.C. Woods, Chem.Phys.Lett. 61, 396 (1979).

(57) T.L. Allen, J.D. Goddard and H.F. Schaefer III, J.Chem.Phys., 73, 3255 (1980).

(58) P.S. Dardi and C.E. Dykstra, Astrophys.J.Lett., 240, L171 (1980).

(59) M.P. Conrad and H.F. Schaefer III, Nature, 274, 456, (1978).

(60) T. Ha and M.T. Nguken, Chem.Phys.Lett., 97, 503 (1983).

(61) M.J. McEwan, unpublished results.

(62) N.N. Haese and R.C. Woods, Astrophys.J., 246, L51 (1981).

(63) M. Yoshimine and W.P. Kraemer, Chem.Phys.Lett., 90, 145 (1982).

(64) V.H. Dibeler, R.M. Reese and J.L. Franklin, J.Am.Chem.Soc., 83, 1813 (1961).

(65) O.I. Smith, Int.J.Mass Spectrom.Ion Proc., 54, 55 (1983).

(66) W. Heerma, J.J. de Ridder and G. Dijkstra, Org.Mass Spectrom., 2, 1103 (1969).

(67) W. Heerma and J.J. de Ridder, Org.Mass Spectrom., 3, 1439 (1970).

(68) J. van Thuijl, J.J. van Houte, A. Maquestiau, R. Flammang and C. De Meyer, Org.Mass Spectrom., 12, 196 (1977).

(69) E.K. Chess, R.L. Lapp and M.L. Gross, Org.Mass Spectrom., 17, 475 (1982).

(70) R.G. Cooks, J.H. Beynon and J.F. Litton, Org.Mass Spectrom., 10, 503 (1975).

(71) M.L. Gross and F.W. McLafferty, J.Am.Chem.Soc., 93, 1267 (1971).

(72) P.N.T. van Velzen and W.T. van der Hart, Chem.Phys. 61, 335 (1981).

(73) S.G. Lias and T.J. Buckley, Int.J.Mass Spectrom.Ion Proc., 56, 123 (1984).

(74) F.P. Lossing, Can.J.Chem., 50, 3973 (1972).

(75) K. Raghavachari, R.A. Whiteside, J.A. Pople and P.v.R. Schleyer, J.Am.Chem.Soc., 103, 5649 (1981).

(76) J.L. Holmes and F.P. Lossing, Can.J.Chem., 57, 249 (1979).

(77) P.J. Ausloos and S.G. Lias, J.Am.Chem.Soc., 103, 6505 (1981).

(78) C.C. Van de Sande and F.W. McLafferty, J.Am.Chem.Soc., 97, 4613 (1975).

(79) J.L. Holmes and J.K. Terlouw, Can.J.Chem., 53, 2076 (1975).

(80) J.L. Holmes, J.K. Terlouw and F.P. Lossing, J.Phys.Chem., 80, 2860 (1976).

(81) A.S. Blair and A.G. Harrison, Can.J.Chem., 51, 703 (1973).

(82) R.R. Corderman, P.R. LeBreton, S.E. Butrill, A.D. Williamson and J.L. Beauchamp, J.Chem.Phys., 65, 4929 (1976).

(83) W.J. Bouma, J.K. MacLeod and L. Radom, J.Chem.Soc., Chem.Commun., 724 (1978).

(84) W.J. Bouma, J.K. MacLeod and L. Radom, J.Am.Chem.Soc., 101, 5540 (1979).

(85) H. Lischka and H.J. Kohler, Chem.Phys.Lett., 63, 326 (1979).

(86) K.M.A. Refeay and W.A. Chupka, J.Chem.Phys., 48, 5205 (1968).

(87) A.G. Harrison, C.D. Finney and J.A. Stark, Org.Mass Spectrom., 5, 1313 (1971).

(88) R.H. Staley, R.R. Corderman, M.S. Foster, J.L. Beauchamp, J.Am.Chem.Soc., 96, 1260 (1974).

APPENDIX A:

Definitions of Non-S.I. Units

Quantity	Non-SI Unit	Definition
E/N	Townsend(Td)	$10^{-21}Vm^2$
Pressure	Torr	133.3Pa
Pressure	Millibar	100Pa
Energy	Electron volt(eV)	$96.5kJmol^{-1}$
Dipole moment	Debye(D)	$3.33564X10^{-30}Cm$
Mobility	$cm^2V^{-1}s^{-1}$	$10^{-4}m^2V^{-1}s^{-1}$
Diffusion coefficient	cm^2s^{-1}	$10^{-4}m^2s^{-1}$
Rate coefficient	$cm^3molec^{-1}s^{-1}$	$1.66X10^{-18}m^3mol^{-1}s^{-1}$
Mass	atomic mass unit	$1.6605X10^{-27}kg$

APPENDIX B: LISTINGS OF COMPUTER PROGRAMS

PULSE Page 1 of 3

```
100 REM INITIALIZE PIAs
110 P1=58116:Q1=58118:P2=58120:Q2=58122:P3=58124:Q3=58126
115 P4=58132:Q4=58134:P5=58136:Q5=58138:P6=58140:P6=58142
120 POKEP1+1,0:POKEP1,0:POKEP1+1,4
123 POKEP2+1,0:POKEP2,0:POKEP2+1,4
125 POKEP3+1,0:POKEP3,0:POKEP3+1,4
127 POKEP4+1,0:POKEP4,0:POKEP4+1,4
130 POKEQ1+1,0:POKEQ1,0:POKEQ1+1,4
133 POKEQ2+1,0:POKEQ2,255:POKEQ2+1,4
136 POKEQ3+1,0:POKEQ3,255:POKEQ3+1,4
140 POKEQ4+1,0:POKEQ4,255:POKEQ4+1,4
145 POKEQ5+1,0:POKEQ5,255:POKEQ5+1,4
150 DIMIS(371),SS(371):PRINTCHR$(26)
155 DISKOPEN,6,"PULDAT":DISK!"IO ,02"
160 PRINT"** MEASUREMENT OF ARRIVAL TIME DISTRIBUTIONS **":PRINT
170 PRINT"** RUN 1000 to calculate drift tube voltages **":PRINT
175 PRINT"TYPE 'D' to recover data from DISK"
180 INPUT"SOURCE POSITION (scale)";DD$:IFDD$="D"THEN2000
185 DD=VAL(DD$):PRINT
200 INPUT"MINIMUM TIME , >=6 us";MN:IFMN<60RMN>370THEN200
250 INPUT"MAXIMUM TIME , <=370 us";MX:IFMX>370THEN250
255 TC=(MX+50)/1E6
270 INPUT"TIME INCREMENT (us)";T
300 INPUT"SAMPLE TIME per POINT (sec)";CY:TT=CY:CY=CY/TC
310 CY=INT(CY/256):IFCY=0THENPRINT"TOO SHORT":GOTO300
320 IFCY>255THENPRINT"TOO LONG":GOTO300
350 INPUT"No. of SCANS";NS:PRINT:FORJ=1TONS
355 DISK!"CA 6000=38,1"
360 POKE24813,CY  :REM $60ED
370 EP=24611+INT((MX-3.999)/2):POKEEP,76:POKEEP+1,221:POKEEP+2,96
390 PRINT"SCAN ";J:PRINT"ARRIVAL        ACCUMULATED"
391 PRINT"TIME (us)      ION SIGNAL":PRINT
400 FORDP=MNTOMXSTEPT
410 DI=INT(DP/2):CA=24600+DI
500 RESTORE:FORI=CATOCA+8:READD
510 POKEI,D:NEXTI
520 DATA 140,10,227,234,234,234,141,10,227
530 REM  STY $E30A;NOP;NOP;NOP;STA $E30A
541 IFDI*2<>DPTHENPOKE24797,234:POKE24602,72:GOTO548
542 POKE24602,234:POKE24797,72
548 PRINTDP;TAB(15);
550 DISK!"GO 6000"
560 FORI=CATOCA+8:POKEI,234:NEXT
565 CNT=65536*PEEK(P2)+256*PEEK(P3)+PEEK(P1):IS(DP)=IS(DP)+CNT
566 PRINTIS(DP)
570 NEXTDP
580 PRINT:PRINT:NEXTJ
600 DP=DP-T:T2=2*T
605 PRINT#6,MN:PRINT#6,DP:PRINT#6,T
610 FORI=MNTODPSTEPT:PRINT#6,IS(I):NEXTI
612 PRINT#6,DD$:PRINT#6,NS:PRINT#6,TT
615 DISKCLOSE,6
```

```
620 SS(MN)=IS(MN):SS(MN+T)=IS(MN+T)
630 SS(DP-T)=IS(DP-T):SS(DP)=IS(DP)
650 FORI=MN+T2TODP-T2
660 SS(I)=(-3*IS(I-T2)+12*IS(I-T)+17*IS(I)+12*IS(I+T)-3*IS(I+T2))/35
670 NEXTI
700 REM LANGRANGE INTERPOLATION
710 FORI=MN+T2TODP-T2:IFSS(I)>LSTHENLS=SS(I):IM=I
712 NEXTI
715 DEFFNL4(X)=((X-IM-T)*(X-IM)*(X-IM+T)*(X-IM+T2))/24*T
720 DEFFNL3(X)=((X-IM-T2)*(X-IM)*(X-IM+T)*(X-IM+T2))/-6*T
725 DEFFNL2(X)=((X-IM-T2)*(X-IM-T)*(X-IM+T)*(X-IM+T2))/4*T
730 DEFFNL1(X)=((X-IM-T2)*(X-IM-T)*(X-IM)*(X-IM+T2))/-6*T
735 DEFFNL0(X)=((X-IM-T2)*(X-IM-T)*(X-IM)*(X-IM+T))/24*T
740 DEFFNLA(X)=FNL0(X)*SS(IM-T2)+FNL1(X)*SS(IM-T)+FNL2(X)*SS(IM)
745 DEFFNLB(X)=FNLA(X)+FNL3(X)*SS(IM+T)+FNL4(X)*SS(IM+T2)
750 I=IM-.75*T:LM=0
755 LB=FNLB(I):IFLB>LMTHENLM=LB:I=I+.25*T:GOTO755
757 PRINTCHR$(26):DISK!"IO ,03"
758 PRINT:PRINT"DRIFT DISTANCE =";10-DD/10+.04;"cm   (";DD$;")
759 PRINTNS;" SCAN(S) WITH ";TT;" SECOND COUNTING":PRINT
760 PRINT"Signal MAXIMUM after";(I-.25*T);"us":PRINT
835 PRINT"TIME   EXP SIG   SMOOTH SIG   NORM. SIG"
840 FORI=MNTODPSTEPT:PRINTI;TAB(7)IS(I);TAB(18)INT(SS(I)+.5);
845 PRINTTAB(30)INT(SS(I)/LS*1000+.5):NEXTI
850 PRINT:DISK!"IO ,02"
900 PRINT:INPUT"GRAPH on PRINTER";G$:IFG$<>"Y"THEN999
910 PRINT#1:FORI=MNTODPSTEPT:PRINT#1,I;TAB(5+SS(I)/SS(IM)*34)"*":NEXTI
999 END
1000 PRINT:GOSUB31000:PRINT#1
1002 INPUT"ION,BUFFER";S$:PRINT#1,"ION ,BUFFER >>";S$
1005 INPUT"TEMPERATURE (Celcius)";T:PRINT#1,"TEMP.=";T;"C";
1010 T=T+273:PRINT#1,"  ("T"K)
1020 INPUT"PRESSURE (torr)";PR:PRINT#1,"PRESSURE =";PR;"TORR"
1030 INPUT"E/N Td";EN:PRINT#1,"E/N =";EN;"Td"
1040 E=EN*96.58*PR/T:PRINT#1,"E =";E;"V/cm":PRINT"E =";E;"V/cm"
1050 PRINT#1,"V(RINGS) =";10.5*E
1060 PRINT#1:PRINT#1,"DISTANCE    V(TRACKING)"
1070 FORD=90TO10STEP-5:PRINT#1,D;((100-D)/10+.04)*E:NEXT
1099 END
2000 PRINTCHR$(26):REM REREAD DATA FROM DISK
2005 DISK!"EX D100=39"
2010 INPUT#6,MN,DP,T:T2=2*T
2020 FORI=MNTODPSTEPT:INPUT#6,IS(I):NEXTI
2025 INPUT#6,DD$,NS,TT
2030 GOTO620
9999 END
```

```
31000 REM READ CLOCK SUBROUTINE
31010 DA=57344:CA=DA+1
31020 DB=DA+2:CB=DB+1
31040 C$="JANFEBMARAPRMAYJUNJULAUGSEPOCTNOVDEC"
31050 D$="SUNMONTUEWEDTHUFRISAT"
31060 GOSUB31160:FORAD=7TO2STEP-1:POKEDA,AD
31070 GOSUB31180:T(AD)=TI:NEXTAD:DISK!"IO ,03"
31080 PRINTMID$(D$,T(5)*3-2,3);"  ";MID$(C$,T(7)*3-2,3);T(6);"    ";
31090 IFT(4)>=12THENPM=1
31100 IFT(4)>=13THENT(4)=T(4)-12
31110 IFT(4)=0THENT(4)=12
31120 PRINTT(4);":"T(3)":"T(2);"  ";
31130 IFPM=1THENPRINT"PM    ":GOTO31150
31140 PRINT"AM    "
31150 PM=0:DISK!"IO ,02":RETURN
31160 POKECA,58:POKEDA,31:POKECA,62
31170 POKECB,58:POKEDB,0:POKECB,62
31180 POKEDA,ADD:POKECA,54:DTA=PEEK(DB):POKECA,62
31190 MS=DTAAND240:MS=(MS/16)*10:LS=DTAAND15:TIME=MS+LS:RETURN
```

ASSEMBLED SOURCE CODE for PULSE

```
 10 6000                    *= $6000
 20 E30A=                   P2B=$E30A
 30 E30B=                   CR= $E30B
 40 0048=                   V = $48
 50 6000 A900     INIT      LDA #0
 60 6002 8548               STA V
 70 6004 8549               STA V+1
 80 6006 A990               LDA #$90
 90 6008 8D0AE3             STA P2B
100 600B A980               LDA #$80
110 600D 8D0AE3             STA P2B
120 6010 A2C0               LDX #$C0
130 6012 A000               LDY #0
140 6014 8E0AE3  PULSE      STX P2B
150 6017 8D0AE3             STA P2B
160 60DD         DLYST  *=*+195
170 60DD 48      DLYEND FHA
180 60DE 68                 PLA
190 60DF 18                 CLC
200 60E0 A548               LDA V
210 60E2 6901               ADC #1
220 60E4 8548               STA V
230 60E6 A549               LDA V+1
240 60E8 6900               ADC #0
250 60EA 8549               STA V+1
260 60EC C9FF               CMP #$FF
270 60EE F005               BEQ NEXT
280 60F0 A980               LDA #$80
290 60F2 4C1460             JMP PULSE
300 60F5 A9A0     NEXT      LDA #$A0
310 60F7 8D0AE3             STA P2B
320 60FA A990               LDA #$90
330 60FC 8D0AE3             STA P2B
340 60FF 60                 RTS
```

DRIFT Page 1 of 2

```
10 REM  ATD Calculation for PRIMARY ions
12 REM
15 DIMFLUX(50):PRINTCHR$(26)
16 PRINT"** CALCULATION OF ARRIVAL TIME DISTRIBUTION **"
17 PRINT"**          FOR DRIFT TUBE                  **":PRINT
20 REM ALL CALCULATIONS IN SI UNITS ALTHOUGH
21 REM INPUTS MAY BE IN COMMONLY USED UNITS
22 REM
30 RO=.001:REM RAD OF SOURCE APERTURE
40 AE=8.11E-07:REM AREA OF EXIT(m2)
50 PI=3.14159
60 SN=1000:REM INITIAL SURFACE ION DENSITY
61 INPUT"TEMPERATURE (Celcius)";T:T=T+273.16
62 INPUT"TOTAL PRESSURE (Torr)";P:NT=9.663E18*P/T
63 INPUT"E/N (Td)";EN
64 E=EN/1E15*NT:PRINT:PRINT"E =";E/100;"V/cm"
65 INPUT"HIGH OR LOW FIELD (H/L)";F$:IFF$="L"THEN500
70 PRINT: INPUT"DRIFT VELOCITY (cm/s)";VD:VD=VD/100
80 INPUT"LONGITUDINAL DIFF. COEFF(cm2/s)";DL:DL=DL/10000
90 INPUT"TRANSVERSE DIFF.COEFF(cm2/s)";DT:DT=DT/10000
100 INPUT"DISTANCE SOURCE-EXIT (cm)";Z:Z=Z/100
110 INPUT"REACTION RATE CONST(cm,molec,s)";KR:IFKR=0THEN128
115 INPUT"ORDER of REACTION";RO:IFRO<>2ANDRO<>3THEN115
120 INPUT"% REACTANT IN GAS";NR:NR=NR/100*NT
122 IFRO=2THENAL=KR*NR:GOTO126
125 AL=KR*NR*NT
126 PRINT"COLLISION FREQUENCY ="AL"/s"
127 PRINT"AVERAGE LIFETIME ="1/AL"s"
128 PRINT:INPUT"Calculate TOTAL flux (Y/N)";F$:IFF$="Y"THENGOSUB800
130 PRINT:INPUT"START AND FINISH TIMES (us)";TS,TF
140 INPUT"TIME INCREMENT (us)";IN
141 IF(TF-TS)/IN<=45THEN145
142 PRINT"TOO MANY STEPS":GOTO140
145 TS=TS/1E6:TF=TF/1E6:IN=IN/1E6
149 I=0:SZ=0
150 T=TS+I*IN:IFT>TFTHEN230
155 I=I+1
200 GOSUB700:FLUX(I)=FLUX
210 PRINTT*1E6,FLUX(I)
215 SZ=SZ+FLUX(I)
220 GOTO150
230 PRINT:PRINT"TOTAL FLUX =";SZ*IN:PRINT
235 PRINT"Hit RETURN to continue"
240 IFPEEK(57100)<>246THEN240
300 REM GRAPH ROUTINE
310 PRINTCHR$(26)
320 FORSL=53248TO55104STEP64:POKESL,156:NEXT
325 POKE55168,169
```

DRIFT Page 2 of 2

```
330 FORSL=55169TO55215:POKESL,154:NEXT
350 FMAX=0
360 FORJ=1TOI:IFFLUX(J)<FMAXTHEN370
365 FMAX=FLUX(J):JMAX=J
370 NEXT
380 FORJ=1TOI
390 POKE55168+J-64*(INT(FL(J)/FMAX*30)),42:NEXT
410 REM FIND MAX BY BISECTION
415 S=1:T=TS+(JMAX-2)*IN:GOSUB700:FA=FLUX:T=T+IN:GOSUB700:FB=FLUX
420 DF=FB-FA:IFABS(DF)/ABS(FB)<1E-8THEN445
430 IFDF>0THENFA=FB:T=T+S*IN:GOSUB700:FB=FLUX:GOTO420
435 S=-S:FB=FA:IN=IN/2:T=T+S*IN:GOSUB700:FA=FLUX:T=T+S*IN:GOTO420
445 PRINTCHR$(26):PRINT"MAXIMUM AFTER";INT((T+5E-10)*1E9)/1E3;"usec"
450 PRINT:INPUT"RERUN NEW DISTANCE or TIMES";T$
455 IFT$="Y"THEN128
460 INPUT"OUTPUT TO PRINTER";P$
465 IFP$<>"Y"THEN999
470 PRINT#1,"TIME (US)","SIGNAL"
475 FORJ=1TOI:FLUX(J)=FL(J)/FL(JMAX)*1000
480 PRINT#1,INT(TS*1E6+(J-1)*IN*1E6+.0001),FL(J)
481 NEXTJ
482 IFF$<>"L"THEN490
483 PRINT#1,"Z =";Z*100;"CM","P =";P;"TORR"
484 PRINT#1,"E =";E/100;"V/CM","E/N =";EN;"TD"
486 PRINT#1,"K0 =";K0*10000;"CM2/VS";"      D =";DL*10000;"CM2/S"
488 PRINT#1,"NORMALISATION FACTOR = ";FMAX
490 GOTO999
500 REM
501 REM CALC. DO FROM EINSTIEN EQ.
510 PRINT:INPUT"REDUCED MOBILITY (cm2/Vs)";K0:K0=K0/10000
550 KP=K0*T/273.16*760/P
560 DO=KP*T*8.61798E-5:VD=KP*E
561 INPUT"MASS of ION ,BUFFER (amu)";MI,MB:PRINT
562 DL=DO+(MB+3.72*MI)/(3*(MB+1.908*MI))*MB*1.036E-8*VD^3/E
565 DT=DO+(MB+MI)/(3*(MB+1.908*MI))*MB*1.036E-8*VD^3/E
582 PRINT"DRIFT VELOCITY =";VD*100;"cm/s"
583 PRINT"LONG. DIFF. COEFF. =";DL*10000;"cm2/s"
585 PRINT"TRANS. DIFF. COEFF. =";DT*10000;"cm2/s":PRINT
590 GOTO100
700 AD=EXP(-(Z-VD*T)^2/(4*DL*T))
710 RD=1-EXP(-R0*R0/(4*DT*T))
720 RL=EXP(-ALPHA*T)/(4*SQR(PI*DL*T))*(VD+Z/T)
730 FLUX=SN*AE*AD*RD*RL
740 RETURN
800 REM CALCULATE TOTAL FLUX
802 EF=SQR(VD*VD/(4*DL)+AL)
803 EG=SQR(Z*Z/(4*DL)+R0*R0/(4*DT))
804 EC=(Z*VD)/(2*DL)
805 TZ=(2*SQR(DL)+VD/EF)*EXP(-Z/SQR(DL)*EF+EC)
806 TZ=TZ-(Z/EG+VD/EF)*EXP(-2*EG*EF+EC)
807 TZ=TZ*SN*AE/(4*SQR(DL))
808 PRINT:PRINT"TOTAL ION FLUX =";TZ:RETURN
999 END
```

DRIFT2 Page 1 of 3

```
10 REM ATD calculation for SECONDARY ions
12 REM
15 DIMFLUX(50):PRINTCHR$(26)
16 PRINT"** CALCULATION OF ARRIVAL TIME DISTRIBUTION **"
17 PRINT"**          FOR DRIFT TUBE                    **":PRINT
20 REM ALL CALCULATIONS IN SI UNITS ALTHOUGH
21 REM INPUTS MAY BE IN COMMONLY USED UNITS
22 REM
30 R0=.002:R2=R0*R0:REM RAD OF SOURCE APERTURE
40 AE=8.11E-07:REM AREA OF EXIT(m2)
50 PI=3.14159
60 SS=1000:REM INITIAL SURFACE ION DENSITY
61 INPUT"TEMPERATURE (Celcius)";T:T=T+273.16
62 INPUT"TOTAL PRESSURE (Torr)";P:NT=9.663E18*P/T
63 INPUT"E/N (Td)";EN
64 E=EN/1E15*NT:PRINT:PRINT"E =";E/100;"V/cm"
65 INPUT"DRIFT VELOCITY OR MOBILITY (V/M)";F$:IFF$="M"THEN500
70 PRINT: INPUT"DRIFT VELOCITY A (cm/s)";VA:VA=VA/100
72 INPUT"LONGITUDINAL DIFF. COEFF A (cm2/s)";LA:LA=LA/10000
74 INPUT"TRANSVERSE DIFF.COEFF A(cm2/s)";TA:TA=TA/10000
80 PRINT: INPUT"DRIFT VELOCITY B (cm/s)";VB:VB=VB/100
82 INPUT"LONGITUDINAL DIFF. COEFF B (cm2/s)";LB:LB=LB/10000
84 INPUT"TRANSVERSE DIFF.COEFF B(cm2/s)";TB:TB=TB/10000
90 PRINT
100 REM
110 PRINT:INPUT"REACTION RATE A-B (cm,molec,s)";K1:IFK1=0THEN138
115 INPUT"ORDER of REACTION";RO:IFRO<>2ANDRO<>3THEN115
120 INPUT"% REACTANT IN GAS";NR:NR=NR/100*NT
122 IFRO=2THENAA=K1*NR:GOTO126
125 AA=K1*NR*NT
126 PRINT:PRINT"REACTIVE COLLISION FREQ. A ="AA"/s"
127 PRINT"AVERAGE LIFETIME A="1/AA*1E6"us"
130 PRINT:INPUT"REACTION RATE B-? (cm,molec,s)";K2:IFK2=0THEN138
131 INPUT"ORDER of REACTION";RO:IFRO<>2ANDRO<>3THEN131
132 IFRO=2THENAB=K2*NR:GOTO134
133 AB=K2*NR*NT
134 PRINT:PRINT"REACTIVE COLLISION FREQ. B ="AB"/s"
135 PRINT"AVERAGE LIFETIME B="1/AB*1E6"us"
138 PRINT:PRINT:INPUT"DISTANCE SOURCE-EXIT(cm)";Z:Z=Z/100
139 PRINT:INPUT"START AND FINISH TIMES (us)";TS,TF
140 INPUT"TIME INCREMENT (us)";IN
141 IF(TF-TS)/IN<=45THEN145
142 PRINT"TOO MANY STEPS":GOTO140
145 TS=TS/1E6:TF=TF/1E6:IN=IN/1E6
149 I=0:SZ=0
150 T=TS+I*IN:IFT>TFTHEN230
155 I=I+1
200 GOSUB700:FLUX(I)=FLUX
210 PRINTT*1E6,FLUX(I)
215 SZ=SZ+FLUX(I)
220 GOTO150
230 PRINT:PRINT"TOTAL ION SIGNAL =";SZ*IN:PRINT
```

```
235 PRINT"Hit RETURN to continue"
240 IFPEEK(57100)<>246THEN240
300 REM GRAPH ROUTINE
310 PRINTCHR$(26)
320 FORSL=53248TO55104STEP64:POKESL,156:NEXT
325 POKE55168,169
330 FORSL=55169TO55215:POKESL,154:NEXT
350 FMAX=0
360 FORJ=1TOI:IFFLUX(J)<FMAXTHEN370
365 FMAX=FLUX(J):JMAX=J
370 NEXT
380 FORJ=1TOI
390 POKE55168+J-64*(INT(FL(J)/FMAX*30)),42:NEXT
400 IFPEEK(57100)<>246THEN400
410 PRINTCHR$(26):INPUT"FIND PRECISE MAXIMUM";M$:IFM$<>"Y"THEN460
415 S=1:T=TS+(JMAX-2)*IN:GOSUB700:FA=FLUX:T=T+IN:GOSUB700:FB=FLUX
420 DF=FB-FA:PRINT".";:IFABS(DF)/ABS(FB)<1E-8THEN445
430 IFDF>0THENFA=FB:T=T+S*IN:GOSUB700:FB=FLUX:GOTO420
435 S=-S:FB=FA:IN=IN/2:T=T+S*IN:GOSUB700:FA=FLUX:T=T+S*IN:GOTO420
445 PRINT:PRINT"MAXIMUM AFTER";INT(T*1E9)/1E3;"usec":PRINT
460 INPUT"OUTPUT TO PRINTER";P$
465 IFP$<>"Y"THEN482
470 PRINT#1,"TIME (US)","SIGNAL"
472 FJ=FLUX(JMAX)
475 FORJ=1TOI:FLUX(J)=FL(J)/FJ*1000
480 PRINT#1,INT(TS*1E6+(J-1)*IN*1E6+.0001),FL(J):NEXTJ
482 INPUT"GRAPH ON PRINTER";G$:IFG$<>"Y"THEN488
483 FJ=FL(JM)
484 FORJ=1TOI:FL=INT(FL(J)/FJ*32+7)
485 PRINT#1,INT(TS*1E6+(J-1)*IN*1E6+.0001);TAB(FL);"*":NEXTJ
488 INPUT"RERUN NEW DISTANCE or TIMES";T$
489 IFT$="Y"THEN138
490 GOTO999
500 REM Calculation of drift velocities and diffusion coefficients
510 PRINT:INPUT"REDUCED MOBILITY ION A (cm2/Vs)";KA:KA=KA/10000
550 KP=KA*T/273.16*760/P
560 DO=KP*T*8.61798E-5:VA=KP*E
561 INPUT"MASS of ION A, BUFFER (amu)";MA,MG:PRINT
562 LA=DO+(MG+3.72*MA)/(3*(MG+1.908*MA))*MG*1.036E-8*VA^3/E
565 TA=DO+(MG+MA)/(3*(MG+1.908*MA))*MG*1.036E-8*VA^3/E
582 PRINT"DRIFT VELOCITY A=";VA*100;"cm/s"
583 PRINT"LONG. DIFF. COEFF. A=";LA*10000;"cm2/s"
585 PRINT"TRANS. DIFF. COEFF. A=";TA*10000;"cm2/s"
610 PRINT:INPUT"REDUCED MOBILITY ION B (cm2/Vs)";KB:KB=KB/10000
650 KP=KB*T/273.16*760/P
660 DO=KP*T*8.61798E-5:VB=KP*E
661 INPUT"MASS of ION B (amu)";MB:PRINT
662 LB=DO+(MG+3.72*MB)/(3*(MG+1.908*MB))*MG*1.036E-8*VB^3/E
665 TB=DO+(MG+MB)/(3*(MG+1.908*MB))*MG*1.036E-8*VB^3/E
682 PRINT"DRIFT VELOCITY B=";VB*100;"cm/s"
683 PRINT"LONG. DIFF. COEFF. B=";LB*10000;"cm2/s"
685 PRINT"TRANS. DIFF. COEFF. B=";TB*10000;"cm2/s":PRINT
690 GOTO100
```

DRIFT2 Page 3 of 3

```
699 REM Numerical integration usisg Simpson's rule
700 NZ=2*INT(T*2.5E5)+20:H=T/NZ:SN=0
705 U=0:GOSUB750:SN=SN+DU
708 U=T:GOSUB750:SN=SN+DU
710 FORJ=2TONZ-2STEP2:U=J*H:GOSUB750:SN=SN+2*DU:NEXTJ
715 FORJ=1TONZ-1STEP2:U=J*H:GOSUB750:SN=SN+4*DU:NEXTJ
720 FLUX=SS*AA*AE*H/3*SN:RETURN
750 A=4*TA*T-4*(TA-TB)*U
752 B=4*LA*T-4*(LA-LB)*U
754 C=VA*T-(VA-VB)*U:ZC=Z-C
756 D=AA*T-(AA-AB)*U
760 DU=1/SQR(PI*B)*(1-EXP(-R2/A))*(2*LB*(ZC)/B+VB)*EXP(-D-(ZC)*(ZC)/B)
770 RETURN
999 END
```